Titre: Title:	Metabolomics and Dynamic Metabolic Flux Analysis in ABE (Acetone-Butanol-Ethanol) Fermentation
Auteur: Author:	Xinhe Zhao
Date:	2017
Type:	Mémoire ou thèse / Dissertation or Thesis
Référence: Citation:	Zhao, X. (2017). Metabolomics and Dynamic Metabolic Flux Analysis in ABE (Acetone-Butanol-Ethanol) Fermentation [Thèse de doctorat, École Polytechnique de Montréal]. PolyPublie. https://publications.polymtl.ca/2700/

UNIVERSITÉ DE MONTRÉAL

METABOLOMICS AND DYNAMIC METABOLIC FLUX ANALYSIS IN ABE (ACETONE-BUTANOL-ETHANOL) FERMENTATION

XINHE ZHAO

DÉPARTEMENT DE GÉNIE CHIMIQUE

ÉCOLE POLYTECHNIQUE DE MONTRÉAL

THÈSE PRÉSENTÉE EN VUE DE L'OBTENTION

DU DIPLÔME DE PHILOSOPHIAE DOCTOR

(GÉNIE CHIMIQUE)

JUIN 2017

UNIVERSITÉ DE MONTRÉAL

ÉCOLE POLYTECHNIQUE DE MONTRÉAL

Cette thèse intitulée :

METABOLOMICS AND DYNAMIC METABOLIC FLUX ANALYSIS IN ABE (ACETONE-BUTANOL-ETHANOL) FERMENTATION

présentée par : ZHAO Xinhe

en vue de l'obtention du diplôme de : Philosophiae doctor

a été dûment acceptée par le jury d'examen constitué de :

M. PERRIER Michel, Ph. D., président

M. JOLICOEUR Mario, Ph. D., membre et directeur de recherche

M. TAVARES Jason-Robert, Ph. D., membre

M. GARNIER Alain, Ph. D., membre

DEDICATION

To my wife and daughter.

ACKNOWLEDGEMENTS

First, I would like to thank the financial support of the BioFuelNet Canada, a network focusing on the development of advanced biofuels. BioFuelNet is a member of the Networks of Centres of Excellence of Canada program (NSERC grant # 419517), and the Natural Science and Engineering Research Council of Canada.

Especially, I would like to express my sincere thanks to my supervisor, Professor Mario Jolicoeur, for his patient guidance, thoughtful advices, continuous encouragement and other various supports during my thesis. I particularly appreciated his kind attention helping me to learn all along my thesis. I am also greatly humbled by his continuous guidance while developing and on model calibration.

I would also like to thank Jingkui Chen for his training work and all cooperation during sample analysis. I would like to thank my colleague and wife, Xiaojie Ren for her support both on work and life.

Least but not last, I would like to thank Stefan Condruz, Mayssa Kasbi, Julien Robitaille, Benoit Laflaquière and Dr. Sabine Peres for their cooperation during lab work and modeling process. Meanwhile, warm thanks to all my colleagues in the lab, especially Eric Karengera, Chi-Yuan Chang, Prajwal Kumar, Zhihui Yi, Irina Valitova and Edwige Arnold.

Finally, I must thank my mother and mother-in-law and all my family for their support to my life and study.

RÉSUMÉ

De nos jours, les hydrolysats d'hémicelluloses, des matières premières riches en glucides issues des procédés papetier et forestier, sont largement étudiés pour le développement de procédés de bioraffinerie forestière pour la production de biobutanol, un biodiésel de remplacement du pétrole. Une des avenues biotechnologiques les plus étudiées à ce jour est la fermentation ABE (acétone-butanol-éthanol) par la bactérie *Clostridium acetobutylicum.* Cependant, certains inhibiteurs de la fermentation ABE sont générés lors du procédé de prétraitement et d'hydrolyse, ce qui limite grandement l'utilisation de ces biomasses riches en substrats peu coûteux. D'autre part, les pratiques actuelles de culture mènent à des rendements en butanol qui ne sont pas suffisants pour assurer la mise en place d'unités industrielles de production qui soient économiquement profitables. L'objectif de ce projet de recherche visait donc à améliorer la productivité du bioprocédé de fermentation ABE, dans un contexte de bioraffinage forestier, par l'amélioration des connaissances et le développement de stratégies de culture. Un milieu synthétique contenant du xylose comme source principale de carbone a été utilisé pour simuler un hydrolysat d'hémicelluloses d'épinette noire pour un bioprocédé de fermentation avec la bactérie *Clostridium acetobutylicum*.

Tout d'abord, nous avons étudié l'effet d'une concentration élevée en chlorure de sodium sur le comportement du bioprocédé. En effet, une quantité élevée en hydroxyde de sodium est ajouté lors du procédé de délignification des copeaux de bois, au préalable de l'étape d'hydrolyse, cet ajout tient au fait du contrôle pH ainsi que pour son pouvoir caustique comme agent de nettoyage. Ainsi, compte tenu de l'intérêt à utiliser cette solution d'hydrolysats d'hémicellulose, il est considéré comme crucial d'évaluer l'effet de cette haute concentration en sodium sur la fermentation ABE. Une concentration seuil de sodium de 200 mM, soit ce qui est normalement mesuré en industrie, a été utilisée et comparée à une culture témoin avec la souche *Clostridium acétobutylicum* ATCC 824. Les résultats ont révélé que la biomasse et l'ABE étaient sérieusement inhibés par une concentration élevée en sodium, avec une diminution respectivement de 19.50 ± 0.85 % (biomasse), 35.14 ± 3.50 % (acétone), 33.37 ± 0.74 % (butanol) et 22.95 ± 1.81 % (éthanol). De manière intéressante, les productivités spécifiques cellulaires en solvants ont été maintenues comparativement à la culture témoin. Une étude approfondie du métabolisme intracellulaire a permis d'identifier que l'effet principal d'une concentration élevée en sodium se concentre principalement sur la phase d'acidogénèse, phase préalable et requise pour procéder en phase solvantogénèse lors de laquelle les solvants sont produits. Les intermédiaires métaboliques associés

à la voie des pentoses phosphates et à la glycolyse ont alors été respectivement inhibés de 80.73 ± 1.47 % et de 68.84 ± 3.42 % face à la culture contrôle sans ajout de sodium. Cependant, l'ATP et le NADH ont été accumulés pendant cette période alors que le ratio entre le $NADP^+$ et le NADPH est demeuré constant pour toute la durée de la culture; un phénomène pouvant être relié à la forte hausse de productivité spécifique en solvants.

Dans un deuxième temps, l'effet de la présence d'acétate sur la fermentation ABE a été étudié, compte tenu que ce composé est généré en quantité non négligeable lors de l'étape d'hydrolyse des hémicelluloses. Or, par un heureux hasard, les cultures implémentées initialement avec une concentration en acétate de sodium de 60 mM ont mené à la production d'une quantité élevée de riboflavine, atteignant un maximum ~ 0,2 g L^{-1} (0,53 mM) contre 0,057 mM dans la culture témoin, soit une augmentation d'un facteur 10x. Parallèlement à une augmentation marquée de production de riboflavine, la production de solvants et le rendement en biomasse ont même été simultanément favorisés. De façon intéressante, l'addition d'acétate a également stimulé l'accumulation intracellulaire de NADH, ce qui a pu contribuer, finalement, à affecter d'autres voies métaboliques par régulation redox. L'analyse métabolique intracellulaire a également permis de spéculer sur les flux stimulés ou inhibés en présence d'acétate et qui les métabolites accumulés lors de l'étape d'acidogénèse vers la phase de solvantogénèse pour la production de solvants.

Finalement, un modèle métabolique cinétique a été développé pour simuler ce système de production ABE coproducteur de riboflavine, et utilisé pour l'analyse de la dynamique des flux métaboliques. La cinétique de chaque flux métabolique ainsi que de la croissance de la biomasse sont décrites selon une cinétique de type Michaelis-Menten. Le mécanisme d'activation de la formation de riboflavine et de butanol par l'acétate, ainsi que les mécanismes d'inhibition de la croissance de la biomasse et l'absorption du xylose par le butanol ont été décrits. Le modèle comprend 24 réactions, 23 métabolites et 72 paramètres. La structure du modèle ainsi que la valeur de ses paramètres biocinétiques ont été déterminées en confrontant les simulations du modèle à des données expérimentales en bioréacteur de 3,5 L, en concentrant l'étude des paramètres sensibles identifiés par une étude de sensibilité. Ainsi, le modèle a montré être en mesure de simuler divers phénomènes métaboliques reliés à la transition de la phase acidogène à la phase solvantogène, soit une étape cruciale à l'induction de la production en solvants. Parallèlement, l'analyse dynamique des flux métaboliques, via les simulations du modèle, a permis de révéler que les taux de formation de riboflavine (ribA) et de guanosine triphosphate (GTP, précurseur de la riboflavine) (PurM),

étaient tous deux fortement stimulés par l'ajout d'acétate, avec une activité de 9,4 fois et 9,7 fois au moment initial, respectivement. Cette étude supporte donc notre hypothèse que l'ajout d'acétate favorise une stimulation de flux les métabolites accumulés lors de l'acidogénèse vers la production de solvants dans la phase de solvantogénèse. Enfin, une simulation différente de la concentration initiale en acétate a montré que ce modèle était robuste pour prédire l'ABE et la coproduction de riboflavine dans un milieu de culture contrôle sans ajout d'acétate.

En conclusion, cette thèse portant sur l'étude du comportement métabolique d'un bioprocédé de fermentation ABE à l'aide de *Clostridium acetobutylicum* ATCC 824, apporte des idées, des résultats et des outils qui contribueront à l'établissement de bioprocédés de production de biobutanol, valorisant des résidus d'hydrolysats d'hémicellulose, qui soient économiquement viables.

ABSTRACT

Nowadays, hemicellulose hydrolysates - sugar-rich feedstocks issued from the pulp-and-paper and forestry industries - are being greatly investigated in butanol biorefinery. Among various biotechnological platforms under study to produce butanol, the acetone-butanol-ethanol (ABE) fermentation process with *Clostridium acetobutylicum* seems to be the most studied avenue. However, some inhibitors are generated in the pre-treatment and hemicellulose hydrolysis processes, with compounds which are inhibitors of ABE fermentation. Moreover, the productivity yields of the ABE bioprocess are still low and barely enable the economic feasibility of such a bioprocess at an industrial scale, despite the low cost of these feedstocks. Therefore, the main objective of this thesis is focused on ameliorating our fundamental knowledge of ABE fermentation in order to enable the identification of potential bioprocess improvement strategies. The aim of this research is thus to contribute to the development of biobutanol industrialization. A synthetic medium with xylose as the main carbon source was used to simulate hemicellulose hydrolysates of black spruce, used in the pulp-and-paper and forestry industries, and *Clostridium acetobutylicum* was the culture used to perform ABE fermentation.

In the first part, we evaluated the effect of a high sodium chloride concentration in ABE fermentation, since large amounts of sodium hydroxide are applied to wood chips during the hydrolysis process such as in delignification, pH control, and as caustic cleaning agents. These processes then artificially increase the sodium concentration of the resulting solution, and since this solution is to be used as a culture medium for ABE fermentation, it is crucial to characterize the effects of such a high sodium content. A sodium concentration of 200 mM, a level normally observed in industry, was thus assessed and compared to a control culture. The *Clostridium acetobutylicum* ATCC 824 strain was studied, and a high sodium condition was shown to affect biomass growth and ABE yield, but not the cell-specific productivity in ABE. A further metabolomics study showed that a high sodium concentration mainly influenced the acidogenic phase and biomass synthesis. The ABE fermentation process normally requires an acidogenic phase first, in order to proceed to the solventogenic phase during which solvents are produced, so during acidogenesis, high sodium conditions were shown to inhibit the intermediate metabolites concentration of the pentose phosphate pathway and glycolysis pathways of up to 80.73 ± 1.47 % and 68.84 ± 3.42 %, respectively. However, ATP and NADH were stimulated at high sodium,

while the $NADP^+$-to-NADPH ratio was constant for the entire culture duration, a phenomenon which may explain the robustness of solvents' specific productivities even under a sodium stress.

In the second part, we investigated the effect of supplementing acetate on ABE fermentation, since this compound is generated in non-negligible amounts during the hemicellulose hydrolysis step. Indeed, supplementing the culture medium at 60 mM sodium acetate led to the production of a yellow sediment clearly identified as riboflavin. We thus observed that a 60 mM acetate supplementation leads to a 10-fold increase of riboflavin, reaching up to ~ 0.2 g L^{-1} (0.53 mM) compared to 0.057 mM in the control culture. A metabolomic study showed that acetate supplementation resulted in a higher consumption of GTP, which is the precursor of riboflavin. Moreover, solvents production and biomass yield were also promoted when adding acetate. Interestingly, acetate addition clearly stimulated the accumulation of the reduced form of nicotinamide-adenine dinucleotide (i.e. NADH), which could have affected other metabolic pathways though redox regulation mechanisms. Our metabolomic study also suggests that a high acetate condition stimulates the mobilization of various metabolic intermediates accumulated in acidogenesis towards solvents production in solventogenesis.

In the third part, a kinetic metabolic model was developed in order to better understand the effect of adding acetate by simulating the ABE-coproducing riboflavin process and performing a dynamic metabolic flux analysis. Each step in flux kinetics, as well as the biomass specific growth rate, was described using the Michaelis-Menten type approach. The activation mechanism of riboflavin and butanol formation by acetate, as well as the inhibition mechanisms of biomass growth and xylose uptake by butanol, were described. The model includes 24 reactions, 23 metabolites, and 72 parameters. Model structure as well as kinetic parameter value were determined by minimizing simulation errors of experimental data for 3.5-L bioreactor cultures at 60 mM acetate condition. Indeed, the model was shown to be capable of adequately simulating experimental data and predicting culture behavior without acetate addition, as well as the transition from acetogenesis to solventogenesis - a crucial step in the induction of solvents production. Moreover, a dynamic metabolic flux analysis suggests that the riboflavin (ribA) and guanosine triphosphate (GTP, precursor of riboflavin) formation rates (PurM) were strongly stimulated by high acetate with 9.4-fold and 9.7-fold activity early following inoculation, respectively. This *in silico* study further suggests that a high acetate condition stimulates fluxes which dredged accumulated metabolites in acidogenesis for solvents production.

In conclusion, this work on the investigation of the metabolic behavior of ABE fermentation with *Clostridium acetobutylicum* ATCC 824 has brought thoughts, results, and tools which may contribute to enabling the economic feasibility of producing butanol valorizing hemicellulose hydrolysates wastes.

TABLE OF CONTENTS

DEDICATION III

ACKNOWLEDGEMENTS IV

RÉSUMÉ V

ABSTRACT VIII

LIST OF TABLES XV

LIST OF FIGURES XVI

LIST OF SYMBOLS AND ABBREVIATIONS XXI

LIST OF APPENDICES XXIV

CHAPTER 1 INTRODUCTION 1

1.1 Energy crisis and bioenergy 1

1.2 Biobutanol 2

1.3 Hemicellulose hydrolysates: feedstocks of ABE fermentation 3

1.3.1 Hemicellulose hydrolysates are xylose enriched 3

1.3.2 Various inhibitors limit the utilization of hemicellulose hydrolysates in ABE fermentation 5

1.4 Modeling ABE fermentation 8

1.5 Project objectives 9

1.6 Organization of the thesis 10

CHAPTER 2 LITERATURE REVIEW 12

2.1 Microbial strains and feedstocks investigated for ABE fermentation 12

2.2 Metabolic pathways involved in ABE fermentation 15

2.2.1 Metabolic pathway analysis 16

2.2.2 Genomic and transcriptomic analyses 20

2.2.3 Proteomic analyses 23

2.3 Modeling ABE fermentation biosystem 25

CHAPTER 3 METHODOLOGY 27

3.1 Culture method 27

3.2 Metabolomic analysis 27

3.2.1 Sample collection and extraction 27

3.2.2 Intracellular sugar phosphates and organic acids 28

3.2.3 Intracellular nucleotides 29

3.2.4 Riboflavin purification and identification 29

3.2.5 The analysis of the ABE 30

3.2.6 Acetic acid and butyric acid 30

3.2.7 Amino acids analysis 31

3.2.8 Xylose analysis 31

3.3 Dynamic modeling 32

CHAPTER 4 ARTICLE 1: A QUANTITATIVE METABOLOMICS STUDY OF HIGH SODIUM RESPONSE IN *CLOSTRIDIUM ACETOBUTYLICUM* ATCC 824 ACETONE-BUTANOL-ETHANOL (ABE) FERMENTATION 35

4.1 Abstract 36

4.2 Keywords 36

4.3 Introduction 37

4.4 Methods 39

4.4.1 Cell culture 39

4.4.2 Culture sampling and metabolites extraction 40

4.4.3 Analytical and calculation methods 41

4.5 Results and Discussion 41

4.5.1 Identifying sodium threshold concentration affecting biomass growth 41

4.5.2 Sodium affects biomass and ABE production metabolism 44
4.5.3 High sodium stimulates energy metabolism in acidogenesis 48
4.5.4 High sodium affects cell central carbon metabolism 51
4.5.5 The cell redox state is robustly controlled 58
4.6 Conclusion 61
4.7 Acknowledgements 62
4.8 Authors' contributions 62
CHAPTER 5 ARTICLE 2: A DYNAMIC METABOLIC FLUX ANALYSIS OF CO-PRODUCING RIBOFLAVIN IN ABE (ACETONE-BUTANOL-ETHANOL) FERMENTATION BY *CLOSTRIDIUM ACETOBUTYLICUM* ATCC 824 63
5.1 Abstract 64
5.2 Key words: 64
5.3 Introduction 65
5.4 Materials and methods 66
5.4.1 Cell culture 66
5.4.2 Riboflavin purification and identification 67
5.4.3 Metabolites analysis 68
5.4.4 The dynamic metabolic model 68
5.5 Results and Discussion 69
5.5.1 Sodium acetate induces riboflavin production in ABE fermentation 69
5.5.2 Supplementing NaAc promotes ABE fermentation 74
5.5.3 Carbon flux analysis supplementing 60 mM NaAc 76
5.5.3.1 Evolving from acidogenesis to solventogenesis 76
5.5.3.2 Central carbon metabolism slightly leaks to riboflavin synthesis 78
5.5.3.3 GTP plays a key role in riboflavin production 81

5.5.3.4 Redox nucleotide concentration behaviour was affected by adding acetate 83
5.5.3.5 Amino acid metabolic analysis 85
5.6 Conclusion 87
5.7 Acknowledgements 88
5.8 Author Contributions 88
5.9 Supplementary material 1 89
5.9.1 Model hypothesis and description 89
5.9.2 Model calibration and parameters sensitivity analysis 99
5.10 Supplementary material 2 103
5.11 Supplementary material 3 104
CHAPTER 6 GENERAL DISCUSSION 108
CHAPTER 7 CONCLUSION 113
CHAPTER 8 RECOMMENDATIONS 115
BIBLIOGRAPHY 117
APPENDICES 135

LIST OF TABLES

Table 1. 1 Energy density and specific energy of butanol, ethanol and gasoline 2

Table 2. 1 Study of various strains in ABE fermentation 13

Table 2. 2 Different feedstocks and strains used along with maximum solvents and productivities achieved (Jurgens et al., 2012) 15

Table 2. 3 *C. acetobutylicum* DSM 1731 and Rh 8 strains compared for their proteins expression level (Bao et al., 2014). 25

Table 4. 1 Growth and productivity of *C. acetobutylicum* ATCC 824 batch culture on xylose with or without a 170 mM NaCl supplement. All values are maximum values taken from Figure 4.2 and Figure 4.3 or calculated using two successive points, identifying the maximum value; ± values represent standard deviation for n=3. 45

Table 4. 2 Energetics of *C. acetobutylicum* ATCC 824 batch culture on xylose with or without a 170 mM NaCl supplement. All values are maximum values taken from Figure 4.4 or calculated using two successive points, identifying the maximum value; ± values represent standard deviation for n=3.....50

Table 4. 3 *C. acetobutylicum* ATCC 824 content in sugar phosphates, pyruvate and redox nucleotides in batch culture on xylose with or without a 170 mM NaCl supplement. All values are maximum values taken from Figure 4.6 and Figure 4.7 or calculated using two successive points, identifying the maximum value; ± values represent standard deviation for n=3. 56

Table S 1. Stoichiometric of reactions in the model 90

Table S 2. Kinetic equations of the metabolic fluxes in the model.....91

Table S 3. Mass balances equations of the model.....94

Table S 4. State variables initial values.....97

Table S 5. Parameters values.....98

LIST OF FIGURES

Figure 1. 1 Global distribution of final energy consumption in 2011 (Popp et al., 2014) 1

Figure 1. 2 Low cost sugar feedstocks for ABE fermentation 4

Figure 1. 3 Hydrolysate components analysis result from black liquor 5

Figure 1. 4 Composition of wood, and list of compounds generated from dilute-acid hydrolysis (Alriksson, 2006)**.**.....6

Figure 1. 5 Effect of representative lignocellulosic biomass degradation products on ABE production in *Clostridium beijerinckii* 592 (Blaschek et al., 2010) 7

Figure 2. 1 Central metabolism of *C. acetobutylicum* (Lutke-Eversloh, 2014). 17

Figure 2. 2 Two possible mechanisms for the conversions of butyrate to butanol (Al-Shorgani et al., 2011)**.**.....18

Figure 2.3 Proposed metabolic pathway for riboflavin production by *Ashbya gossypii*, *Bacillus subtilis,* and *Candida famate*. (Abbreviations: G-6P, Glucose-6-phosphate; 3PG, 3-phosphoglycerate; PEP, Phosphoenolpyruvate; Ribu-5P, Ribulose-5-phosphate; OAA, Oxaloactate; Asp, Aspatate; Thr, Thre- onine; Gly, Glycine; Ser, Serine; GTP, Guanosine triphos-phate; GMP, Guanosine monophosphate; XMP, Xanthine monophosphate; IMP, Inosine monophosphate; DRTP, 2, 5-diamino-6-ribosylamino-4 (3H)-pyrimidinedione 5-phosphate; ARP, 5-amino-6-ribitylamino-2, 4 (1H, 3H)-pyrimidine; DBP, L-3, 4-dihydroxy-2-butanone-4-phosphate; DMRL, 6, 7- dimethyl-8-ribityllumazine (Lim et al., 2001).....20

Figure 3.1 Algorithm of resolution for determining a model kinetic parameters value.....33

Figure 4. 1 Effect of NaCl addition to CGM medium on *C. acetobutylicum* ATCC 824 grown on xylose. Axis unit is optical density at 600nm. Error bars represent standard deviations from three independent replicates (n=3). 42

Figure 4. 2 Effect of NaCl addition on (a) *C. acetobutylicum* ATCC 824 biomass growth in batch culture on xylose; (b) pH; (c) xylose concentration; (d) xylose specific consumption rate. ● 170 mM NaCl addition culture and ○ the control culture. Error bars represent standard deviations from three independent replicates (n=3). 43

Figure 4. 3 Effect of NaCl addition on ABE yield and specific productivity profiles on acetone (a, b), butanol (c, d), ethanol (e, f), acetic acid (g, h), butyric acid (i, j) in *C. acetobutylicum* ATCC 824 batch culture on xylose. ● 170 mM NaCl addition culture and ○ the control culture. Error bars represent standard deviations from three independent replicates (n=3).....47

Figure 4. 4 Effect of NaCl addition on *C. acetobutylicum* ATCC 824 energy state in batch culture on xylose. (a) ATP; (b) ADP; (c) AMP; (d) ATP-to-(ATP+ADP+AMP) ratio. ● 170 mM NaCl addition culture and ○ the control culture. Error bars represent standard deviations from three independent replicates (n=3). 49

Figure 4. 5 Comparative analysis of metabolites concentration behaviour involved in *C. acetobutylicum* ATCC 824 during acidogenesis with and without supplementing sodium. Light blue shade indicates metabolites measured in this study, in which: blue-written metabolites refer to concentration decrease and red-written metabolites refer to concentration increase, all compared to control low sodium concentration, whereas black-written metabolites were not quantified being below the detection limit of the analytical method (i.e. TCA metabolites) or showing unaffected concentrations (i.e. $NADP^+$-to-NADPH ratio) at high sodium concentration during acidogenesis. G1P: glucose 1-phosphate; G6P: glucose 6-phosphate; F6P: fructose 6-phosphate; X5P: xylulose 5-phosphate; R5P: ribose 5-phosphate; PYR: pyruvic acid; α-KG: α-ketoglutaric acid; SUC: succinic acid; FUM: fumaric acid; MAL: malic acid; (ISO)CIT: (iso) citric acid; Fd Ox: Ferredoxin (oxidized) ; Fd Red: Ferredoxin (reduced).....53

Figure 4. 6 Effect of NaCl addition on PPP and glycolysis pathway in *C. acetobutylicum* ATCC 824 batch culture on xylose. (a) X5P; (b) R5P; (c) F6P; (d) G6P; (e) G1P; (f) PYR. ● 170 mM NaCl addition culture and ○ the control culture. Error bars represent standard deviations from three independent replicates (n=3). 55

Figure 4. 7 Effect of NaCl addition on redox level and ratio on *C. acetobutylicum* ATCC 824 batch culture on xylose. (a) NADH; (b) NAD^+; (c) NADPH; (d) $NADP^+$; (e) NAD^+-to-NADH ratio;

(f) $NADP^+$-to-NADPH ratio. ● 170 mM NaCl addition culture and ○ the control culture. Error bars represent standard deviations from three independent replicates (n=3).....59

Figure 5. 1 Images of riboflavin obtained in *C. acetobutylicum* ATCC 824 bioreactor culture (56 h) with xylose and 60 mM sodium acetate. (a) Microscopic image of riboflavin crystal: 1000X magnification under bright field optical microscopy (Leitz Laborlux S Microscope); (b) 400X magnification under bright field optical microscopy. (c) Centrifuged fermentation broth: the orange sediment is riboflavin and white sediment is biomass. 70

Figure 5. 2 Metabolic pathways described in the model. The dashed line delimits the cell membrane. 71

Figure 5. 3 Metabolites concentrations and flux rates simulation results related to riboflavin and acetate metabolisms for a xylose culture of *C. acetobutylicum* ATCC 824. Solid line refers to simulation results for the 60 mM NaAc culture and dashed line to the control culture. Solid circle is experimental data for 60 mM NaAc; open triangle is experimental data in control culture. Error bars represent standard deviations from two independent bioreactor culture replicates. (a) riboflavin; (b) acetate; (c) ribA flux rate; (d) net acetate productivity (PTA minus CoATa); (e) ribA -to- XR ratio; (f) ribA -to- the specific growth rate (μ) ratio; (g) ribA -to- PurM ratio; (h) ribA -to- BYDH ratio. 73

Figure 5. 4 Simulation results of biomass, solvents production and carbon consumption status for a xylose culture of *C. acetobutylicum* ATCC 824. Solid line refers to simulation results for the 60 mM NaAc culture, and dashed line to the control culture. Solid circle is experimental data for 60 mM NaAc, and open triangle is experimental data in control culture. Error bars represent standard deviations from two independent bioreactor culture replicates. (a) biomass; (b) xylose; (c) butanol; (d) acetone; (e) ethanol; (f) pH. 75

Figure 5. 5 Dynamic metabolic flux analysis results for a xylose culture of *C. acetobutylicum* ATCC 824 from model simulation. Solid line refers to simulation results for the 60 mM NaAc culture and dashed line to the control culture. (a) CoATa -to- PTA ratio; (b) CoATb -to- PTB ratio; (c) CoATa -to- CoATb ratio; (d) XR -to- (CoATa-PTA) ratio; (e) flux rate of BYDH; (f) flux rate of AYDH; (g) flux rate of AADC; (h) flux rate of CoATa. 77

Figure 5. 6 Simulation results of intracellular carbon metabolites for a xylose culture of *C. acetobutylicum* ATCC 824. Solid line refers to simulation results for the 60 mM NaAc culture and dashed line to the control culture. Solid circle is experimental data for 60 mM NaAc; open triangle is experimental data in control culture. Error bars represent standard deviations from two independent culture replicates. (a) X5P&Ru5P; (b) R5P; (c) F6P; (d) GTP; (e) GA3P&DHAP; (f) PYR. 79

Figure 5. 7 Comparison of *C. acetobutylicum* ATCC 824 metabolic flux distribution at 10 h and 60 h for 60 mM NaAc supplement culture (a, b) and control culture (c, d) from model simulations. Brown colour represents PPP pathway; green colour represents glycolytic pathway; red colour represents riboflavin pathway; and blue colour represents acids to solvents conversion pathway. Flux unit is in mmol gDW^{-1} h^{-1}.....81

Figure 5. 8 Effect of NaAc on *C. acetobutylicum* ATCC 824 energetic state. Solid circle is experimental data for 60 mM NaAc; open triangle is experimental data in control culture. Error bars represent standard deviations from two independent culture replicates. Error bars represent standard deviations from two independent culture replicates. (a) AMP; (b) ADP; (c) ATP; (d) GTP -to- AMP ratio; (e) GTP -to- ADP ratio; (f) GTP -to- ATP ratio.....82

Figure 5. 9 Effect of NaAc on *C. acetobutylicum* ATCC 824 redox states. Solid circle is experimental data for 60 mM NaAc; open triangle is experimental data in control culture. Error bars represent standard deviations from two independent culture replicates. (a) NAD; (b) NADH; (c) NADP; (d) NADPH; (e) NADH -to- NAD ratio; (f) NADPH -to- NADP ratio. 84

Figure 5. 10 Fifteen amino acids degradation in test and control cultures in xylose by *C. acetobutylicum* ATCC 824. Open square and circle symbols are two parallar test culture in 60 mM NaAc condition, triangle is control.....87

Figure S 1. Sensitivity analysis of model parameters for 60 mM NaAc supplemented culture. Vertical axis value represents percentage change in the objective function for parameter change from - 50 % to + 100 % around the optimized value. Parameters not shown have percentage changes less than 10 %. 100

Figure S 2. Parameter estimates with error bars representing 95 % confidence intervals for highly sensitive parameters of (a) PPP pathway and growth; (b) solvents production; (c) km values; (d) acids and solvents conversion.....101

Figure S 3. Model simulation results of intracellular metabolites for which no experimental data were available. Solid line is for the 60 mM NaAc supplementation culture, dashed line is for the control culture without NaAc addition. (a) DNA; (b) G13DP; (c) PEP; (d) ACoA; (e) AACoA; (f) ACA; (g) BCoA. 102

Figure S 4. Riboflavin identification by comparing 60 mM sodium acetate bioreactor culture sample to pure riboflavin standard by HPLC/MS/MS analysis. Riboflavin standard analysis by (a) UV detector and (b) MS/MS, and sample analysis by (c) UV detector and (d) MS/MS. 103

Figure S 5. Main products, biomass, pH, and xylose consumption in two parallel batches in a 60 mM NaAc condition for the xylose culture of *C. acetobutylicum* ATCC 824. (a) riboflavin; (b) acetate; (c) xylose; (d) cell dry weight; (e) pH; (f) acetone; (g) butanol; (h) ethanol; (i) butyrate.....106

Figure S 6. Energy and redox status in two parallel batches in a 60 mM NaAc condition for a xylose culture of *C. acetobutylicum* ATCC 824. (a) ATP; (b) ADP; (c) AMP; (d) GTP; (e) NAD; (f) NADH; (g) NADP; (h) NADPH. 106

Figure S 7. Main carbon metabolites in two parallel batches in a 60 mM NaAc condition for a xylose culture of *C. acetobutylicum* ATCC 824. (a) X5P; (b) R5P; (c) PYR; (d) GA3P; (e) F6P. 107

LIST OF SYMBOLS AND ABBREVIATIONS

a	coefficient of cell death
AACoA	acetoacetyl coenzyme A
AADC	acetoacetate decarboxylase
ACA	acetoacetate
ACoA	acetyl coenzyme A
ADP	adenosine diphosphate
A_i	activator concentration
AMP	adenosine monophosphate
ATP	adenosine triphosphate
AYDH	acetaldehyde dehydrogenase
BCoA	butyryl coenzyme A
BHBD	β-hydroxybutyryl-CoA dehydrogenase
BYDH	butyraldehyde dehydrogenase
$C_{\_BuOH}$	butanol concentration
CoATa	acetoacetyl-CoA-acetate-CoA-transferase
CoATb	acetoacetyl-CoA-butyrate-CoA-transferase
DNA	deoxyribonucleic acid
DPO1	nucleoside-diphosphate kinase
eACE	extracellular acetate
eACTO	extracellular acetone
eBuOH	extracellular butanol
eBUT	extracellular butyrate
eCO2	extracellular carbon dioxide
eEtOH	extracellular ethanol
eLAC	extracellular lactate
ePRPO	extracellular Propanol
eRIBO	extracellular riboflavin
eXYL	extracellular xylose
F6P	fructose 6-phosphate
Fd Ox	ferredoxin (oxidized)

Fd Red	ferredoxin (reduced)
G13DP	glycerate-1,3-bisphosphate
GA3P	glyceraldehyde 3-phosphate
GA3PDH	glyceraldehyde-3-phosphate dehydrogenase
GTP	guanosine triphosphate
$K_{activation}$	activation constant
K_{i_BuOH}	inhibition parameter by butanol
$K_{inhibition}$	inhibition constant
LDH	lactate dehydrogenase
n	number of substrates and co-factors involve in each reaction
NAD	nicotinamide adenine dinucleotide (oxidized)
NADH	nicotinamide adenine dinucleotide (reduced)
NADP	nicotinamide adenine dinucleottide phosphate
NADPH	nicotinamide adenine dinucleottide phosphate (reduced)
PEP	phosphoenolpyruvate
PFK	phosphofructokinase
PFOR	pyruvate-ferredoxin oxidoreductase
PGK	phosphoglycerate kinase
PK	pyruvate kinase
PTA	phosphotransacetylase
PTB	phosphotransbutyrylase
PurM	purine metabolism
PYR	pyruvate
R5P	ribose 5-phosphate
ribA	GTP cyclohydrolase II
rpiA	ribose 5-phosphate isomerase A
SADH	secondary alcohol dehydrogenase
S_i	substrate of each enzyme
THL	thiolase
tktA	transketolase
V	reaction rate of each intracellular

$V_{\max}$	constant of the maximum reaction rate
X	biomass
X5P	xylulose 5-phosphate
XR	xylose reductase
μ	biomass specific growth rate
μ_{max}	maximum biomass specific growth rate
α	constant
β	constant

LIST OF APPENDICES

Appendix A – Correlation of cells dry weight and optical density 135

Appendix B – Culture medium 136

Appendix C – Exploration on ABE culture with hydrolysate and pretreatment liquor 137

Appendix D – Matlab files 140

CHAPTER 1 INTRODUCTION

1.1 Energy crisis and bioenergy

The current global warming problem has made the finding of renewable and environmentally-friendly alternative fuels a high priority. Indeed, the Kyoto Protocol, which was adopted by the UNFCCC (United Nations Framework Convention on Climate Change) in 1997 and signed by 183 countries (including Canada), aims to decrease emissions of the main anthropogenic greenhouse gases (GHGs) (www.unfccc.int). Apart from environmental pollution created by burning fossil fuels - a side effect affecting our health - energy-based conflicts also radically affect people's lives around the world. Therefore, the energy problem is not only an important issue to national economies, but also a key for world peace and stability. Consequently, developing an alternative renewable energy source is a valuable option agreeing with the sustainable development paradigm.

Bioenergy is one of the renewable energy sources with the most potential, since it is based on the transfer of free solar energy to biomass hydrocarbon-based storage through photosynthesis. Indeed, the utilization of biomass to develop an alternative economical, renewable, and environmentally-friendly energy source has been made a high priority (George W. Huber, 2006). In fact, plant (and algae) biomass is a unique sustainable resource which can be used to produce liquid transportation fuels. Although plant biomass is the largest energy storage in the world, its utilization accounts for a low level in the total world energy production (George W. Huber, 2006), and only 0.8 % of biofuels (Figure 1.1) (Popp et al., 2014). There is thus a huge potential for increasing the use of biomass as a source of bioenergy.

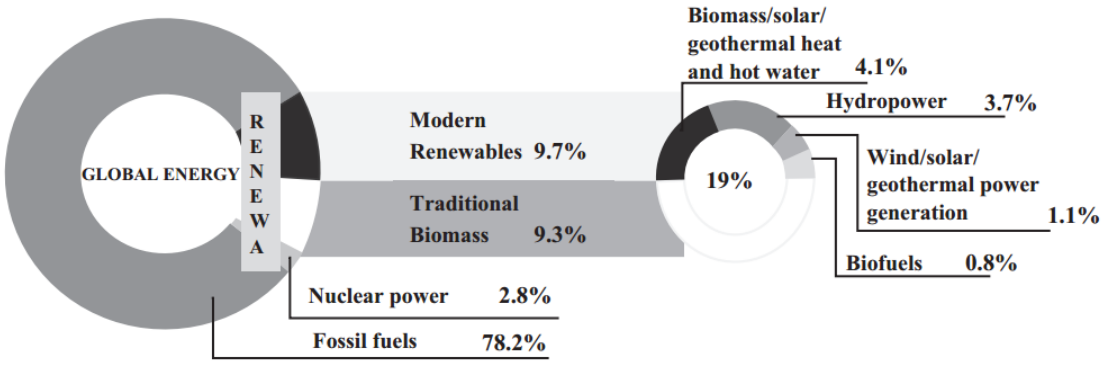

Figure 1. 1 Global distribution of final energy consumption in 2011 (Popp et al., 2014)

Several alternative liquid biofuels have been investigated, either to replace gasoline or be blended with liquid fuels. Bioethanol, defined as the first generation biofuel, is one successful case used for transferring biomass into bioenergy. The United States of America and most other developed countries have allowed the blending of a portion of bioethanol with gasoline for many years. However, ethanol utilization presents various disadvantages such as its low energy content, and thus a poor performance when blended to gas, as well as the fact that it causes damages to engines, to name a few.

1.2 **Biobutanol**

Biobutanol, an energy efficient alternative fuel, is now considered a second-generation biofuel. Table 1.1 compares the differences between butanol, ethanol, and gasoline (Brown, 2003). In its use as a biofuel, butanol thus presents better characteristics than ethanol for many reasons. Butanol contains 25 % more energy than ethanol, and has a greater miscibility than ethanol in gasoline. The air-to-fuel ratio for butanol is close to that of gasoline, which could enable it to completely replace gasoline, so it can be directly used without any engine modifications. Butanol is less hygroscopic, has a lower vapor pressure than ethanol, and is less corrosive, which makes it easier to transport. Compared with ethanol, butanol has a higher ignition point, a supplemental trait favoring the addition of butanol into gas (Yousheng, 2009). Consequently, butanol represents a valuable biofuel of the future. In addition, ethanol fermentation processes could be retrofitted to work with butanol, since both ethanol and butanol fermentation are anaerobic processes using the same bioreactors. Therefore, the updating of biofuel production from ethanol to butanol is clearly feasible.

Table 1. 1 Energy density and specific energy of butanol, ethanol and gasoline

Fuel Type	Density (kg/m^3)	Specific energy (kJ/g)	Energy content (MJ/L)
n-butanol	810	36	29.2
Ethanol	794	26.5	23.5
Gasoline	740	44	32.6

Acetone-Butanol-Ethanol (ABE) fermentation has a long history which can be traced back to 1861 when Pasteur discovered the process from anaerobic cultivation. For instance, before the 1950s,

two thirds of industrially-used butanol were produced by ABE fermentation in the USA, especially during the Second World War. However, due to the development of the petrochemical industry, the high cost of fermentative raw materials has removed it from the market.

With the development of chemical synthesis, the industry moved away from fermentation processes for economic considerations. However, because of the global warming problem, the idea of the bio-production of butanol re-emerged in recent years (Bankar et al., 2013). In 2007, the USA passed the new energy bill (H.R.6) which defined butanol as "advanced biofuel", and moreover, the U.S. Navy has also recently cooperated with the Cobalt Technologies Company to develop biobutanol as a military and jet fuel (www.cobalttech.com). Aside from the actions of the USA, some multinational companies have also taken part in this competitive race to produce economical butanol. For instance, DuPont has joined BP, Europe's biggest oil company, to produce biobutanol and replace ethanol as a gasoline additive in the future (Hess, 2006). The current international price of biobutanol is about $4 per gallon, and the worldwide market is about 350 million gallons per year with a 3 % growth. It can be estimated that the total market value is about $2 billion per year in 2017 (Ranjan & Moholkar, 2012). Being a potential biofuel, as well as a valuable C4 feedstock for chemical synthesis, biobutanol has gained attention as its worldwide market has expanded (Bankar et al., 2013).

1.3 Hemicellulose hydrolysates: feedstocks of ABE fermentation

1.3.1 Hemicellulose hydrolysates are xylose enriched

As mentioned previously, biobutanol production from sugars was commercialized at the beginning of the 20th century. In 1912, Dr. Weizmann successfully produced butanol by using starch and molasses - a cheap sugar source - and this process was widely used during the First World War. However, the cost of raw materials took up 60 % - 70 % of the entire processing cost, which seriously limited the development of the ABE fermentation industry (Liu et al., 2011). Indeed, the substrate cost had become the main bottleneck of the microbial production of butanol. With the development of fossil fuel extraction technology, ABE fermentation lost competitive potential - even corn starch still costs more than petrochemical-based processes. *Clostridium* species, which enable ABE fermentation, allow the use of a wide range of substrates from hexoses (glucose, fructose, etc.) and pentoses (xylose, arabinose, etc.), to starch, xylan, and other polysaccharides, to

produce butanol. This bacterial trait thus provides a chance to identify cheaper biomass feedstocks enabling the economic feasibility of ABE fermentation.

Low-cost sugar substrates have been investigated for biobutanol production including corn, algal biomass, and other agriculture wastes (Figure 1.2). Indeed, some industrial wastes present abundant carbohydrate contents. For instance, the black liquor issued from the waste water of pulp and paper mills contains abundant levels of hemicelluloses, which have been shown to release high levels of xylose after the hydrolyzation process (Figure 1.3), xylose being a candidate substrate for ABE fermentation (Zheng et al., 2009).

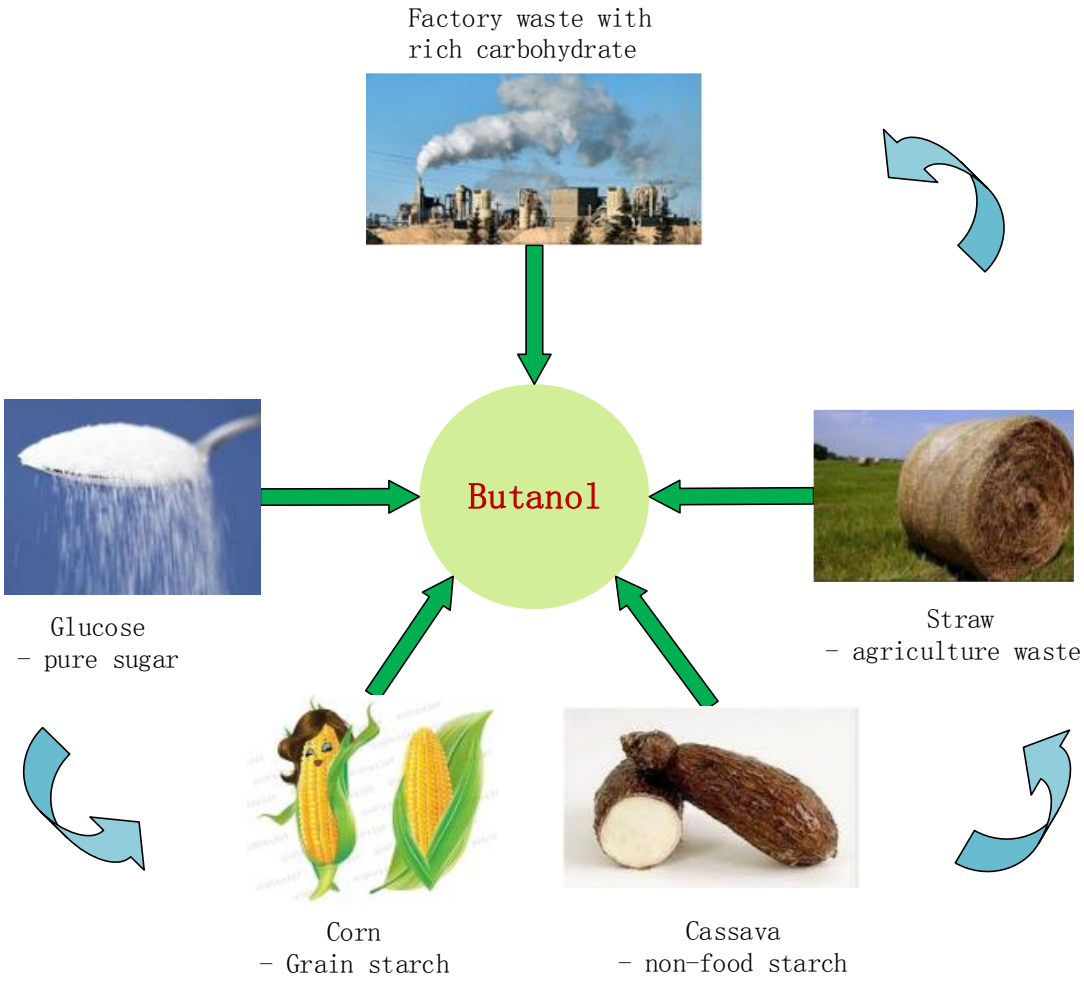

Figure 1. 2 Low cost sugar feedstocks for ABE fermentation

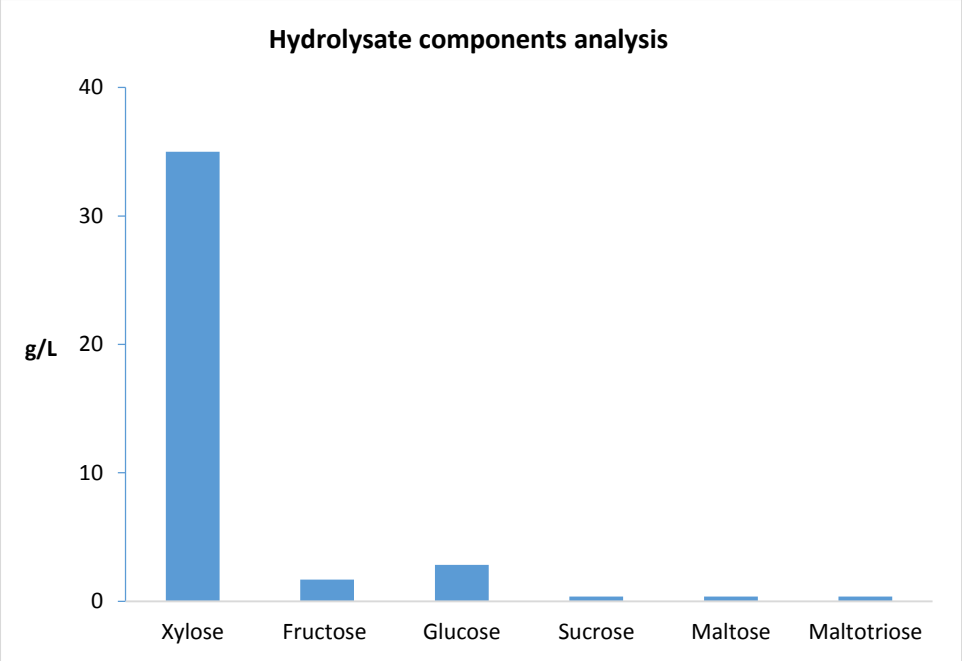

Figure 1. 3 Hydrolysate components analysis result from black liquor (Prof. Jolicoeur's laboratory unpublished results)

Therefore, this black liquor, a waste stream from the pulp and paper industry, represents a valuable cheap source of sugar for the ABE fermentation process.

1.3.2 Various inhibitors limit the utilization of hemicellulose hydrolysates in ABE fermentation

Although there are abundant amounts of cheap biomasses available as feedstocks to feed the ABE fermentation process, the breakdown of macromolecular storage sugars (e.g. cellulose, starch, lipids, etc.) is first required in order to obtain simple sugars which can be processed by microbes. For instance, the *Clostridium* species cannot directly use hemicellulose and lignocellulose as substrates - these first need a pretreatment consisting of enzymolysis or hydrolysis. Fermentable substrates will then become available as hexose or pentose sugars (Figure 1.4).

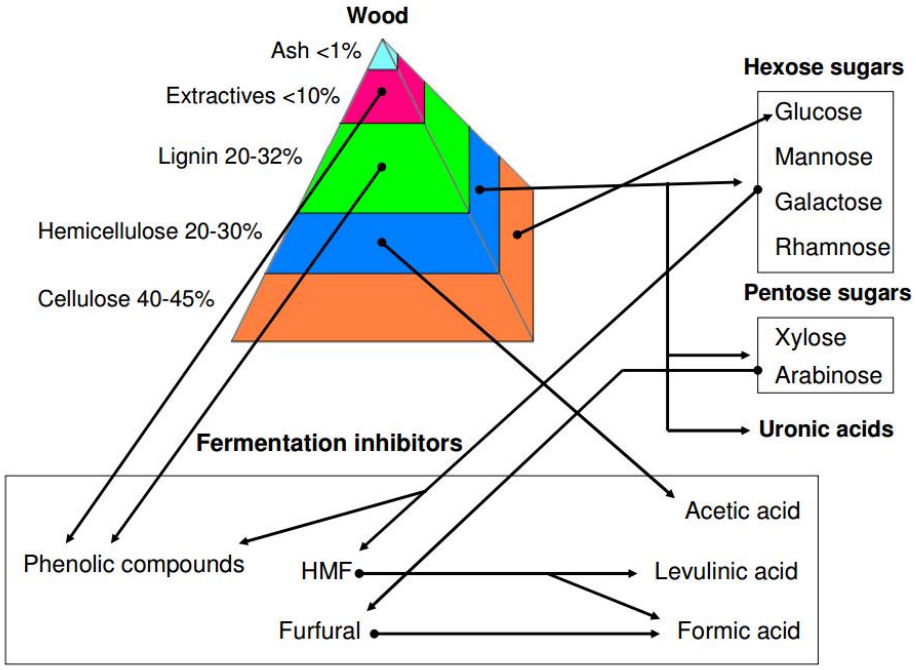

Figure 1. 4 Composition of wood, and list of compounds generated from dilute-acid hydrolysis (Alriksson, 2006).

However, some compounds which are known as inhibitors of microbial development, and thus of ABE fermentation, are generated as byproducts in the pretreatment process, such as coumaric acid, ferulic acid, furfural, formic acid, and syringaldehyde (Figure 1.4). Most of them will limit ABE production at different levels, and consequently, a detoxication step is required before proceeding with fermentation.

Many researches have studied the effects of various inhibitors on ABE fermentation. Ezeji and Blaschek (2010) concluded that the main inhibitors which limit solvents generation include furfural, hydroxymethyl furfural (HMF), syringaldehyde, coumaric acid, glucuronic acid, and ferulic acid (Figure 1.5). Wang et al. (2011) also studied formic acid, another byproduct generated in the pretreatment. Since formic acid is a microscale byproduct in hydrolysate, few people have paid attention to it as an inhibitor in ABE fermentation. However, recent results have indicated that even 1 mM of formic acid can limit butanol production (Wang et al., 2011), and it has also been found that the existence of formic acid will lead to “acid crash” - a phenomenon limiting solvents generation from acids (Maddox et al., 2000).

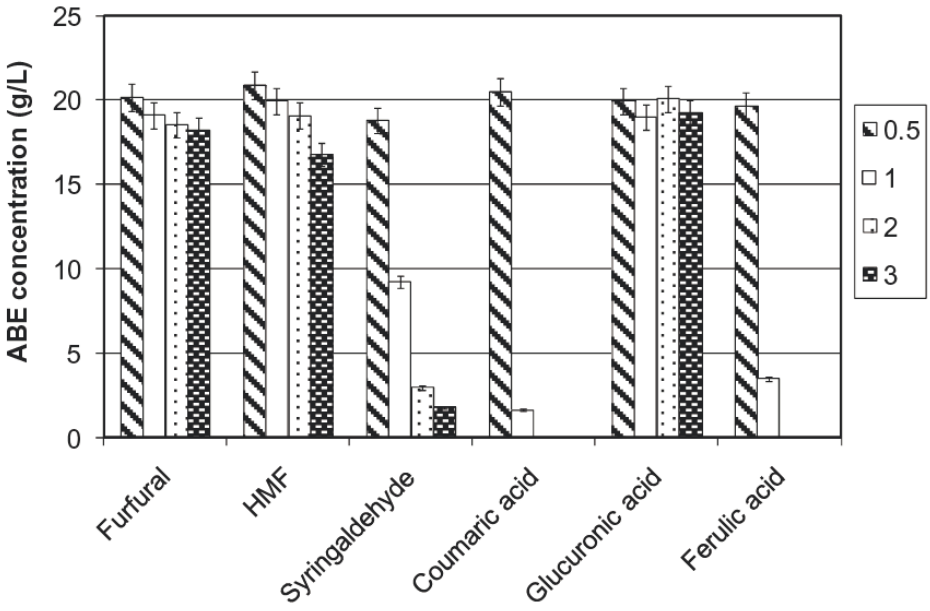

Figure 1. 5 Effect of representative lignocellulosic biomass degradation products on ABE production in *Clostridium beijerinckii* 592. Lignocellulosic biomass particules of 0.5 (inclined dashed bars), 1 (white bars), 2 (light dotted bard), and 3 (dense dotted bars) mm diameters were analyzed. (Ezeji and Blaschek, 2010)

Moreover, when using the hydrolysate of pulp and paper "black liquor" as feedstock, significant amounts of sodium hydroxide may remain with the solution since it is applied in delignification, chemical regeneration, pH control, and as a caustic cleaning agent (Murray, 1992). Among the ions with concentration increases along the various process steps enumerated above, sodium requires specific attention. Furthermore, acetate is generated during hydrolysis as a byproduct, a compound reaching up to 60 - 70 mM (Awes et al., 1998). In addition, various published works have reported that the presence of acetate in the fermentation medium could improve solvents generation effectively (Chen & Blaschek, 1999a; Chen & Blaschek, 1999b; Husemann & Papoutsakis, 1990). Indeed, in 1990, Michael. H. W. Husemann and his colleagues discovered that adding 30 mM of acetate could lead to a two-fold increase of butanol production (Husemann & Papoutsakis, 1990), and attributed this phenomenon to the acetate buffering effect and enzyme overexpression. Chih-Kuang Chen et, al., observed a modified expression of CoA transferase, acetate kinase, butyrate kinase, and phosphotransbutyrylase when adding 20 mM of sodium acetate, along with enhanced solvents production (Chen & Blaschek, 1999b). In 2009, Yang Gu et al., using cassava as a substrate to culture the *Clostridium acetobutylicum* EA2018 strain, found that a 30 mM acetate

supplement could obtain butanol 14.1 ± 0.3 and 9.9 ± 0.4 g L^{-1} in the corn and cassava mediums, respectively. They have also investigated the expression level of the main enzymes (*ask, buk, adc, ctfAB, adhE, bdhB,* etc) and concluded that ammonium acetate could maintain the robust expression of enzymes associated with acidogenesis and solventogenesis (Gu et al., 2009).

1.4 **Modeling ABE fermentation**

ABE fermentation is a two-phase complex biosystem - acidogenesis/solventogenesis - with the accumulation of acids during the first phase, which are then consumed and transformed into solvents in the second phase. Indeed, highly regulated pathways compete for the same metabolic intermediates. Therefore, in such a complex case, a mathematical model describing cell growth and the biochemical network of reactions, from sugar substrate to solvents production, can be useful to the understanding of the phenomena involved.

Approaches such as Metabolic Flux Analysis (MFA) and Flux Balance Analysis (FBA) have been used to describe carbon flow from the substrates to the products (Stephanopoulos et al., 1998). These also allow the testing of hypotheses for the identification of branch nodes and revealing unknown fluxes, the examination of the influence of alternative pathways, and the calculation of maximum theoretical yields (Nielsen, 1998; Orth et al., 2010). In complement, the precise determination of flux rates and direction for complex systems such as reversible and cyclic reactions can be carried out by the use of isotopic tracers within labeled substrates (e.g. ^{13}C,^{15}N). Specifically, the FBA approach relies on objective functions looking at the optimization of specific fluxes, flux ratios, cell specific growth rate, or yields (Orth et al., 2010). Finally, the Metabolic Control Analysis (MCA) approach has been developed to evaluate the control enzymes of a metabolic network (Almaas et al., 2004; DA, 1998; Stephanopoulos et al., 1998).

However, current MFA, FBA, and MCA approaches have all been developed and applied to biosystems at a steady state. Some recent attempts have been proposed to perform a dynamic analysis adapting the FBA approach, but it is still a hybrid view with sequential steady states (Sousa et al., 2016). Indeed, past macroscopic approaches such as that initiated by Monod (Kovárová-Kovar & Egli, 1998) and which can describe kinetically a time-continuous biosystem behavior are now applied to metabolic networks (Cloutier et al., 2007; Ghorbaniaghdam et al., 2013; Leduc et al., 2006). Such dynamic models, with flux kinetics described, aim to understand the dynamic

behavior of metabolic fluxes, metabolites concentrations, and enzyme activity along with time. Dynamic models can not only be used to understand and explain key dynamic behaviors, but also to perform dynamic metabolic flux analysis, which is especially useful in various works from biomedical applications (Robitaille et al., 2015) to bioprocess optimization (Cloutier et al., 2008). Buehler and Mesbah demonstrated a dynamic metabolic model simulating continuous fermentation culture, which tried to offer insight into cell behavior for optimizing the ABE fermentation process (Buehler & Mesbah, 2016), while Shinto et al. simulated batch culture metabolism in both glucose and xylose conditions with extracellular experimental data (Shinto et al., 2008; Shinto et al., 2007). However, these models have only simulated substrates, biomass, and main products rather than any intracellular metabolites, which lacks experimental validation.

1.5 **Project objectives**

This work aims to characterize the performance of ABE fermentation with hemicellulose hydrolysates from pulp and paper mills using black spruce. A synthetic medium proposed in literature was complemented with xylose as the main carbon source to simulate hemicellulose hydrolysates under defined conditions. *Clostridium acetobutylicum*, the model species for ABE production, was used as the living biocatalyst. We have studied how the major by-products encountered industrially, from the use of sodium hydroxide in the pretreatment processes of hemicelluloses, affects solvents production and particularly butanol. This research project included the following sub-objectives.

The first sub-objective consisted of evaluating the effect of the high sodium content expected from the hemicellulose pre-treatment and hydrolysis process in solvents production. To precisely characterize how a high sodium content affects bacterial cell behavior, a metabolomic study was performed in order to identify the reaction pathways involved in ABE production inhibition. This was achieved by investigating central carbon metabolism and pathways related to solvents synthesis, including energetic and redox metabolism. This work revealed that high sodium inhibition does not directly affect ABE metabolism, but the intermediates related to biomass synthesis, which further affects solvents production yield.

A second objective then consisted of characterizing the effect of supplementing the culture medium with acetate, a by-product obtained during the hemicellulose hydrolysis process. While performing

these assays, we observed the production of riboflavin, a vitamin (B_2) of commercial interest, when supplementing the culture medium with sodium acetate. This objective was then implemented with a focus on the understanding of how riboflavin production had been stimulated, as well as solvents production. To achieve this goal, we performed a metabolomics study and developed a dynamic metabolic model to identify the mechanisms of acetate influence on both solvents and riboflavin production. The former helped us to understand the complex interplay between carbon utilization, energy regulation, and the biosynthetic pathways of ABE and riboflavin, while the latter helped us to identify the key fluxes related to the enhancement of riboflavin as well as ABE metabolisms. Thus, this work provided a way of enhancing the bioprocess' economic feasibility by co-producing riboflavin. The dynamic metabolic model could be further developed and serve as an *in silico* platform to seek the maximizing of the riboflavin-ABE fermentation yields, as well as to bring insight on potential genetic manipulations meant to improve the bioprocess yield.

Overall, this thesis has significantly contributed to the enhancement of the understanding of the ABE bioprocess using hemicellulose hydrolysates, as well as demonstrating ways to improve the economic potential of the bioprocess.

1.6 **Organization of the thesis**

This thesis includes eight chapters:

- In chapter one, we introduce the current situation of the expected energy crisis and the global warming problem, emphasizing the importance of developing renewable and sustainable bioenergy sources. Identified as a second-generation renewable and sustainable biofuel, butanol - which can be obtained from the bacterial fermentation of various cheap biomasses - is described. Then, the development of feedstocks for biobutanol production from ABE (including acetone-butanol-ethanol solvents) fermentation and their specific utilization are presented. A new feedstock of interest in Canada, hemicellulose hydrolysates obtained from the pulp and paper industry and studied in this thesis as a potential feedstock in ABE fermentation, is presented along with the thesis' research problems and objectives.

- Chapter two presents a literature review on the ABE bioprocess, fermentation strains, cellular metabolisms, as well as co-products such as riboflavin. Then, literatures on proteomic,

genomic, and transcriptomic works on ABE fermentation are reviewed to draw the state-of-the-art understanding of the ABE bioprocess at the cell level. Finally, mathematical modelling approaches already used to describe ABE fermentation and others are identified as being useful to finely describe and study the metabolic link between the carbon source (i.e. xylose) and culture condition to ABE and co-product (e.g. riboflavin) production and productivity.

- Chapter three presents all the materials and methods used in this work, including metabolomic analysis methods (intracellular and extracellular metabolites extraction and analysis), as well as the modelling methodology.

- Chapter four presents a quantitative metabolomics study of the high sodium response in ABE fermentation - work published in the Scientific Reports journal. High sodium condition has been shown to affect biomass growth with a lower activity of the central carbon metabolism, and this work suggests that performing fermentation maximizing biomass inoculum concentration may be an efficient strategy to reach expected butanol production counteracting a high sodium effect.

- Chapter five presents the development of a dynamic model describing ABE fermentation as well as riboflavin synthesis. Model simulation results suggest the validity of the dynamic model for this biosystem for the further exploration of enzyme reaction dynamics - this work is currently under submission in the Biotechnology and Bioengineering journal.

- Chapter six presents the general discussion in which this thesis' results are analyzed in the context of the butanol market and its economic feasibility, especially from the use of hemicellulose hydrolysates. Then, the thesis' originality and major contributions to the industrial development of ABE fermentation are presented. Finally, riboflavin production and market development are also discussed.

- Chapter seven presents the general conclusion of this thesis, and Chapter eight proposes recommendations for further work thought to improve the efficiency and economic feasibility of the ABE fermentation industrial process.

CHAPTER 2 LITERATURE REVIEW

2.1 Microbial strains and feedstocks investigated for ABE fermentation

With the pioneer discovery of butanol production in the *Clostridium* species by Dr. Weizmann, various attempts have been carried out over the last century to isolate and identify potential species. Among many, *Clostridium acetobutylicum* ATCC 824 and *Clostridium beijerinckii* NCIMB 8052 are considered to be classical species with high solvents production capability. *Clostridium acetobutylicum* ATCC 824, a typical strain with completed genome sequencing, is also called the "Weizmann Organism". *Clostridium* species are strict anaerobic gram-positive bacteria (Mermelstein & Welker, 1994). During their vegetative growth, they are rod-shaped with both ends obtuse or acute, and have peritrichous flagella at one end (Mitchell, 1997). Compared to yeasts, which are used for ethanol production, *Clostridium* can metabolize various types of raw materials, giving a higher industrial potential.

Strain selection is a timeless step. Selected for their characteristics, such as metabolizing specific or a variety of raw materials, the appropriateness of a strain will rely on specific objectives. *C. beijerinckii* BA101 and *C. beijerinckii* P 260 have been studied for many years and have been demonstrated to be outstanding strains for industrialization, and *C. beijerinckii* BA 101 was derived before 1997 from *C. beijerinckii* NCIMB 8052. Based on a P2 medium containing 6 % glucose, the butanol yield can reach up to 19 g L^{-1}, which represents an increase of 100 % compared with its parental line NCIMB 8052. *C. beijerinckii* BA 101 also performed efficiently in continuous culture fermentation, with a butanol yield of up to 1.74 g L^{-1} h^{-1} at a dilution rate of 0.2 h^{-1}, while that of NCIMB 8052 was only 1.17 g L^{-1} h^{-1} (Formanek, 1997). *C. beijerinckii* P260, which was derived earlier in the 1950s and patented by the Commercial Solvents Corporation, reached up to 21.9 g L^{-1} of total solvent concentration (Ranad Shaheen, 2000).

Table 2. 1 Study of various strains in ABE fermentation

Strain	**Butanol yield (g L^{-1})**	**T (°C)**	**Reference**
C. acetobutylicum ATCC 824	11-17	37	(Bankar et al., 2012; Li et al., 2010; Sun & Liu, 2012; Van der Wal et al., 2013; Yen & Wang, 2013)
C. beijerinckii NCIMB 8052	8-12.3	35-37	(Guo et al., 2011; Van der Wal et al., 2013; Zhang et al., 2012)
C. saccharoperbutylacetonicum N1-4 (ATCC 13564)	10-20.1	30	(Al-Shorgani et al., 2012; Thang et al., 2010; Zheng et al., 2013)
C. beijerinckii BA101	13-19	37	(Ezeji et al., 2007; N Qureshi, 2001)
C. beijerinckii P260	14	35	(Qureshi et al., 2007)
C. beijerinckii ATCC 10132	20	37	(Isar & Rangaswamy, 2012)
C. beijerinckii DSM 6423	11.2	37	(Survase et al., 2013)
C. beijerinckii mutant RT66	9.3	35	(Guo et al., 2013)
C. beijerinckii ATCC 55025 (derived from ATCC 4259)	8.8	37	(Liu et al., 2010)
C. acetobutylicum DSM 792	9.5-11	37	(Survase et al., 2012)
C. acetobutylicum B3 (CGMCC 5234)	15.4	37	(Liu et al., 2013b)
C. acetobutylicum JB200 (derived from ATCC 55025)	19	37	(Xue et al., 2013)
C. acetobutylicum mutant NT642 (D64)	15.4	37	(Liu et al., 2012)
C. acetobutylicum BKM19 (derived from PJC4BK)	17.6	37	(Jang YS, 2013)
C. acetobutylicum EA 2018 (CCTCC M94061)	13	37	(Gu et al., 2009)
C. tyrobutylicum ATCC 25755	16-20.5	37	(Yu et al., 2012; Yu et al., 2011)
C. saccharobutylicum DSM 13864	13.4	35	(Ni et al., 2012; Ni et al., 2013)
C. pasteurianum CH4	13.3	37	(Kao et al., 2013)
C. pasteurianum MBEL_GLY2 (derived from *C. pasteurianum* ATCC 6103)	10.8	37	(Malaviya et al., 2012)

Apart from *Clostridium*, species such as *E. coli* were genetically engineered for butanol production. Atsumi *et al.* cloned a set of genes (*thl, hbd, crt, bc, etfAB and ashE2*) into *E. coli* for butanol-specific production, with 139 mg/L of butanol produced under anaerobic conditions (Atsumi et al., 2008). Inui *et al.* cloned butanol-producing genes (*thiL*, *hbd*, *crt*, *bcd-etfB-etfA*, and *adhe*) from *C. acetobutylicum* ATCC 824, reaching 1.2 g/L in *E. coli (Inui et al., 2008)*. Steen *et al.* transferred

the butanol biosynthetic pathway in *Saccharomyces cerevisiae* and reached 2.5 mg/L (Steen et al., 2008). However, compared to the final yield, the original *Clostridium* species is still dominating biobutanol production.

Aside from investigations to identify or develop high biobutanol-producing strains, recent research has also paid attention to the feedstocks' substrates among which crops, agricultural waste, forestry resources, and industrial waste attract attention because these raw materials contain an abundant quantity of carbohydrates to be fermented. It is quite obvious that simple sugars, which are readily fermentable, lead to higher yields in butanol. For instance, *Clostridium acetobutylicum* ATCC 824 led to 15 g L^{-1} and then to 16.9 g L^{-1} butanol with glucose (Bankar et al. 2012; Yen & Wang, 2013), while corn stover led to 10.1 g L^{-1} (He & Chen, 2013), 12 g L^{-1} on cassava (Li et al., 2012), 12 g L^{-1} on marine microalgae (Huesemann & Kuo, 2012), and 7 g L^{-1} on sugar maple wood (Sun & Liu, 2012). However, the economical evaluation must consider both the yield in butanol as well as the cost of the feedstocks per gram of butanol obtained. Jurgens *et al*. summarized the raw materials that have been assessed and their application in ABE fermentation (Table 2.2) (Jurgens et al., 2012).

Table 2. 2 Different feedstocks and strains used along with maximum solvents and productivities achieved (Jurgens et al., 2012)

Feedstock	**Hydrolysis method**	**Strain used**	**Yield [a] (g/g)/ Productivity [b] (g/L/h)**	**Total ABE (g/L)**	**Reference**
Wheat straw	H_2SO_4, enzyme	*C. beijerinckii* P260	0.60/0.42	25	(Qureshi et al., 2007)
Wheat straw	H_2SO_4, enzyme	*C. beijerinckii* P260	0.41/0.31	21.42	(Qureshi et al., 2008b)
Corn fiber	H_2SO_4	*C. beijerinckii* BA101	0.39/0.10	9.3	(Qureshi et al., 2008a)
Palm oil mill effluent, sago starch	Enzyme	*C. saccharoperbutylace-tonicum* N1-4	0.40/0.10	14.38	(Hipolito et al., 2008)
Dried distillers' grains and soluble (DDGS)	Ammonium fiber expansion, enzyme	*C. beijerinckii* BA101	0.34/0.14	10.4	(Ezeji & Blaschek, 2008)
Rice bran and defatted rice bran	HCl, enzyme	*C. beijerinckii* NCIMB 8052	0.31/0.26	16.42	(Lee, 2009)
Barley straw	H_2SO_4, enzyme	*C. beijerinckii* P260	0.43/0.39	26.64	(Qureshi et al., 2010a)
Corn stover	H_2SO_4, enzyme	*C. beijerinckii* P260	0.44/0.31	26.27	(Qureshi et al., 2010b)
Switchgrass	H_2SO_4, enzyme	*C. beijerinckii* P260	0.39/0.17	14.61	(Qureshi et al., 2010b)
Wheat bran	H_2SO_4	*C. beijerinckii* ATCC 55025	0.32/0.16	11.8	(Liu et al., 2010)
SO_2–ethanol–water (SEW) spent liquor	SO_2-ethanol-water	*C. acetobutylicum* DSM 792	0.20/0.09	8.79	(Survase et al., 2011)
Sugar maple wood	Hot water extraction, sulfuric acid	*C. acetobutylicum* ATCC 824	0.22/0.15	11	(Sun & Liu, 2012)
Rice straw	H_2SO_4, enzyme	*C. acetobutylicum* MTCC 481	1.04[c]/0.017	3	(Sun & Liu, 2012)
Cassava baggase	Enzyme	*C. acetobutylicum JB200*	0.39/0.62	33.87	(Sun & Liu, 2012)
Maize stalk juice	–	*C. beijerinckii* NCIMB 8052	0.27[c]/0.30	11.5	(Wang & Blaschek, 2011)

[a] Gram of solvents per gram of substrate.

[b] Sum of solvents production.

[c] Only butanol yield and productivity.

2.2 **Metabolic pathways involved in ABE fermentation**

Acquiring knowledge about the cell network of reactions, from the uptake of substrates to the excretion of end-products of interest, brings a unique view about the carbon flow and can thus allow identifying strategies of bioprocess management to maximize its productivity. Dealing with

this knowledge, the metabolic engineering approach allows the analysis of metabolic flux rates and distribution, as well as evaluating the strategies of metabolic pathways modification (Stephanopoulos et al., 1998). It is based on experimental data on cell physiology and cell metabolism, as well as fundamental knowledge in biology, biochemistry, cell physiology, and applied microbiology (Mayank et al., 2013; Stephanopoulos, 1999).

2.2.1 Metabolic pathway analysis

ABE synthesis pathways have been well-described in literature (Figure 2.1), with the particularity of a biphasic fermentation process and a transition from acidogenesis to solventogenesis. At first, glucose is metabolized through the glycolysis pathway (or Embden-Meyerof-Parnas Pathway: EMP), then converted to pyruvate, while pentoses such as xylose are metabolized through the Pentose Phosphate Pathway (PPP) to result in 6-phosphate fructose and 3-phosphate glyceraldehyde, which then enter the EMP pathway. Pyruvate is then catalyzed to acetyl-CoA by the iron oxidation protein-pyruvate oxidoreductase. Then, phosphate acyltransferase (Pta) and acetate kinase (Ack) catalyze the following steps of acetyl-CoA to synthesize acetic acid. In a parallel pathway, Acetyl-CoA is catalyzed by a series of enzymes - Thl (thiolase), Hbd (3-hydroxybutyryl-CoA dehydrogenase), Crt (crotonase), Bcd (butyryl-CoA dehydrogenase), Ptb (phosphotransbutyrylase), and Buk (butyrate kinase) - to generate butyrate (Jones & Woods, 1986; Lee et al., 2008; Lutke-Eversloh, 2014; Lutke-Eversloh & Bahl, 2011). During acidogenesis, acetic and butyric acids are accumulated concurrently to the cells' exponential growth. In acidogenesis, NADH is accumulated to provide the reducing power required for generating solvents in the subsequent solventogenic phase (Mann & Lutke-Eversloh, 2013). Cells then access solventogenesis with solvents accumulation while growth reduces and reaches a stationary phase. In solventogenesis, previously secreted acetic and butyric acids are re-uptaken to feed pathways of acetone and butanol production. Acetoacetyl-CoA transferase and acetate/butyrate-CoA transferase are the key enzymes in charge of generating acetyl-CoA and butyryl-CoA, which are then converted to acetone and butanol. Meanwhile, ethanol is synthesized from acetyl-CoA, which is catalyzed by aldehyde/alcohol dehydrogenase and accompanied by two moles of NAD(P)H consumption.

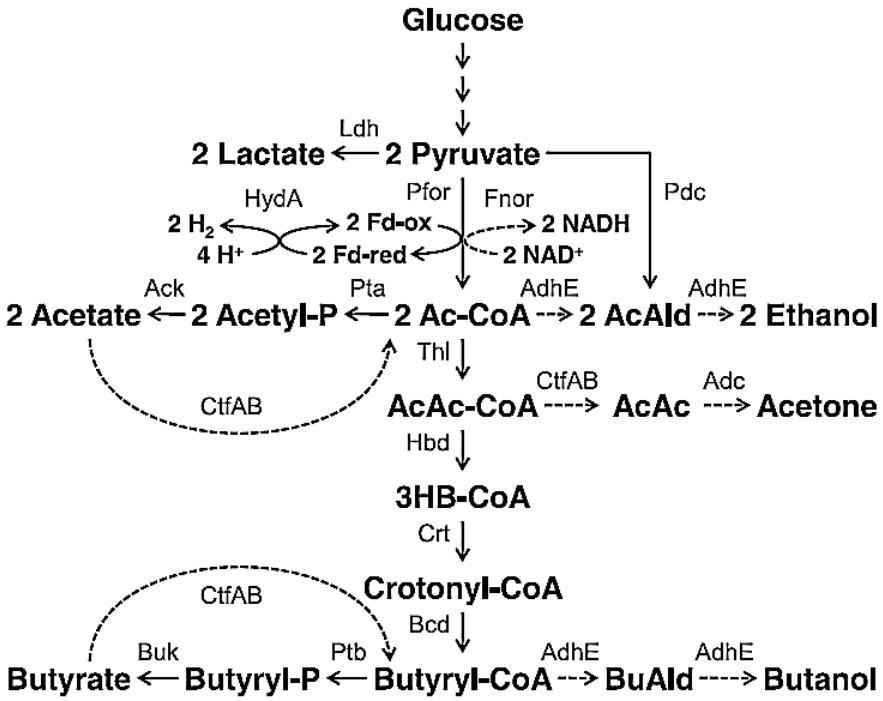

Figure 2. 1 Central metabolism of *C. acetobutylicum* (Lutke-Eversloh, 2014).

The transformation from acid to solvent is a special character of ABE fermentation. Therefore, abundant literatures focused on the metabolic mechanisms of the *Clostridium* species involved during the acidogenic-solventogenic phase transition. The conversion from acids accumulation to solvents generation causes a pH change in the culture medium. Acid (acitic and butyric acids) over-production is accompanied, under uncontrolled pH culture condition, to the "acid crash" phenomenon followed by the inhibition of the solventogenesis phase. During the pH phase transition, two ways of conversion from butyrate to butanol were revealed by Al-Shorgani et al (Figure 2.2). Both pathways go through the CoA transferase pathway and require two molecules of NADH, which are recycled from glucose and other sugars' catabolic pathways, and also played as co-factors of the following reactions involving BADH (butyraldehyde dehydrogenase) and BDH (butanol dehydrogenase) enzymes. Similarly to the other biofuel production bioprocesses, glucose has been widely studied in ABE fermentation (Al-Shorgani et al., 2011). Najeeb *et al.* studied the bioconversion of butyric acid to butanol by *C. asccharoperbutylacetonicum* N1-4, and showed that 10 g L^{-1} butyric acid leads to 13 g L^{-1} butanol in the presence of 20 g L^{-1} of glucose, but only 0.7 g L^{-1} butanol was produced without glucose (Al-Shorgani et al., 2011). While using *C. beijerinckii* TISTR 1461, 12 g L^{-1} of butanol were obtained from 15 g L^{-1} of glucose and 10 g L^{-1} of butyric acid (Loyarkat et al., 2013).

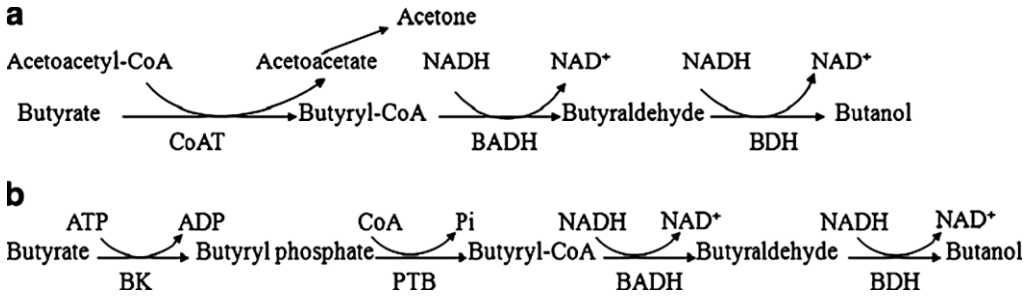

Figure 2. 2 Two possible mechanisms for the conversions of butyrate to butanol (Al-Shorgani et al., 2011).

In 2011, Amador-Noguez et al. conducted a metabolomics study of the acidogenic-solventogenic transition in *C. acetobutylicum*, using isotope tracers and quantitative flux modelling, with 114 metabolites tracked along with an acidogenic-solventogenic transition. These authors reported that amino acids, glycolytic, pyruvate, acetyl-CoA, NAD(P)H, and nucleotide triphosphates metabolisms decreased when cells evolved from acidogensis to solventogenesis (Amador-Noguez et al., 2011).

Riboflavin is a secondary metabolite which plays a significant role in cell metabolism as a vitamin (B2) and is widely found in plants and microorganisms, but not in higher animals. Indeed, a two-milligram dose of vitamin B_2 per day is necessary in the human diet (Cai & Bennett, 2011). Currently, the global market of riboflavin is estimated at 3,000 tons per year, with an industrial production by chemical, biochemical synthesis, and fermentation methods (Lim et al., 2001). Since the 1940s, various microorganisms have been found to produce riboflavin (Arzberger, 1943). Bacteria such as clostridia, yeasts species such as *Candida flareri*, *Candida guilliermondii*, *Candida famata*, and *Mycobacerium pheli*, as well as fungi species such as *Aspergillus terreus*, *Eremotheciumashbyii*, and *Ashbyagossypii*, have been used to produce riboflavin (Lim et al., 2001). Bacteria and yeast express low levels of riboflavin, and various methods were assessed to improve their production yield. For instance, the *C. acetobutylicum* ATCC 824 strain reached 70 mg L^{-1} of riboflavin after work in genetic engineering (Cai & Bennett, 2011), *C. acetobutylicum* reached 100 mg L^{-1} of riboflavin under bipyrimidine induction (Legg & Beesch, 1945), and *Candida flareri* produced 600 mg L^{-1} of riboflavin in an optimized medium. Of interest, fungi species (*Ashbyagossypii*) are currently often used in the industrial production of riboflavin,

expressing a high level of riboflavin at ~ 5 g L^{-1} compared to yeasts and bacteria (Lim et al., 2001). However, due to an increasing global market for riboflavin, there is room for alternative methods of riboflavin production. As previously mentioned, riboflavin is a by-product of ABE fermentation by *C. acetobutylicum* (Burgess et al., 2009), but after decades of improvement attempts as mentioned above, its yield of riboflavin is still quite low. However, as reported, when the riboflavin yield reaches 1 g L^{-1}, it will become competitive to the current market (Cai and Bennett, 2011), so promoting riboflavin yield in the ABE fermentation system is significant. With respect to *C. acetobutylicum*, the typical strain for ABE fermentation, its commercial application in the biobutanol industry is unparalleled. Riboflavin as a by-product which adds to biobutanol production may confer a higher economic competitiveness. Therefore, obtaining substantial riboflavin as a by-product of ABE in *C. acetobutylicum* is a new concept to the riboflavin industry, as well as the biobutanol industry.

Lim, et al. (2001), summarized three metabolic pathways of riboflavin in *Ashbya gossypii*, *Bacillus subtilis*, and *Candida famate*, which represented fungi, bacteria, and yeast, respectively (Lim et al., 2001). Depending on the proposed pathway, *C. acetobutylicum* synthesizes riboflavin and should pass key joint ribulose-5-phosphate (Ru5P), which is generated from the PPP pathway. It then goes to purine metabolism for GTP synthesis through different ways (Figure 2.3). Therefore, GTP is the key joint of riboflavin synthesis, which is catalyzed to 2, 5-diamino-6-ribosylamino-4 (3H)-pyrimidinedione 5-phosphate (DRTP), 5-amino-6-ribitylamino-2,4 (1H, 3H)-pyrimidine (ARP), 6,7-dimethyl-8-ribityllumazine (DMRL), and finally to riboflavin. The riboflavin is the major precursor of flavin mononucleotide (FMN) and flavin adenine dinucleotide (FAD), and although it can be regenerated by FMN and FAD, this was considered negligible compared to the denovo synthesis from GTP. FMN and FAD are mainly used as the prosthetic group for many flavoproteins and play a fundamental role in electron transfer. Instead of free FMN or FAD, they are connected to the flavoproteins by a solid non-covalent bond. Therefore, depending on a proposed negligible interconversion from FMN and FAD, riboflavin synthesis was defined mainly through the PPP and purine metabolic pathways, which is reasonable and in agreement with the reported literature (Lim et al., 2001, Cai & Bennett, 2011).

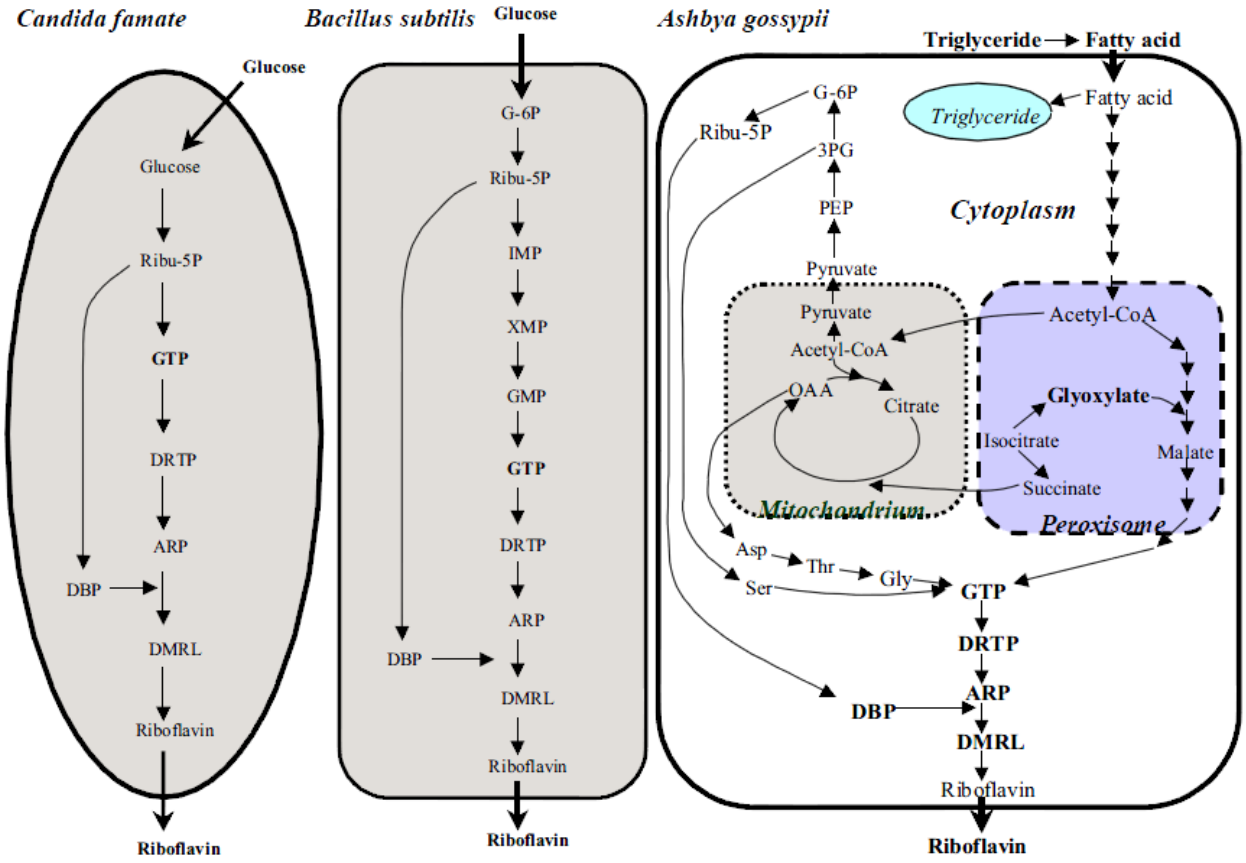

Figure 2.3 Proposed metabolic pathway for riboflavin production by *Ashbya gossypii*, *Bacillus subtilis*, and *Candida famate*. (Abbreviations: G-6P, Glucose-6-phosphate; 3PG, 3-phosphoglycerate; PEP, Phosphoenolpyruvate; Ribu-5P, Ribulose-5-phosphate; OAA, Oxaloactate; Asp, Aspatate; Thr, Thre- onine; Gly, Glycine; Ser, Serine; GTP, Guanosine triphos-phate; GMP, Guanosine monophosphate; XMP, Xanthine monophosphate; IMP, Inosine monophosphate; DRTP, 2, 5-diamino-6-ribosylamino-4 (3H)-pyrimidinedione 5-phosphate; ARP, 5-amino-6-ribitylamino-2, 4 (1H, 3H)-pyrimidine; DBP, L-3, 4-dihydroxy-2-butanone-4-phosphate; DMRL, 6, 7- dimethyl-8-ribityllumazine (Lim et al., 2001).

2.2.2 Genomic and transcriptomic analyses

As a typical strain used in ABE fermentation, the *C. acetobutylicum* ATCC 824 whole genome was sequenced in 2001 and includes 3.9 Mb chromosomes and 3740 open reading frames (ORFs) (Hartmanis & Gatenbeck, 1984; Nolling et al., 2001). Abundant functional genes related to butanol productivity, cell tolerance, and other positive effects were investigated based on genomic knowledge. Inactivation and overexpression of the *spo0A* gene in *C. acetobutylicum* ATCC 824

revealed that it is a crucial regulating gene for solvents formation and cell sporulation. Spo0A is the transcriptional regulator of the solventogenic operon *aad-ctfA-ctfB* and *adc*, and multiple sporulation factor genes involving the sigF operon, *spoIIGA, sigE, and sigG (Gheshlaghi et al., 2009; Harris et al., 2002).* A similar study also revealed a positive mutant strain of *C. acetobutylicum* EA2018 (hyper-butanol production) showing a higher level of the transcriptional factor of *spo0A,* compared to the wild strain ATCC 824 (Hu et al., 2011).

The recently available genome sequence information for *C. beijerinckii* NCIMB 8052 has allowed for the examination of the gene expression profile during the shift from acidogenesis to solventogenesis with time (Shi & Blaschek, 2008b). Their study revealed that the expression of the acetate formation genes encoding for phosphotransacetylase (*pta*) and acetate kinase (*ack*), as well as the butyrate formation gene encoding for butyrate kinase (*buk*), all increased up to two-fold during the acidogenic phase and declined with the onset of solvent formation. Specifically, in *C. beijerinckii* 8052, the onset of solventogenesis was concurrent to the initiation of the sporulation process. *C. beijerinckii* NCIMB 8052 was also compared to its positive mutant BA101 at the transcriptional level by real-time quantitative reverse transcription-PCR (Q-RT-PCR). The comparison was based on acid formation genes, butyryl-CoA formation genes, solventogenic genes, early sporulation genes, putative sig E-regulated genes, putative sigG-regulated genes, the phosphotransferase system (PTS), glycolytic genes, and chemotaxis genes. Compared to *C. beijerinckii* 8052, *C. beijerinckii* BA101 showed an increased expression of butyryl-CoA and butanol formation genes during the solventogenic phase. It has also been suggested that the *C. beijerinckii* BA101 gene expression of sporulation and PTS (e.g. *manIIAB* and *manIIC* were 5- to 10-fold lower) is less efficient than for the 8052 strain, while the genes of the primary metabolism and chemotaxis/motility (e.g. *bdc* was 3-fold higher) are overexpressed compared to the 8052 strain (Shi & Blaschek, 2008b).

The positive mutant strain *C. acetobutylicum* EA 2018 (not producing spores, and with a greater solvent production capability) also exhibited abundant overexpressed genes compared to the wild strain *C. acetobutylicum* ATCC 824. Aside from the *spo0A* and *adhEII* overexpression benefits to solvents formation, most of the genes related to acid formation have shown lower expression levels in the EA2018 strain. Looking at substrate utilization genes, EA2018 shows enhanced pentose uptake capacity - for instance, *xylB,* which is involved in xylose and xylan metabolism, was

expressed at a higher level, while *xylD* and xylanase genes (CEA_P0115 and CEA_P0053) also showed higher expression levels in EA2018. The results also showed that the variation of CEA_G2622 (CAC2613 in ATCC 824), a putative transcriptional regulator involved in xylose utilization, might also be involved in the accelerated utilization of the xylose substrate. This information could be valuable for further genetic modification of *C. acetobutylicum* maximizing butanol production, as it may also benefit hemicellulose fermentation in the near future (Hu et al., 2011).

Butyric acid induction has been demonstrated to promote butanol production in ABE fermentation. Wang et al. (2013) investigated the effect of butyrate supplementation on gene transcription and expression related to glycolysis, acidogenesis, and solventogenesis; sporulation genes, putative *abrB* genes, and putative sensory kinase genes; as well as genes related to cell motility, sugar transport, and granulose formation. Results have indicated that the PTS encoding gene cluster (Cbei_4911-4911 and Cbei_1844), CoA biosynthesis-related genes (Chei_260-2610), and alcohol dehydrogenase genes (Cbei_2181 and Cbei_2243) were overexpressed in a butyrate-supplemented condition. Moreover, *pta* (Cbei_1164) and *ack* (Cbei_1165) genes related to acetic acid formation, *ptb* (Cbei_0203) and *buk* (Cbei_0204) genes related to butyrate formation, as well as the genes related to acetoacetyl-CoA and butyryl-CoA synthesis were also shown to be overexpressed. All of these genes were upregulated from the very beginning of the fermentation process when supplementing butyrate. Similar results for the sol operon genes *ald-ctfA-ctfB-adc, ald* (Cbei_3832, encoding aldehyde dehydrogenase), *ctfA* (Cbei_3833), *ctfB* (Cbei_3834), and *adc* (Cbei_3835), sporulation genes *spo0H* (Cbei_0135) and *spo0A* (Cbei_1712), and *sigF* operon (*spoIIAA-spoIIAB-sigF*) were all overexpressed earlier in butyrate-supplemented culture compared to un-supplemented culture (Wang et al., 2013).

Tomas et al., compared the solvent-tolerant strain 824 (pGROE1) to the wild-type control strain 824 (pSOS95del). Comparing their transcriptional profiles for genes which are likely to play a role in the general butanol stress response showed that these have similar expression patterns, while genes likely to be associated to increased tolerance to butanol showed opposite expression patterns. The butanol dose-dependent production increased with the upregulation of most of the stress protein genes (*groES, dnaKJ, hsp18,* and *hsp90*), solvent formation genes (*aad, ctfA, ctfB, adc,* and *bdhA/B*), butyrate formation genes (*ptb* and *buk*), and butyryl-CoA biosynthesis operon genes,

while the major fatty acid synthesis operon genes, several glycolytic genes, and a few sporulation genes were downregulated (Tomas et al., 2004).

Therefore, genomic and transcriptomic studies have provided abundant knowledge on the specific genes in hyper-butanol productivity strains, tolerant stains, and other positive effects in various strains. They have revealed key gene encoding for sporulation, acid and solvent formation, PTS, chemotaxis, as well as for glycolytic and other control metabolites regulation. This knowledge can be beneficial to further proteomic and metabolomics analyses.

2.2.3 **Proteomic analyses**

Aside from genomic and transcriptomic studies, people have also focused on the proteomic study in various conditions by ABE fermentation.

Based on the discovery that the *spo0A* gene significantly affects butanol productivity, Sullivan et al. compared *C. acetobutylicum* ATCC824 and *spo0A* mutant strain for their proteomic profile. In the *spo0A* knockout strain, six proteins - Ppi, ChW14, Adc, Spo0A, ChW16, and ChW17 - were absent. Meanwhile, *spo0A* overexpression affected proteins involved in glycolysis, translation, heat shock stress response, and energy production (Sullivan & Bennett, 2006). Therefore, *spo0A*-related proteins have received more attention for their multi-functional regulation roles.

In 2011, Sivagnanam et al. compared *C. acetobutylicum* ATCC 824 proteomics in glucose and xylose cultures. They reported that the flagellar protein and chemotaxis proteins CheW/CheV were downregulated and absent in xylose culture (Sivagnanam et al., 2011). These authors also investigated different protein expressions in both exponential and stationary phases in xylose culture. A total of 109 and 57 proteins were identified during the exponential and stationary phases, respectively. Related to central carbon metabolism, phosphate acetyltransferase, xylulose kinase, butyrate-acetoacetate CoA-transferase (subunit B), NADH-dependent butanol dehydrogenase B, acetoacetate decarboxylase, and acetyl-CoA acetyltransferase were upregulated in the exponential phase compared to the stationary phase (Sivagnanam et al., 2012). Meanwhile, Sivagnanam et al. identified 14 proteins in the ABC transport system and three proteins in the PTS system - phosphocarrier protein (Hpr), phosphoenolpyruvate protein kinase (PTS system enzyme I), and PTS enzyme II ABC component - which were all expressed in both glucose and xylose cultures

(Sivagnanam et al., 2011). During the transition from the exponential phase to the stationary phase, xylulose kinase was reduced by 86 %, phosphate acetyltransferase by 65 %, acetyl-CoA acetyltransferase by 72.7 %, acetoacetate decarboxylase by 77 % and butyrate-acetoacetate CoA-transferase by 62 % (Sivagnanam et al., 2012). Mao et al. (2011) observed that some transport proteins were downregulated in solventogenesis, such as glutamine ABC transporter (CAC0112), oligopeptide ABC transporters (CAC3628, CAC3629, and CAC3632), and the ABC transporter ATP-binding proteins (CAC0147 and CAC2867) (Mao et al., 2011). In *C. acetobutylicum* ATCC 824, enzymes of glucokinase and glucose-6-phosphatase were identified in xylose culture, proving the existence of the gluconeogenesis pathway (Sivagnanam et al., 2011).

Han et al. (2013) performed a proteomic analysis investigating the effect of a calcium supplementation in *C. beijerinckii* NCIMB 8052 (Han et al., 2013). They observed the increase at various levels of heat shock proteins (GrpE and DnaK), sugar transporters, and proteins involved in various cellular processes such as DNA synthesis, repair, recombination and replication, sporulation stage II protein D, nucleoside triphosphate hydrolase (conserved domain), and arsenite-activated ATPase. However, no effect on the expression of key enzymes in the solventogenic pathway were observed, aside from upregulated activities of coenzyme A transferase (CoAT), acetate kinase (AK), and acetoacetate decarboxylase (ACDC). CoAT is the central enzyme for acetate and butytate re-uptake (which, in turn, is needed for subsequent conversion to butanol), as well as the rate-limiting enzyme for acetone production. These authors have speculated that the Ca^{2+} ion is enhancing ABE fermentation from the stimulation of sugar transport, butanol tolerance, energy metabolism, and various enzyme activities (Han et al., 2013).

Mao et al. compared the wild strain DSN 1731 to its mutant Rh8, identified for its tolerance to butanol (Shaoming Mao et al., 2010). In comparison to the wild strain *C. acetobutylicum* DSN 1731, its mutant Rh8 showed that the chaperone and solvent formation-related proteins were upregulated, while amino acid metabolism and protein synthesis-related proteins were downregulated in both the acidogenic and solventogenic phases, which, respectively, are only upregulated or downregulated in the solventogenic phase in the wild type strain (Table 2.3). This suggests that Rh8 cells have developed a mechanism to prepare for butanol inhibition prior to its production, which may explain the increased butanol yields observed.

Table 2. 3 *C. acetobutylicum* DSM 1731 and Rh 8 strains compared for their proteins expression level (Bao et al., 2014).

Classify of proteins	**Related proteins**	**Protein level in Rh8 compare to DSN1731**
acid and solvent formation-related proteins	CtfB, CtfA, Adlhel, Adc, THL, BdhB and BdhA	upregulated
	PflB, AskA, Ptb (upregulated in acidogenesis)	downregulated
chaperone proteins	Hspl8, GroES, ClpC, GrpE, YacI, Phase shock protein A, Rubrerythrin, TufA, GroEL, GreA, N-terminal fragment of elongation factors Ts, ClpP, DanK, HtpG, HtrA	upregulated
	Map (upregulated in acidogenesis)	downregulated

Comparing the proteomic study results with those of the transcriptomic study for tolerant mutant strain - solvent-tolerant strain 824 (pGROE1) (Tomas et al., 2004) - the patterns of solvent formation and chaperone proteins were consistent with their transcriptional levels. However, despite the transcriptional level of acid formation-related genes, the butyryl-CoA biosynthesis operon genes, major fatty acid synthesis operon, and several central metabolism genes (glycolytic genes) were downregulated in mutant 824 (pGROE1). Li Yin et, al. also studied the membrane proteome of *C. acetobutylicum* and 73 differentially expressed proteins which were identified in the mutant strain, and speculated that butanol tolerance is associated to membrane stability (Mao et al., 2011).

Summarizing all of the above, in comparing wild strains to positive mutant strains or induced strains, it is clear that the proteins involved in central carbon metabolism - Pentose phosphate pathway (PPP) and Glycolysis, Pyruvate metabolism, acid and solvent formation related proteins, chaperones proteins, phase shock proteins, heat shock stress response proteins, sporulation and energy metabolism-related proteins, metabolite transporters, cellular membrane proteins, chemotaxis proteins, and flagellar/motility proteins express differentially.

2.3 **Modeling ABE fermentation biosystem**

This section summarizes the state of development of metabolic models for ABE fermentation. In 1984, Papoutsakis derived a stoichiometric equation system in the *Clostridium* species (Papoutsakis, 1984), which paved the foundation for the metabolic engineering of ABE fermentation (Smid et al., 2005). In 1986, Votruba et al. developed a mathematical model to

describe the physiological aspects of growth and metabolite synthesis, which represented bioreactor mass balances for the substrate, biomass, and main products ABE. In this model, growth is based on the history of the microbial culture (population age) and a variable environment (the metabolic activity derived from the variable morphological culture image). The macroscopic fermentation rates were expressed with substrate consumption and butanol inhibitory effects. However, further carbon metabolism is not simulated in this system. A kinetic metabolic model was developed in 2007 by Shinto *et al.*, which presented a dynamic metabolic model describing 19 reactions and with 45 parameters in *C. saccharoperbutylacetonicum* N1-4 (Shinto et al., 2008; Shinto et al., 2007). Shinto's dynamic model was based on Papoutsakis' stoichiometric equations, introducing time variables into the model conferring a dynamic behavior to all metabolic reactions. This model considered enzyme kinetic character in reaction rates. They tried to open the "black box" of intracellular metabolic process in a dynamic method. In that model, glucose uptake inhibition and product inhibition by butanol were both considered. However, although Shinto established a comprehensive dynamic model, there were some limitations. First, it did not consider ATP and NADP metabolisms, which are known to impact the main metabolism. Second, only substrates, biomass and main products were simulated rather than any intracellular metabolites, which limited the model's output capacity. To describe biomass growth, only acetyl-CoA was considered as contributing to biomass, and the contributions of 5-phosphate ribose and amino acids were ignored (Shinto et al., 2008; Shinto et al., 2007). Li *et al.* also discussed the fact that the Shinto model included lumped reactions between butyrate and butyryl-CoA. These authors further developed Shinto's model investigating the behavior of the key metabolite butyryl phosphate, ameliorating simulation results compared to experimental results (Li et al., 2011). However, after reviewing the models proposed in literature to describe ABE fermentation, we considered that there is still a lack of a comprehensive kinetic model with identified parameters, and that describes the key metabolic pathways linking xylose metabolism to solvents production and productivity.

CHAPTER 3 METHODOLOGY

3.1 Culture method

Clostridium acetobutylicum ATCC 824 is stored in our lab and applied in all the following work. Modified Reinforced Clostridia broth (MRC) medium (ATCC Medium No. 2107, listed in appendix B) was used as a seed medium - it is rich in nutrition and suitable for biomass accumulation. Modified Clostridia Growth Medium (CGM, appendix B) (Choi et al., 2012) was applied as a production medium, which is popularly used for ABE production in *Clostridium sp*. Both culture mediums were applied with xylose as their main carbon source. Based on different research purposes, sodium chloride (0, 5, 10 and 15 g L^{-1}) or sodium acetate (60 mM) were added to test their effects on ABE fermentation. In the sodium chloride culture of Chapter 4, calcium carbonate (5 g L^{-1}) was used to maintain culture pH, while in the sodium acetate culture of Chapter 5, acetate itself was provided as a buffer. All cultures were performed at 37 ˚C either in an incubator (New Brunswick Scientific, series 25D) or in a 3.6 L bioreactor (Infors-HT, Bottmingen, Switzerland) with 2 L of medium. All cultures and inoculations were operated anaerobically by 100 % pure filtered nitrogen gas protection, and resazurin (0.025 %, 4 mL L^{-1}) was used as an oxygen indicator. Bottle cultures were grown anaerobically under 150 rpm, while the bioreactor culture was agitated at 100 rpm with Rushton impellers.

3.2 Metabolomic analysis

3.2.1 Sample collection and extraction

Samples were taken at different time intervals (around 12 h), and centrifuged at 20,000 *g* for 10 min at 4 ˚C. Then, the supernatant was separated from cell pellets and stored at -80 ˚C for extracellular compound analyses, which included ABE, acetate, butyrate, xylose, and amino acids (Riboflavin is not only in the supernatant, which should be specifically proceeded as below). The collected biomass was rinsed twice with 2 mL PBS (Phosphate buffer solution) and centrifuged at 20,000 *g* for 10 min at 4˚C, and the cell metabolism of the collected biomass was then quenched by adding 500 µL 50 % methanol and homogenized with votexer (Fisher Scientific). The suspension was put into an ultrasonic bath with ice water (Crest, 1000 W, 20 kHz) for 30 min, then centrifuged for 10 min (4 ˚C, 20,000 *g*). The supernatant was transferred to a new tube, and cells

were re-extracted with 500 µl 50 % cold methanol following the previous steps. Then, the two successive extracts of the same cell sample were combined in a unique tube and stored in –80 ˚C for further analysis of intracellular sugarphosphates, organic acids, and nucleotides. With respect to riboflavin collection and quantification, culture sample was taken from the stirring bioreactor and diluted 10-fold with distilled water until all the yellow sediment was dissolved, and the suspension was then centrifuged at 20,000 *g*, 4 ˚C for 10 min). The supernatant was mixed with NaOH (1 M) at ratio 4:1 to maintain the stability of riboflavin. Then, a 20 % potassium phosphate buffer (pH 6.0, 0.1 M) was added for neutralization. The final solution was detected and quantified with spectrophotometer (UV-2100, UNICO, Canada) under an absorption wavelength of 444 nm (A444) (Sauer et al., 1996). The concentration was calculated using a calibration curve established using a pure standard of riboflavin (Sigma, Oakville, Canada, cat. # 83885), as described in (Sauer et al. 1996). More details are described in 4.4 and 5.4.

3.2.2 Intracellular sugar phosphates and organic acids

Sugar phosphates - G1P, G6P, F6P, X5P, Ru5P, R5P, and GA3P - and organic acids - PYR, SUC, FUM, MAL, (ISO) CIT, and α-KG - were analyzed with UPLC/MS/MS (Agilent, Quebec, Canada), which was equipped with a 1290 infinity binary pump, an autosampler, a column temperature controller, and a 6460A triple quad mass spectrometer. 20 µL cell extraction was injected into the column after passing through 0.22 µm PTFE filters (Millipore, Ontario, Canada). Sugar phosphates and organic acid were separated on a Hypercarb column (100 × 2.1 mm, 5 µm) and a Hypercarb pre-column (2.1 × 10, 5 µm) (Thermo Fisher, Ontario, Canada) with mobile phase A: 20 mM ammonium acetate at pH 7.5, and mobile phase B: 10 % (v/v) methanol in water at a flow rate of 0.3 mL min^{-1}. The mobile phase gradient was: 0-5 min at 10 % A, 5-10 min at linear gradient from 10 to 20% A, 10-20 min at linear gradient from 20 to 100 % A, 20-30 min at 100 % A, 30-32 min at linear gradient from 100 to 10 % A, and 32-40 min at 10 % A. The negative electrospray ionization model was selected for the analysis with Agilent Jet Stream source. The mass spectrometer operation conditions were set as follows: gas temperature 300 ˚C, gas flow rate 7 L min^{-1}, nebulizer 40 Psi, sheath gas temperature 300 ˚C, sheath gas flow 12 L min^{-1}, and capillary voltage -3.5 kV.

3.2.3 Intracellular nucleotides

Nucleotide concentrations of ATP, ADP, AMP, GTP, NAD(H), and NADP(H) pairs were determined by ion-pairing liquid chromatography-electrospray ionization mass spectroscopy (positive mode) using a UPLC/MS/MS system (Agilent, Quebec, Canada) equipped with a Symmetry C18 column (150 × 2.1 mm, 3.5 µm) (Waters) and a Security C18 guard-column (Waters, 10 × 2.1mm, 3.5 µm). DMHA was used as an ion-pair reagent to improve the signal-to-noise ratio with positive ionization mode. Mobile phase A: 10 mM ammonium acetate, 15 mM DMHA at pH 7.0, and mobile phase B: 40 % (v/v) acetonitrile in water. The flow rate was set at 0.3 mL min L^{-1} using the following gradient: 0-10 min at 15 % B, 10-12 min at linear gradient from 15 to 40 % B, 12-30 min at linear gradient from 40 to 70 % B, 30-35 min at 70 % B, 35-37 min at linear gradient from 70 to 15 % B, and 37-45 min at 15% B.

3.2.4 Riboflavin purification and identification

For the yellow sediment, we first conducted a literature review to find its probability, and found that the *Clostridium* species could generate riboflavin, which is a yellow crystal. Therefore, we compared both the crystal shape and MS/MS of our sediment with standard riboflavin to find out whether they are the same compound, as follows: the yellow sediment was collected from the fermentation broth by first centrifuging at 20,000 *g* for 10 min at room temperature, and washing twice with distilled water. Then, the yellow-rich sediment was purified as follows by repeating the procedure at least three times. The sediment (~ 0.1 g) was first dissolved in 2 mL of 100 % methanol at room temperature and centrifuged at 20,000 *g* (10 min, room temperature), and the supernatant (riboflavin-saturated methanol solution) was stored at -20 ˚C overnight to favour riboflavin crystal precipitation. The purified crystal sample was dissolved in 1 mL of 70 % methanol for the identification step, and a pure riboflavin standard (Sigma, Oakville, Canada, cat. # 83885) was also dissolved in 70 % methanol for comparison.

Riboflavin identification and alignment were carried out on a UPLC-UV-MS/MS (Agilent, Quebec, Canada), which was equipped with a 1290 infinity binary pump, an autosampler, a column temperature controller, a UV detector and a 6460A triple quad mass spectrometer. 2uL samples were injected into the column after passing through 0.22 µm PTFE filters (Millipore, Ontario, Canada) before injection. Riboflavin was separated on an ACQIUITY UPLC BEH Amide column

(100×2.1 mm, 1.7 μm) (Waters, Montreal, Canada) with mobile phase A: 10 mM ammonium acetate and 0.04 % NH_4OH in 70 % acetonitrile (v/v), and mobile phase B: 10 mM ammonium acetate and 0.04 % NH_4OH in 80 % acetonitrile (v/v) at a flow rate of 0.13 mL min^{-1}. The mobile phase gradient was: 0-7 min from 100 % B to 30 % B and returned to 100 % B in 1 min. The column was initialized for 17 min at 100 % B before the second injection. The signal was detected by both the UV detector at 265 nm and the MS detector. The positive electrospray ionization model was selected for the analysis with Agilent Jet Stream source at a transition of 375.1 > 255.1 with a flag voltage of 45 V and a collision cell voltage of 10 V. The mass spectrometer operation conditions were set as follows: gas temperature 250 ˚C, gas flow rate 6 L min^{-1}, nebulizer 30 Psi, sheath gas temperature 250 ˚C, sheath gas flow 10 L min^{-1}, and capillary voltage 3.0 kV. The data was processed by mass hunter software.

3.2.5 The analysis of the ABE

The analysis of ABE was developed from the reference (Gerchman et al., 2012). Briefly, the cell culture medium was extracted by ethyl acetate at room temperature, at the ratio of 1:1, with isobutanol as an internal standard for quantification (for more details, please refer to 4.4.2). The analysis of ABE was performed on a Perkin Elmer Clarus 480 (Perkin Elmer, Canada) with an Elite-Wax ETR (30 m × 0.032 mm i.d.) column and a FID detector. A 1 μL sample was injected with an injector temperature of 260 ˚C. ABE was separated with hydrogen (H_2) as a carrier gas at the flow rate of 2 mL min^{-1}, split ratio 50:1. The column was heated from 40 ˚C to 220 ˚C at 6 ˚C min^{-1}, and held at 220 ˚C for another 5 min before returning to 40 ˚C. The serial standard was performed in the same way as the sample. The data was collected at the absorbance of 210 nm and processed by Masslynx 4.0 software (Waters Canada) (Ahmed et al., 2015).

3.2.6 Acetic acid and butyric acid

Extracellular samples were diluted 2-fold by 5 mM H_2SO_4, and filtered with a 0.22 μm filter before the analysis. The analysis of acetic acid and butyric acid was performed on a Waters HPLC system, which was equipped with a 2777 autosampler (Waters Canada), a 1525 binary pump (Waters Canada), and a 996 PDA (Photodiode Array) detector (Waters, Canada). Acetic acid and butyric acid were separated on the Aminex HPX-87H column and the guard column (Bio-rad, Canada) with a mobile phase of 5 mM H_2SO_4 at a flow rate of 0.6 mL min^{-1}. The column temperature was

set at 50 ˚C, and a 20 µL sample solution was injected into the column for a running time of 30 min. The data was collected at the absorbance of 210 nm and processed by Masslynx 4.0 software (Waters Canada) (Ahmed et al., 2015).

3.2.7 **Amino acids analysis**

The culture medium supernatant separated from cell pallets was used for amino acid analysis. A medium sample also contained proteins which precipitated during the HPLC/MS/MS analysis, and thus affected both the analysis performance and the resulted quantification. The sample should be de-proteinated prior to sample injection, by diluting 400 times at 50 % methanol. Thereafter, the diluted sample was mixed with an internal standard - homoarginine hydrochloride (Fisher Sci. #AC169090010), homophenylalanine (Sigma #294357), and methionil-D3 (CDN Isotope #D1292) - buffer of ratio 1:1, which contained 50 % mobile phase A (20 mM $HCOONH_4$, pH 4.0) and 50 % mobile phase B (20 mM $HCOONH_4$ in acetonitrile, pH4.0) to get the same buffer condition as the HPLC mobile phase. Samples should be prepared on the same day of the analysis due to unstable amino acids under acidic condition. Then, the sample was filtered by a 0.22 µm filter before passing through the HPLC/MS/MS system. A 5 µL sample was injected into the 1290 HPLC system, coupled with a 6460 triple quadruple mass spectrometer (Agilent Technologies, Santa Clara, CA, USA), and separated by a 2.1 × 150 mm ZICTM-Hilic column (3.5 mm, 200 A, PEEK) (Merck SeQuant, Peterborough, Canada). A mass spectrometer and the serials of standards were used for identification and quantification purposes.

3.2.8 **Xylose analysis**

A culture medium supernatant was mixed with 70 % acetonitrile (1:1 in volume) before the HPLC/MS/MS injection in order to get the same buffer condition as the HPLC mobile phase (mobile phase A: acetonitrile / H_2O=30 / 70, 0.1 % NH_4OH and mobile phase B: acetonitrile / H_2O = 80 / 20, 0.1 % NH_4OH). Samples were filtered by a 0.22 µm filter before passing HPLC/MS/MS. An Acquity UPLC BEH Amide Column (2.1×100 mm column, 1.7 um, waters # 186004800) was used for sugar separation under a flow rate of mobile phase at 0.13 mL min^{-1}. Mass spectrometer and the serials of standards were used for identification and quantification purposes.

3.3 Dynamic modeling

A kinetic metabolic model in the ABE fermentation system was developed. The model structure included major carbon metabolism such as PPP pathway, glycolysis pathway, acid and solvent formation, purine metabolism, and pathways related to ABE and riboflavin synthesis. The metabolites' initial condition and parameter value were taken either from experimental data or from literature. A model decomposition method proposed by Rizzi et al. was applied and allowed to systematize and accelerate parameter value identification and calibration processes (Rizzi et al. 1997). This method allows the minimizing of the number of kinetic parameters to determine at each step. The resolution algorithm followed is presented in Figure 3.1, illustrating the working process (Roels, 1983).

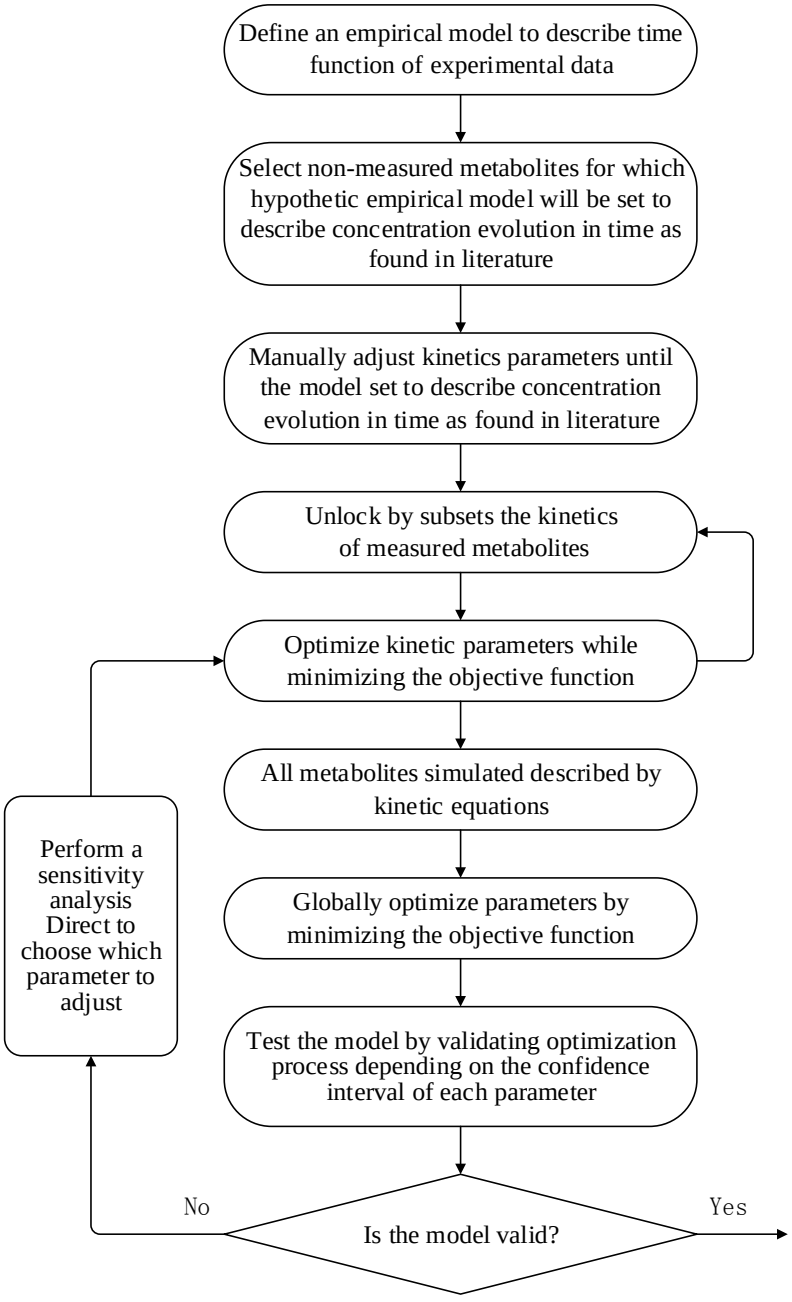

Figure 3.1 Algorithm of resolution for determining a model kinetic parameter value.

Briefly, the principle of this method consists of taking advantage of the experimental data in hand in order to identify a time-function expression which can be used to describe the associated derivative in the mass balance system of equations. One can thus proceed to limiting the changing of only kinetic parameters which are associated with non-measured metabolites first, with the measured ones being well-described. In case this set is too important in size, one can proceed to grouping, for instance, by pathway-related subsets, these ones being under study. Matlab (The

MathWorks Inc., Natick, MA, USA) Optimization Toolbox “lsqcurvefit” was applied to optimize parameters for the minimizing of global simulation error as the objective function. Meanwhile, sensitivity analysis and a 95 % confidence interval were performed to confirm optimization results (for details, refer to 5.11.2).

Moreover, a Matlab code performing the automatic generation of the different Matlab codes in order to perform the resolution of the ordinary differential equation system, developed by Dr. Sabine Peres (S. Peres and M. Jolicoeur, unpublished), was used. The program reads a “.txt” file including the stoichiometry of all reactions, generated kinetic equations, and mass balances files named “equidff.m”. Reaction inhibition and activation mechanisms were also considered. Matlab tool “ode23s” was used to solve the ordinary differential equation system. All files are presented in Appendix D.

CHAPTER 4 ARTICLE 1: A QUANTITATIVE METABOLOMICS STUDY OF HIGH SODIUM RESPONSE IN *CLOSTRIDIUM ACETOBUTYLICUM* ATCC 824 ACETONE-BUTANOL-ETHANOL (ABE) FERMENTATION

Xinhe Zhao, Stefan Condruz, Jingkui Chen, Mario Jolicoeur*

Research Laboratory in Applied Metabolic Engineering, Department of Chemical Engineering, École Polytechnique de Montréal, P.O. Box 6079, Centre-ville Station, Montreal, Quebec, H3C 3A7, Canada.
* Corresponding author: mario.jolicoeur@polymtl.ca

(Published in Scientific Reports, Sci. Rep. 6, 28307; doi:10.1038/srep28307 (2016))

4.1 Abstract

Hemicellulose hydrolysates, sugar-rich feedstocks used in biobutanol refinery, are normally obtained by adding sodium hydroxide in the hydrolysis process. However, the resulting high sodium concentration in the hydrolysate inhibits ABE (acetone-butanol-ethanol) fermentation, and thus limits the use of these low-cost feedstocks. We have thus studied the effect of high sodium on the metabolic behaviour of *Clostridium acetobutylicum* ATCC 824, with xylose as the carbon source. At a threshold sodium concentration of 200 mM, a decrease in both the maximum cell dry weight and ABE yield were observed compared to the control culture. However, solvent specific productivities were not affected by supplementing sodium. The main effects of high sodium on cell metabolism were observed in acidogenesis, during which we observed the accumulation of ATP and NADH, and the inhibition of the pentose phosphate (PPP) and the glycolytic pathways with up to 80.73 ± 1.47 % and 68.84 ± 3.42 % decrease of the associated metabolic intermediates, respectively. However, the $NADP^+$-to-NADPH ratio was constant for the whole culture duration, a phenomenon explaining the robustness of solvent specific productivities. Therefore, high sodium, which inhibited biomass growth through coordinated metabolic effects, did not have any effect on solvent specific productivity.

4.2 Keywords

Clostridium, butanol, xylose, sodium chloride, metabolic, intracellular

4.3 Introduction

Global warming, a result of fossil fuel combustion, has made the production of renewable and environment-friendly fuels a high priority. Biobutanol, a second-generation biofuel that can be produced from sugars of various origins and having physico-chemical properties that are similar to gasoline, has attracted the attention of the industry because of its advantages over ethanol (Wang et al., 2014). Of interest, the *Clostridium* genus has been widely used for biobutanol production for more than a century (Gabriel, 1928; Peterson & Fred, 1932). This bacterium synthesizes acetone-butanol-ethanol (ABE) by fermentation in an average ratio of 3:6:1, respectively. However, the high cost of raw material feedstocks has limited so far biobutanol industrialization.

Lignocellulosic feedstocks, which include non-edible biomasses from agriculture (wheat straw, corn stalks, etc.) and forestry industrial activities (bark, leaves, wood chips and sawmills residues, pulp and paper mills waste streams, etc.) (Wiselogel et al., 1996), have been estimated to account for 50% of the world biomass (Claassen et al., 1999). However, lignocellulose first requires an hydrolysis pretreatment for breaking down complex sugars into fermentable ones, a process generally involving the use of either chemicals or enzymes (Qureshi et al., 2008c). This pretreatment step is normally performed under a severe high temperature environment with the use of acid or alkali solution (Zaldivar et al., 2001). Indeed, such physico-chemical processes incorporate and generate abundant amounts of salts, phenolic acids and aldehydes, all compounds that have been shown to be inhibitory to the subsequent bacterial fermentation step (Alriksson et al., 2006). Especially in the case of the pulp and paper industry, significant amounts of sodium hydroxide is applied in delignification, chemicals regeneration, pH control and as cleaning agent (caustic) (Murray, 1992). Among the ions which concentration increases along the various process steps enumerated above, sodium requires a specific attention. Indeed, sodium ion toxicity has been studied in a wide range of cells (Barth-Jr. et al., 2012; Stubblefield & Mueller, 1960). By removing salts by electrodialysis from wheat straw hydrolysates obtained using alkaline peroxide, ABE production was enhanced from 2.59 to 21.37 g L^{-1} (Qureshi et al., 2008c). Maddox *et al*. suggested high salts concentration diverted ABE fermentation from being solventogenesis to acidogenesis, thus decreasing products yield (Maddox et al., 1995).

ABE fermentation genetics, proteomics and metabolomics has been widely studied. Gheshlaghi, *et al*. identified 21 main functional enzymes in glucose culture, describing enzyme expression characteristics and kinetic parameters (Gheshlaghi et al., 2009). Of interest, ABE fermentation presents a biphasic metabolism starting with acidogenesis followed by solventogenesis. Cell growth occurs during the first stage in batch ABE culture, concurrently with acids accumulation (acetic and butyric acid). Then, solvents accumulate during solventogenesis. In *Clostridium*, the most studied organism performing ABE fermentation, both hexoses and pentoses can be metabolized through glycolysis and pentose phosphate pathway (PPP), respectively. Then, acetic and butyric acids are generated from acetyl-CoA (Lee et al., 2012). Acetic and butyric acids accumulation then stimulates specific sets of enzymes to convert acids (acetic and butyric) into solvents such as acetone and butanol, as well as ethanol (from acetyl-CoA), and the cells enter solventogenesis, a phase revealed by a pH increase (Gheshlaghi et al., 2009).

However, although sodium has been clearly identified as an inhibitory compound, to the best of our knowledge the metabolic effects underlying sodium ion inhibition on ABE production and biomass growth have not been studied to date (Maddox et al., 1995; Qureshi et al., 2008c). In this work, we thus present a quantitative metabolomics characterization of the effect of sodium ion on *C. acetobutylicum* ATCC 824, using NaCl as model compound. We proposed the high NaCl inhibition effect to be mainly attributed to sodium ion rather than from chloride, based on Maddox *et al*. who showed supplementing 10 g L^{-1} NaCl inhibits *C. acetobutylicum* growth rate of 40% but without any significant effect when adding 10 g L^{-1} ammonium chloride (NH_4Cl) (Maddox et al., 1995). Fermentations were performed using a synthetic medium with xylose as the unique carbon source, the major sugar issued from the hydrolysis of black spruce used in the Canadian pulp and paper industry, and the cells metabolome was characterized. Here, we show that *C. acetobutylicum* ABE metabolism is unaffected by sodium inhibition, with a decrease in biomass growth but not the ABE specific productivity.

4.4 **Methods**

4.4.1 **Cell culture**

C. acetobutylicum ATCC 824 was used in this study. The cells were stored at -80 ˚C in 20% (v/v) glycerol. Reinforced clostridia medium (RCM) was used to thaw the cells and for inoculum preparation. RCM consists of peptone (10 g L^{-1}), beef extract (10 g L^{-1}), yeast extract (5 g L^{-1}), xylose (5 g L^{-1}) (glucose replacement), starch (1 g L^{-1}), NaCl (5 g L^{-1}), sodium acetate (3 g L^{-1}), L-cysteinium chloride (0.5 g L^{-1}) and resazurin (0.025%, 4 mL L^{-1})(Rajagopalan et al., 2012). Modified clostridia growth medium (CGM) with xylose (80 g L^{-1}, prepared apart from medium) replacing glucose, was used as fermentation medium. The CGM medium contains K_2HPO_4 (0.75 g L^{-1}), KH_2PO_4 (0.75 g L^{-1}), $MgSO_4 \cdot 7H_2O$ (0.7 g L^{-1}), $MnSO_4 \cdot 5H_2O$ (0.017 g L^{-1}), $FeSO_4 \cdot 7H_2O$ (0.01 g L^{-1}), $(NH_4)_2SO_4$ (2 g L^{-1}) and L-asparagine (2 g L^{-1}), p-aminobenzoic acid (0.004 g L^{-1}), sodium acetate (CH_3COONa) (30 mM or 2.5 g L^{-1}), yeast extract (5 g L^{-1}) and resazurin (0.025%, 4 mL L^{-1}) (Choi et al., 2012). The pH of all media was adjusted at 6.8 using 2 M KOH prior to autoclaving at 121˚C for 20 min, and 5 g L^{-1} $CaCO_3$ was added in CGM fermentation medium as pH buffer (Raganatia et al., 2012; Richmond et al., 2011).

Batch fermentation cultures were performed in 500 mL serum bottles with 200 mL loading volume. All media were continuously sparged with filtered (0.2 um) 100% nitrogen gas for ensuring oxygen removal after autoclaving. Resazurin indicates the presence of oxygen by colour transformation from pink to transparent in the culture media. Culture inocula were grown anaerobically in RCM under 150 rpm for 20 h at 37 ˚C until reaching an optical density (600 nm) of 2.5 - 3.0, and then transferred into the fermentation medium (CGM). Inocula manipulations and culture sampling were performed using sterile syringes and needles, which were nitrogen gas (filter sterilized: 0.22 µm, Millipore) treated for removing O_2 from the syringe reservoir prior to contacting medium. The xylose water solution was filter sterilized (0.22 µm, Millipore) and incorporated into the autoclaved medium under a laminar flow hood. Inoculation volume was at 5 % (v/v) for a resulting initial culture with an OD 600 adjusted at ~ 0.15. NaCl was supplemented at 10 g L^{-1} (i.e. 170mM) in the fermentation medium of the test group, or as described.

4.4.2 Culture sampling and metabolites extraction

Samples were taken every 12 h from 0 h (immediately after inoculation) to 108 h, with 10 time points. Cultures were conducted in triplicate. A total of 10 sampling time points, in triplicate, were used for cell density, pH, cell dry weight and intracellular metabolites quantification (error values are standard deviations). Biomass was first determined by measuring the cell suspension optical density, and the cell dry weight concentration (gDW L^{-1}) was then estimated using a predetermined correlation ($y = 0.2182x + 0.0873$; where y represents cell dry weight (gDW L^{-1}); x represents OD600 value; R^2 is 0.985). Culture samples were first centrifuged at 20,000 g (4 ˚C) for 5 min, and the cells were then re-suspended in distilled water for cell density detection at 600 nm in order to avoid medium components such as resazurin, which interferes with optical density measurements.

To enable the reliable quantification of intracellular compounds including energetic nucleotides (ATP, ADP, AMP, GTP), redox (NAD(H), NADP(H)), sugar phosphates (X5P, R5P, F6P, G1P, G6P, GA3P) and organic acids (PYR, SUC, FUM, MAL, (ISO)CIT, α-KG), the culture samples' volume was taken to obtain about 0.1 g wet weight, the minimum cell mass required for intracellular quantification. Culture samples were centrifuged at 20,000 g (4 ˚C) for 10 min, and the cell pellet was washed two times by PBS, then extracted by 80 % cold methanol (0.5 mL), vortexed for 2 min and placed 10 min for ultrasonic treatment in ice water, and then centrifuged 10 min (4 ˚C; 20,000 g). After transferring the supernatant into a new tube, cells were re-extracted with 0.5 mL of 50 % cold methanol. The two successive extracts of the same cell sample were combined in a unique tube and stored at - 80 ˚C for further analysis. A more precise analysis list and protocols are described in the 3.2 Metabolomic analysis, or as a previous publication (Ghorbaniaghdam et al., 2014).

Extracellular solvents (ABE) were extracted by ethyl acetate. 1 mL of ethyl acetate was introduced into a glass vial containing 0.4 mL of fermentation supernatant, 0.1 mL internal standard (isobutanol 216.7 mM) and 0.1 mL buffer (pH 6.2, 1 M K_2HPO_4 and 1 M KH_2PO_4). The extraction mix was vortexed for 2 min and kept at room temperature for 3 h. Then the upper layer of the organic phase was separated by centrifugation, passed through a 0.22 µm PTFE filter (Millipore, Etobicoke, Canada) and stored at - 80 ˚C for further analysis (Gerchman et al., 2012). Extracellular

acetic and butyric acids were obtained by centrifuging the culture sample at 20,000 g for 10 min, and the suspension was diluted 2 times by 5 mM H_2SO_4, and then filtered and kept at - 80 ˚C for further HPLC analysis.

4.4.3 Analytical and calculation methods

An HPLC system (Agilent, Quebec, Canada) equipped with a 6460 triple quadrupole mass spectrometer was used for analyzing energetic nucleotides, organic acids, and sugar phosphate concentration. All analytical protocols for metabolites quantification were described in Ghorbaniaghdam's article (Ghorbaniaghdam et al., 2014). A Perkin-Elmer Clarus 480 GC with a FID detector (PerkinElmer, Quebec, Canada) equipped with the Elite-WAX ETR (30 m, 0.32 mm I.D.) column was used for ABE analysis. The mobile phase was a mixed gas of air and hydrogen fed at flow rates of 200 mL min^{-1} and 20 mL min^{-1}, respectively (Gerchman et al., 2012). Quantification of acetic and butyric acids were performed on a waters HPLC system, equipped with a 2777 auto-sampler (Waters Canada), 1525 binary pump (Waters Canada) and 996 PDA (Photodiode Array) detector (Waters, Canada). Acetic and butyric acids were separated on Aminex HPX-87H column and guard column (Bio-rad, Canada) with a mobile phase of 5 mM H_2SO_4 at a flow rate of 0.6 mL min^{-1}. The column temperature was set at 50 ˚C. 20 µL sample solution was injected to the column for running time of 30 min. The data was collected at the absorbance of 210 nm and processed by Masslynx 4.0 software (Waters Canada) (Ahmed et al., 2015).

Calculation of the substrates and end-products consumption and synthesis rates were performed using the following equation: $v = \frac{C_{t+12h} - C_t}{12}$, where C_t is a substrate (end-product) concentration at time point t; C_{t+12h} is a substrate (end product) concentration at time point t+12h; and specific rates were calculated dividing the rates v by the average biomass for the time period between time t and t+12h.

4.5 Results and Discussion

4.5.1 Identifying sodium threshold concentration affecting biomass growth

Prior to conducting the metabolomic evaluation of the effect of NaCl inhibition on ABE fermentation, we first determined the inhibitory threshold concentration value of sodium ion under

the experimental conditions of this work. From an initial content of 30 mM sodium acetate (i.e. sodium ion) in clostridia growth medium (CGM) medium, cultures were performed supplementing with 0 g L^{-1} (0 mM), 5 g L^{-1} (85 mM), 10 g L^{-1} (170 mM) and 15 g L^{-1} (256 mM) NaCl. Results (Figure 4.1) confirmed a culture behaviour similar to that reported in literature for *Clostridium*, with a significant cell growth inhibition observed from 10 g L^{-1} NaCl supplement (Richmond et al., 2011). All cultures were repeated three times independently under the four tested concentrations. Error bars represent the standard deviation of the three replicates. Results show that the NaCl inhibition effects under these concentrations were repeatable.

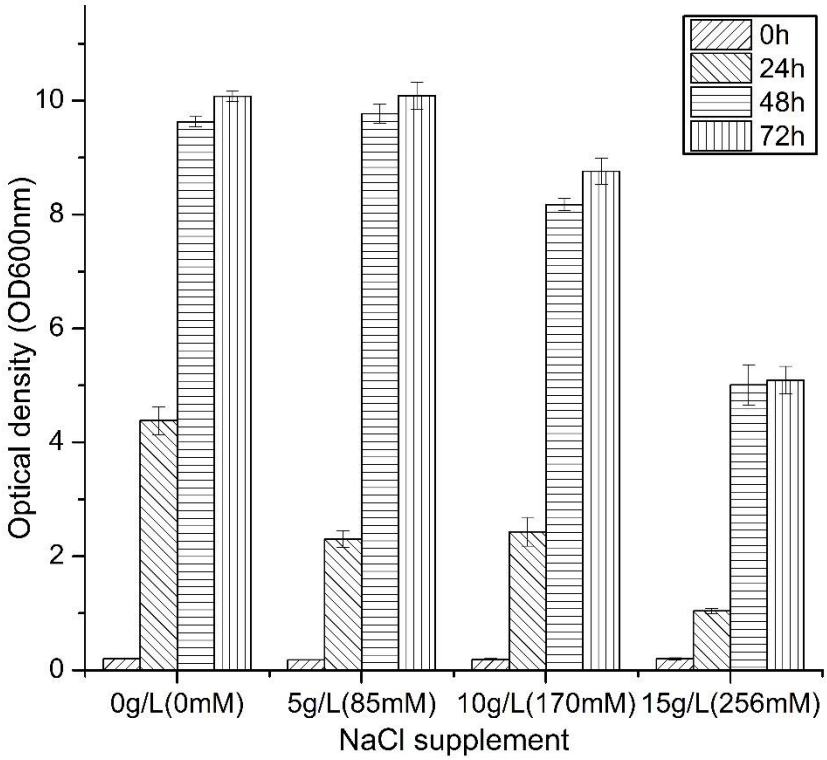

Figure 4. 1 Effect of NaCl addition to CGM medium on *C. acetobutylicum* ATCC 824 grown on xylose. Axis unit is optical density at 600nm. Error bars represent standard deviations from three independent replicates (n=3).

In our study, supplements of 10 and 15 g L^{-1} NaCl resulted in 15.05 ± 1.94 % and 47.99 ± 3.93 % lower maximum biomass levels than the control (0 mM NaCl supplement) at 48 h, and in 13.09 ± 1.51 % and 49.42 ± 2.83 % less biomass at 72 h, respectively. These results are in agreement with that of Qureshi et al. (2008), who studied the *Clostridium* genus showing that 10 g L^{-1} sodium

inhibits biomass growth and ABE production, and that there is no cell growth when it reaches 25 g L^{-1} (Qureshi et al., 2008c). Therefore, since a 170 mM NaCl supplement (for a total of 200 mM sodium ion) affects cell behaviour without being lethal, a prerequisite condition for enabling a reliable quantitative metabolomics analysis, this study has focused on challenging ABE fermentation supplementing with 170 mM NaCl.

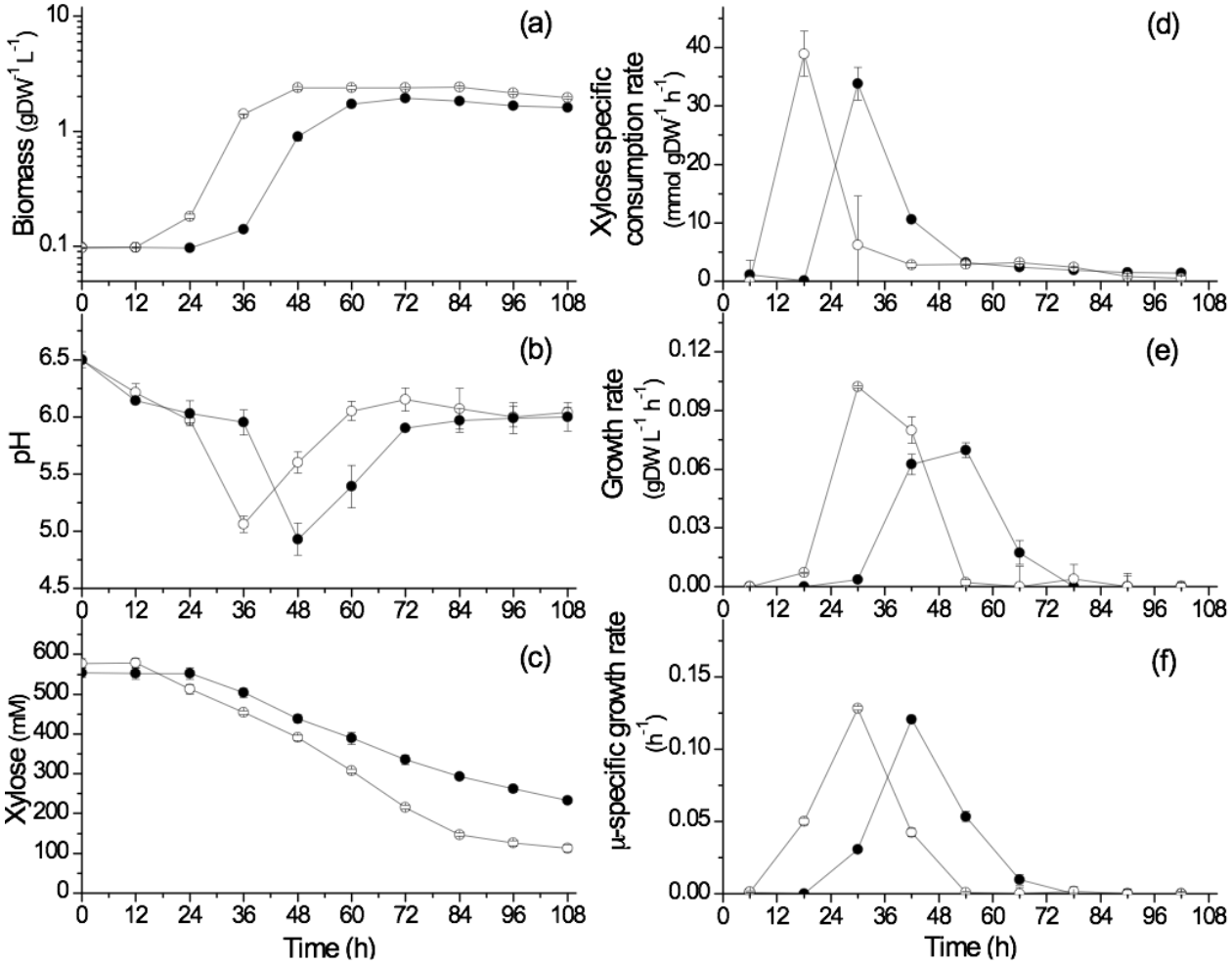

Figure 4. 2 Effect of NaCl addition on (a) *C. acetobutylicum* ATCC 824 biomass growth in batch culture on xylose; (b) pH; (c) xylose concentration; (d) xylose specific consumption rate. ● 170 mM NaCl addition culture and ○ the control culture. Error bars represent standard deviations from three independent replicates (n=3).

4.5.2 Sodium affects biomass and ABE production metabolism

Cultures were performed using a NaCl supplement of 170 mM (i.e. 200 mM sodium ion total). At stationary phase, an average optical density of 7.76 ± 0.55 (OD 600 nm; 60-108h), which corresponds to 1.79 ± 0.12 gDW L^{-1} (cell dry weight), was obtained and represented 74.9 ± 3.33% of that for the control group (average OD600 of 10.47 ± 0.10 and 2.39 ± 0.022 gDW L^{-1} at 48 - 84 h) (Figure 4.2a). Of interest, also supplementing of 170 mM NaCl a culture of *C. beijerinckii* BA101 grown on spray-dried soy molasses medium, Qureshi *et al*. have reported a reduced maximum biomass concentration of 0.6 g L^{-1} compared to 1.7 g L^{-1} in the control group (Qureshi et al., 2001). The inhibitory effect of high sodium also resulted in a lower maximum growth rate with 0.069 ± 0.0038 gDW L^{-1} h^{-1} compared to 0.102 ± 0.0056 gDW L^{-1} h^{-1} (Figure 4.2e). However, in this work the maximum specific growth rate (μ_{max}) was slightly lower in the NaCl group with 0.121 ± 0.0023 h^{-1} compared to the control group (0.128 ± 0.0013 h^{-1}) (Figure 4.2f). In *E. coli*, it has been reported that the μ_{max} decreased by about 80 % when supplemented with 684 mM NaCl (40 g L^{-1}) (Qureshi et al., 2006).

In agreement with our results on cell growth, a lower xylose consumption rate was observed at high sodium. At exponential growth, cells uptake xylose at a rate of 33.83 ± 2.79 mmol gDW^{-1} h^{-1} in the NaCl group, which is 13.2 ± 1.08 % lower than in control group (38.95 ± 3.82 mmol gDW^{-1} h^{-1}) (Figure 4.2d). Moreover, it is clear from our results that high sodium condition affects the growth lag phase, which is prolonged of 12 h compared to the control group, explaining consequently delayed xylose uptake and solventogenesis. As revealed by cultures pH (Figure 4.2b), acidogenesis takes place the first 36 h followed by solventogenesis in the control culture, while a 12 h delay is observed in the high sodium group (i.e. at 48 h). Therefore, high sodium condition postpones cell growth and affects the final biomass and the growth rate of *C. acetobutylicum* ATCC 824. High sodium may thus divert the cell metabolism and resources towards the management of membrane transporters and channels. The cells are thus investing a significant amount of resources for staying functional and this adaptation phenomenon may explain, in part, the observed lag phase. Meanwhile, solvents production decreased under NaCl supplementation (Figure 4.3) Butanol decreased by 33.37 ± 0.74 % with a final butanol concentration of 152.14 ± 2.35 mM (i.e. 11.26 ± 0.17 g L^{-1}) compared to 228.33 ± 1.62 mM (i.e. 16.90 ± 0.12 g L^{-1}) in the control group (84 h;

Figure 4.3c). Acetone and ethanol final concentrations also decreased by 35.14 ± 3.50 % and 22.95 ± 1.81 %, respectively (see details in Table 4.1).

Table 4. 1 Growth and productivity of *C. acetobutylicum* ATCC 824 batch culture on xylose with or without a 170 mM NaCl supplement. All values are maximum values taken from Figure 4.2 and Figure 4.3 or calculated using two successive points, identifying the maximum value; ± values represent standard deviation for n=3.

10g L^{-1} NaCl supplement	**Butanol**	**Acetone**	**Ethanol**	**Acetic acid**	**Butyric acid**
	Solvents and acid production (mM)				
NaCl group	152.14±2.35	73.84±2.45	108.05±4.09	79.40±2.83	22.46±1.71
Control group	228.33±1.62	113.85±2.35	140.24±2.33	69.77±1.56	26.09±0.32
	Specific productivity (mmol gDW^{-1} h^{-1})				
NaCl group	5.09±0.36	2.54±0.13	3.43±0.12	7.93±2.08	3.26±0.37
Control group	4.93±0.14	2.25±0.37	3.05±0.23	6.56±1.15	2.42±0.06
Biomass					
	OD600	Dry weight ($gDW\ L^{-1}$)	Growth rate ($gDW\ L^{-1}\ h^{-1}$)	Specific growth rate (h^{-1})	Xylose specific consumption rate (mmol gDW^{-1} h^{-1})
NaCl group	8.43±0.33	1.94±0.01	0.069±0.0038	0.121±0.0023	33.83±2.79
Control group	10.61±0.21	2.41±0.05	0.102±0.0056	0.128±0.0013	38.95±3.82

Analyzing the cell specific productivity in ABE, we observed maximum acetone and butanol specific productivities of 2.40 ± 0.141 mmol gDW^{-1} h^{-1} and 5.01 ± 0.080 mmol gDW^{-1} h^{-1}, respectively, which were reached simultaneously between 48 h and 60 h at similar levels in both the control and the NaCl groups (Figure 4.3b, d). Productivities, which first rapidly increased from ~ 36 h (control) and ~ 48 h (NaCl) then rapidly decreased at basal levels. Interestingly, ethanol productivity exhibited twin peaks postponed of 12 h between NaCl and control groups (Figure 4.3f). The turning point between the two peaks coincided with the culture shift from acidogenesis to solventogenesis (Figure 4.2b). Aldehyde-alcohol dehydrogenase (AAD) is involved in the synthesis of both butanol and ethanol from butyryl-CoA and acetyl-CoA, respectively. However, Nair and Papoutsakis demonstrated that AAD primary role is the formation of butanol rather than ethanol (Nair & Papoutsakis, 1994). Therefore, butanol formation is obtained in priority when cells

sense a hostile environment (i.e. low pH) during the shift between acidogenesis and solventogenesis, a phenomenon which may explain the ethanol productivity variation.

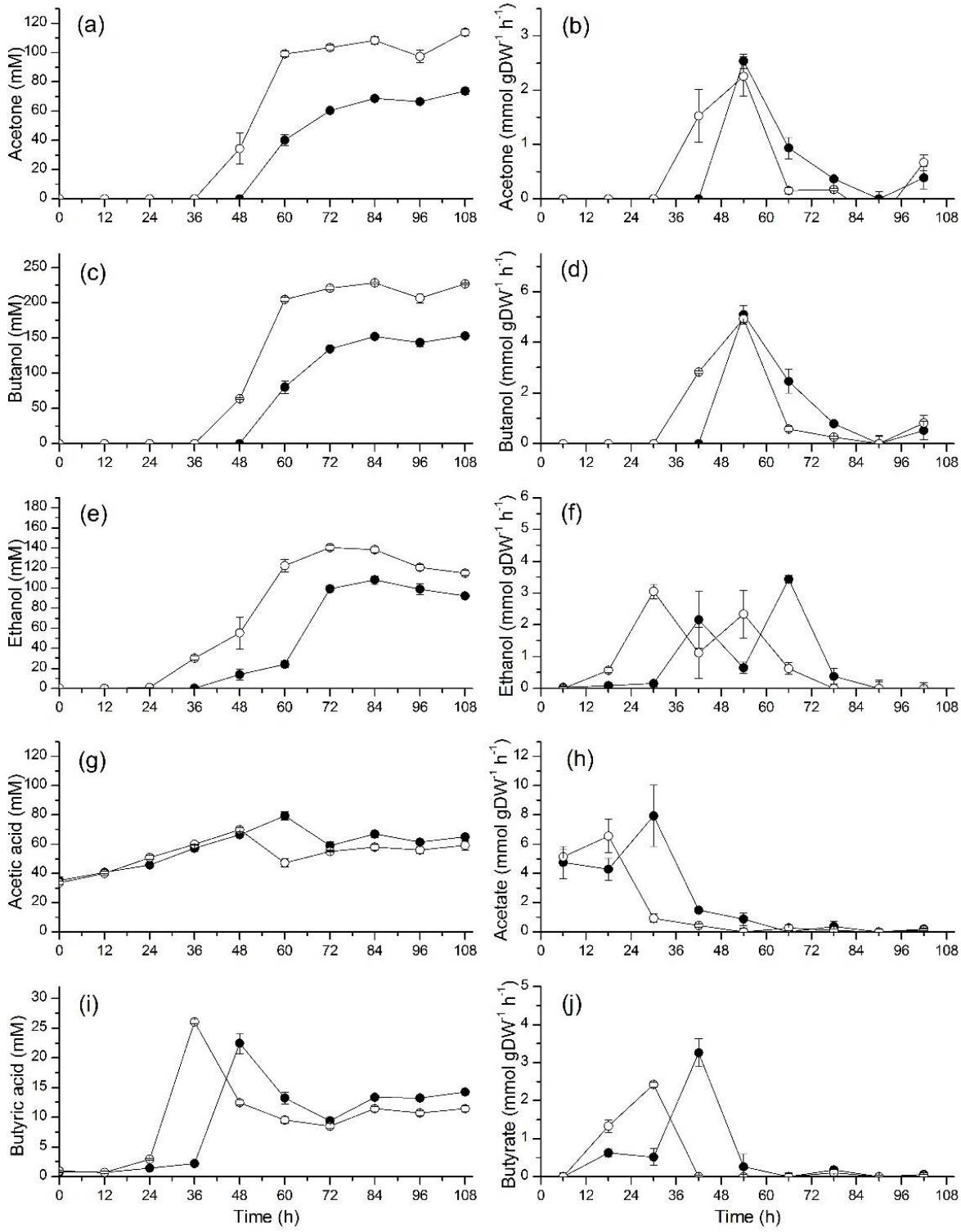

Figure 4. 3 Effect of NaCl addition on ABE yield and specific productivity profiles on acetone (a, b), butanol (c, d), ethanol (e, f), acetic acid (g, h), butyric acid (i, j) in *C. acetobutylicum* ATCC 824 batch culture on xylose. ● 170 mM NaCl addition culture and ○ the control culture. Error bars represent standard deviations from three independent replicates (n=3).

As intermediate products, acetic and butyric acids are the main medium pH effectors. Interestingly, in high sodium group, butyric acid was inhibited at maximum value but acetic acid showed having been promoted. Therefore, these two factors combined may explain the similar pH levels observed in NaCl and control groups. Meanwhile, acetic and butyric acids are also the major metabolic precursors for solvents formation (Wang et al., 2013). Butyric acid reached a peak of 22.46 ± 1.71 mM at 48 h in the NaCl group compared to 26.09 ± 0.32 mM at 36 h in the control group, then decreased to stable levels in both groups (Figure 4.3 i). Acetic acid reached a peak of 79.40 ± 2.83 mM at 60 h in the NaCl group compared to 69.77 ± 1.56 mM at 48 h in the control group, which was postponed by 12 h, the same phenomenon in butyric acid (Figure 4.3g). Of interest, the specific productivity of both acetic and butyric acid remained at higher levels in the NaCl group, which may be related to a depressed conversion rate from acids to solvents. It has been reported that acetoacetyl-CoA:acetate(butyrate) CoA-transferase, which is solely responsible for acetate and butyrate conversion into acetate-CoA and butyrate-CoA (Hartmanis & Gatenbeck, 1984), is inhibited by sodium ions (Hartmanis et al., 1984). Therefore, it seems reasonable that at high sodium the high osmotic pressure led to higher intracellular sodium concentration, which has then resulted in higher extracellular levels in both acetic and butyric acids concentration in NaCl group during solventogenesis (Figure 4.3h, j).

Therefore, high sodium concentration condition was clearly shown to inhibit cell proliferation as well as final solvents and acids production, but it has led, surprisingly, to similar ABE specific productivity levels to those in the control group. With respect to NaCl effect on cells, Shi *et al*. proposed that osmotic pressure is the main effect from supplementing NaCl, dehydrating the cell periphery and thus altering cell membrane permeability (Shi et al., 2011). Meanwhile, Barth *et al*. reported that NaCl has a direct impact blocking DNA amplification from *H. salinarum* cells (Barth-Jr. et al., 2012). Therefore, we have thus extended our study to the cells quantitative metabolomics in order to better understand preserved cell productivities in ABE.

4.5.3 **High sodium stimulates energy metabolism in acidogenesis**

Cell energetics is considered to considerably limits anaerobic organisms (Thauer et al., 1968). However, ATP concentration has been identified as a main signal indicating the shift from acidogenesis to solventogenesis in *C. acetobutylicum* (Grupe & Gottschalk, 1992), which is accompanied by a change in pH. In the present study, in both culture groups where ATP accumulation occurred concurrently to pH decrease (acidogenesis), the pH stopped declining when the ATP reached a maximum value and the cells showed that they had entered solventogenesis, i.e., both cultures of NaCl and control groups reached similar maxima at 48 h (0.429 ± 0.070 vs. 0.465 ± 0.119 µmol gDW^{-1}) (Figure 4.4). This result agrees with what Grupe and Gottschalk (1992) obtained - that the ATP concentration increases while the pH decreases, and reaches a maximum value (~ 6.5 mmol $(mg\ protein)^{-1}$) while the pH stopped declining and the cells accessed the solvent-generating phase (Grupe & Gottschalk, 1992). Meanwhile, under controlled pH conditions, Meyer and Papoutsalis (1989) observed that the ATP concentration was significantly lower in solventogenesis (pH controlled at 6.0) than acidogenesis (pH controlled at 4.0) (Meyer & Papoutsakis, 1989b). The same results were obtained by other researchers - the cell ATP content decreased at low levels when entering the solvent-producing phase (Meyer & Papoutsakis, 1989b; Sivagnanam et al., 2012). Investigating the mechanism, Lutke-Eversloh *et al*. reported that during exponential growth, *C. acetobutylicum* metabolizes carbohydrates into acetic and butyric acids while generating a surplus of ATP (Lutke-Eversloh, 2014). Moreover, Gottwald *et al*. attributed the ATP decrease of *C. acetobutylicum* metabolism to the high acid concentration, where the ATP demand is high to increase membrane active (ATPases) permeability for maintaining physiological internal pH (Gottwald & Gottschalk, 1985).

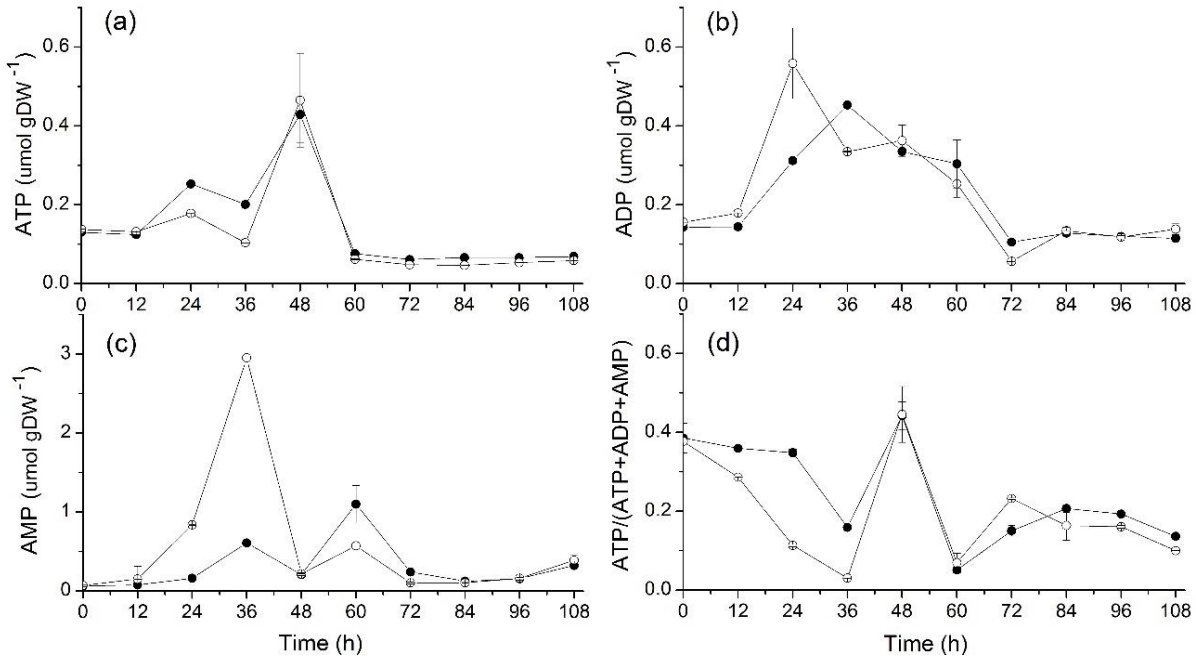

Figure 4. 4 Effect of NaCl addition on *C. acetobutylicum* ATCC 824 energy state in batch culture on xylose. (a) ATP; (b) ADP; (c) AMP; (d) ATP-to-(ATP+ADP+AMP) ratio. ● 170 mM NaCl addition culture and ○ the control culture. Error bars represent standard deviations from three independent replicates (n=3).

In *Clostridium*, Vasconcelos *et al*. observed an ATP concentration of 0.62 ± 0.11 µmol gDW^{-1} using glucose and 1.65 ± 0.15µmol gDW^{-1} with glycerol-glucose in a continuous phosphate-limited culture (Vasconcelos et al., 1994). In the present study, using xylose as the unique carbon source, a maximum ATP value of 0.465 ± 0.119 µmol ATP gDW^{-1} was obtained. One can expect lower cell energetics with xylose, since 5/3 ATP and 5/3 NADH are obtained from each molecule of xylose converted to pyruvate, compared to 2 ATP and 2 NADH for glucose (Gheshlaghi et al., 2009). However, Meyer and Papoutsalis reported 0.64 to 5.1 µmol ATP gDW^{-1} for different glucose feeding rates in continue culture, and even reached a peak of 15 - 20 µmol ATP gDW^{-1} in a pH controlled (pH 4.0) culture with 80 mM glucose and NH_4^+ supply (Meyer & Papoutsakis, 1989b). Therefore, a similar trend is observed for ATP concentration, with an accumulation concurrently to acids generation and a decrease with solvents formation. Meyer and Papoutsalis have also reported that glucose limitation results in a lower ATP concentration in continuous culture, with 0.9 µmol gDW^{-1} versus 4.8 µmol gDW^{-1} (Meyer & Papoutsakis, 1989b). In addition, Girbal and Soucaille have studied the effect of using pyruvate and glucose as carbon sources at

various ratios in *C. acetobutylicum*, and reported that ATP concentration decreased from 1.6 ± 0.15 μmol gDW^{-1} using only glucose to 0.3 ± 0.1 μmol gDW^{-1} using a pyruvate-to-glucose ratio of 0.67, while ADP concentration increased from 1.8 ± 0.2 μmol gDW^{-1} to 2.7 ± 0.4 μmol gDW^{-1} (Girbal & Soucaille, 1994). Therefore, as expected, the carbon source plays a key role on the energetic metabolism behaviour.

Table 4. 2 Energetics of *C. acetobutylicum* ATCC 824 batch culture on xylose with or without a 170 mM NaCl supplement. All values are maximum values taken from Figure 4.4 or calculated using two successive points, identifying the maximum value; ± values represent standard deviation for n=3.

	ATP			**ADP**		
	Concentration (μmol gDW^{-1})	Specific rate (μmol gDW^{-1} h^{-1})		Concentration (μmol gDW^{-1})	Specific rate (μmol gDW^{-1} h^{-1})	
		increasing	decreasing		increasing	decreasing
NaCl	0.429±0.070	0.030±0.002	0.034±0.003	0.453±0.002	0.032±0.004	0.016±0.002
Control	0.465±0.119	0.019±0.001	0.030±0.001	0.559±0.089	0.014±0.002	0.017±0.001
	AMP			**ATP/(ATP+ADP+AMP)**		
	Concentration (μmol gDW^{-1})	Specific rate (μmol gDW^{-1} h^{-1})		Ratio	Specific rate	
		increasing	decreasing		increasing	decreasing
NaCl	1.101±0.138	0.172±0.008	0.228±0.022	0.442±0.035	0.035±0.004	0.030±0.002
Control	2.955±0.060	0.074±0.005	0.072±0.004	0.445±0.071	0.024±0.005	0.032±0.001

Present results also suggested that high sodium concentration favours maintaining high ATP level and ATP-to-(ATP+ADP+AMP) ratio in acidogenesis, but to a negligible extent in solventogenesis (Figure 4.4). At 36 h the ATP level in the control group was ~ 50% lower than in the NaCl group, which indicated the ATP level was stimulated or leading to a lower demand by high sodium during acidogenesis. Meyer and Papoutsakis observed that higher ATP ratio coincides with higher cell growth rate and reduced butanol production in continuous culture under non-limited glucose condition (Meyer & Papoutsakis, 1989a). These authors concluded ATP concentration behaviour may regulate acids and solvents formation and conversion phenomena. Looking at the metabolic pathway (Figure 4.5), only the pathways leading to acetate and butyrate generate one mole ATP each post-glycolysis. Consequently, one can expect high ATP level to be linked to acids

production, and a reduced ATP demand to promote solvents formation. Meanwhile, induction of ATP metabolism has been performed on *C. acetobutylicum* by carbon monoxide (CO) gassing experiment, resulting in a rapid increase of ATP concentration and ATP-to-ADP ratio by almost 400% 1 min after CO feeding (Meyer & Papoutsakis, 1989b). Papoutsakis *et al*. also reported CO feed increases ATP concentration, accompanied by the inhibition of cells growth by 50% and of 100% H_2 formation, but with improved butanol specific production rate. All these findings support that both ATP concentration and turnover rate play a key role during solvents production (Kim et al., 1984; Meyer et al., 1986). In the present study, it was found that high sodium condition reduced the ATP demand and also coincided with lower cell growth rate (Figure 4.2e), but with a negligible impact on solvents specific productivity. Higher ATP level during acidogenesis in NaCl group may partly (with osmotic change, for instance) be attributed to the decrease of membrane permeability, which may affect nutrients uptake mechanisms, explaining reduced cell metabolic activity and biomass accumulation.

4.5.4 **High sodium affects cell central carbon metabolism**

Cell energetic robustness, which can partly explain maintained ABE solvents productivity levels, was further studied investigating the central carbon metabolism. A comparative analysis of the primary and key intermediate metabolites was further performed (Figure 4.5). Firstly, being the entry point product from xylose in the PPP pathway, xylulose-5-phosphate (X5P) plays a key role in controlling carbon flow through the cell metabolic network. X5P maximum cell concentration was inhibited of 79.50 ± 3.82 % under high sodium (0.329 ± 0.034 µmol gDW^{-1} compared to 1.609 ± 0.021 µmol gDW^{-1} in the control group) (Figure 4.6a), and this peak was delayed 12 h so as for the cell growth state (Figure 4.2a, e, f), as discussed previously. Moreover, since xylulose kinase is downregulated at the acid-solvent phase shift, demonstrated by proteomic analysis (Sivagnanam et al., 2012), it was also expected that ribose-5-phosphate (R5P) followed a similar trend than X5P (Figure 4.6b). As the main precursor of DNA synthesis, R5P is related to cell proliferation. R5P concentration behaviour coincided with biomass growth, reaching a maximum value of 1.087 ± 0.051 µmol gDW^{-1} at 36 h in the control group, but only 0.209 ± 0.023 µmol gDW^{-1} in the NaCl group at 48 h, representing an 80.73 ± 1.47 % inhibition of that in the control culture during acidogenesis. However, these peaks (for X5P, R5P, etc) are in sharp contrast with the slow and regular decrease in the extra-cellular xylose concentration time course curve, which suggests that

these intermediaries had accumulated rapidly at the beginning of fermentation (acidogenesis), until solventogenesis started and channelled this overflow of intermediaries. As shown in solventogenesis, X5P and R5P significantly decreased at similar levels under both culture conditions, with even slightly higher levels at 84 h in the NaCl culture. X5P and R5P reached, respectively, 0.15 ± 0.027 and 0.095 ± 0.016 µmol gDW^{-1} in NaCl compared to 0.03 ± 0.002 and 0.014 ± 0.004 µmol gDW^{-1} in the control group. The sugar-phosphates of glycolysis such as glucose-6-phosphate (G6P) (Figure 4.6d), fructose-6-phosphate (F6P) (Figure 4.6c) as well as glucose-1-phosphate (G1P) (Figure 4.6e), also showed slightly higher levels at 84 h in NaCl than in the control. These results thus suggest that the high sodium concentration further affect the main carbon metabolism when cells progress into solventogenesis, but the mechanism of induction is still unclear and requires further focused experimental work.

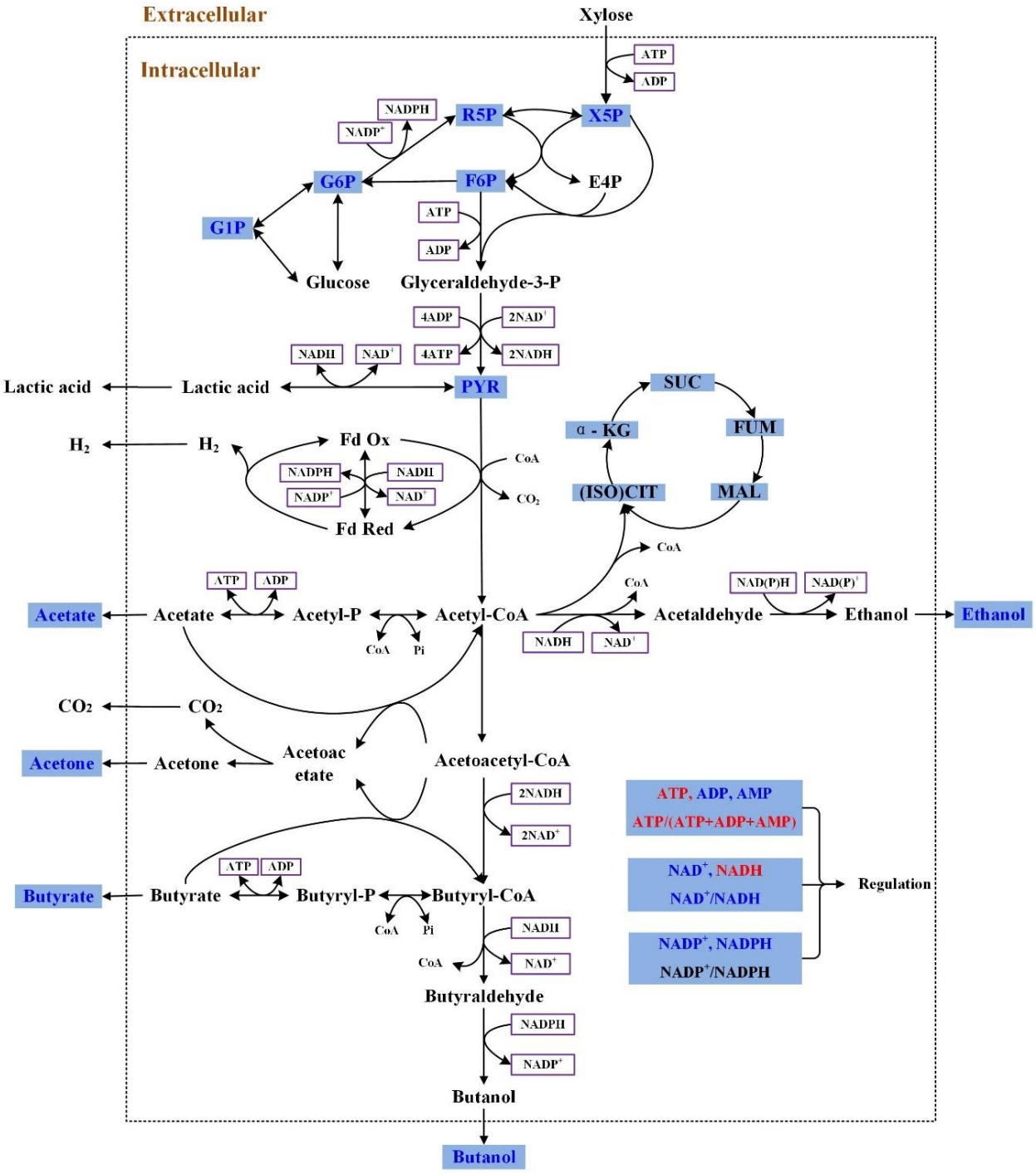

Figure 4. 5 Comparative analysis of metabolites concentration behaviour involved in *C. acetobutylicum* ATCC 824 during acidogenesis with and without supplementing sodium. Light blue shade indicates metabolites measured in this study, in which: blue-written metabolites refer to concentration decrease and red-written metabolites refer to concentration increase, all compared to control low sodium concentration, whereas black-written metabolites were not

quantified being below the detection limit of the analytical method (i.e. TCA metabolites) or showing unaffected concentrations (i.e. $NADP^+$-to-NADPH ratio) at high sodium concentration during acidogenesis. G1P: glucose 1-phosphate; G6P: glucose 6-phosphate; F6P: fructose 6-phosphate; X5P: xylulose 5-phosphate; R5P: ribose 5-phosphate; PYR: pyruvic acid; α-KG: α-ketoglutaric acid; SUC: succinic acid; FUM: fumaric acid; MAL: malic acid; (ISO)CIT: (iso) citric acid; Fd Ox: Ferredoxin (oxidized) ; Fd Red: Ferredoxin (reduced).

More precisely, R5P concentration increased at a specific rate of 0.051 ± 0.003 µmol gDW^{-1} h^{-1} and 0.008 ± 0.0003 µmol gDW^{-1} h^{-1} concurrently to the maximum cell growth phase, respectively in control (24-36 h) and NaCl (36-48 h) group. The increased rate in the control group being 6.37 times that in the NaCl group. A similar trend has also been observed for X5P, the following metabolite of R5P in PPP, with 0.085 ± 0.003 µmol gDW^{-1} h^{-1} and 0.013 ± 0.0004 µmol gDW^{-1} h^{-1} in control (24-36 h) and NaCl (24-36 h) groups, respectively. The rate in the control group being 6.54 times that in the NaCl group. Interestingly, the maximum specific rate of biomass at exponential phase was only 1.48 times that in the NaCl group. Therefore, although X5P and R5P are directly involved in cell growth, NaCl inhibition seems, apparently, to result in the decoupling of biomass growth and metabolites concentration management in the PPP in acidogenesis.

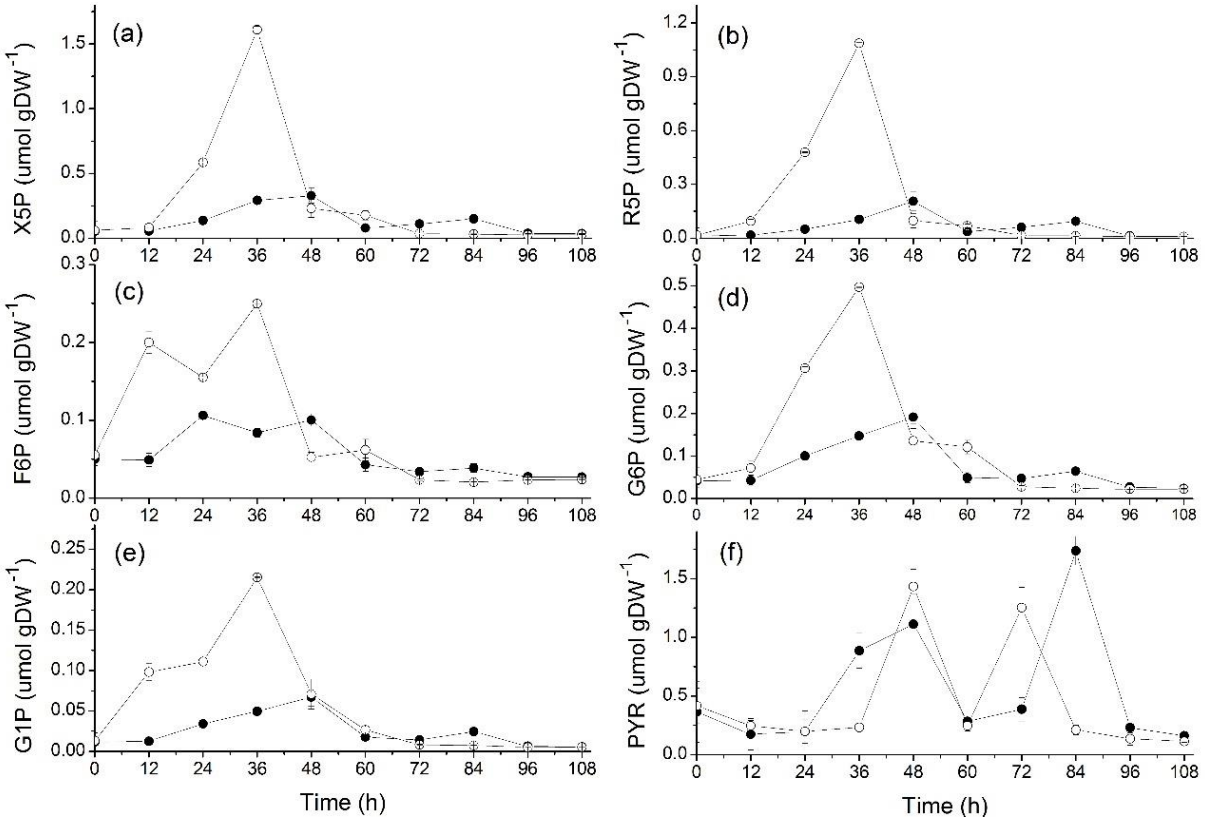

Figure 4. 6 Effect of NaCl addition on PPP and glycolysis pathway in *C. acetobutylicum* ATCC 824 batch culture on xylose. (a) X5P; (b) R5P; (c) F6P; (d) G6P; (e) G1P; (f) PYR. ● 170 mM NaCl addition culture and ○ the control culture. Error bars represent standard deviations from three independent replicates (n=3).

Strongly interconnected to PPP, metabolic intermediates of the glycolytic pathway showed to follow a similar trend, indeed, F6P, G6P and G1P showed being seriously depressed at high sodium. While these metabolic intermediates do increase during acidogenesis (see Table 4.3 for rate values), but to a much lesser extent in the NaCl group, they then decreased to similar values (close to initial basal levels) to that in the control in solventogenesis. The trend for these metabolic intermediates of glycolysis is thus similar to that of R5P and X5P. Interestingly, F6P expressed two peaks during acidogenesis in both culture groups (Figure 4.6c), a phenomenon that may be conditioned by the fact that F6P is at the branch point between PPP and glycolysis pathway, and thus affected by various interconnected and competitive fluxes. We also observed that high sodium resulted in 80.73 ± 1.47 % and 68.84 ± 3.42 % lower metabolic intermediates maximum

concentrations for the PPP and the glycolytic pathway, respectively (Table 4.3). High sodium thus inhibited growth-related metabolism, leading to a lower biomass production.

Table 4. 3 *C. acetobutylicum* ATCC 824 content in sugar phosphates, pyruvate and redox nucleotides in batch culture on xylose with or without a 170 mM NaCl supplement. All values are maximum values taken from Figure 4.6 and Figure 4.7 or calculated using two successive points, identifying the maximum value; ± values represent standard deviation for n=3.

	X5P	**R5P**	**F6P**	**G6P**	**G1P**	**PYR**
	Concentration value (µmol gDW^{-1})					
NaCl group	0.329±0.034	0.209±0.023	0.106±0.002	0.191±0.011	0.067±0.001	1.737±0.121
Control group	1.609±0.021	1.087±0.051	0.250±0.012	0.497±0.004	0.215±0.003	1.431±0.148
	Increasing specific rate (µmol gDW^{-1} h^{-1})					
NaCl group	0.013±0.0004	0.008±0.0003	0.005±0.0003	0.005±0.0002	0.001±0.0001	0.113±0.010
Control group	0.085±0.003	0.051±0.003	0.012±0.001	0.022±0.003	0.009±0.001	0.124±0.006
	NADH	**NAD^+**	**NADPH**	**$NADP^+$**	**NAD^+ /NADH**	**$NADP^+$ /NADPH**
	Concentration value (µmol gDW^{-1})					
NaCl group	21.87±0.821	5.38±0.921	0.702±0.024	1.112±0.032	8.06±0.235	1.584±0.032
Control group	19.76±0.346	6.98±0.033	1.060±0.042	1.595±0.057	24.03±0.190	1.689±0.013
	Increasing specific rate (µmol gDW^{-1} h^{-1})					
NaCl group	1.804±0.073	0.254±0.014	0.046±0.001	0.074±0.015	0.313±0.018	/
Control group	1.631±0.018	0.359±0.033	0.049±0.002	0.066±0.001	0.602±0.013	/

Pyruvate (PYR) is at the main branch point of the central carbon metabolism leading to anabolic pathways. According to proteomic analysis, pyruvate kinase (CAC0518), pyruvate-formate lyase (CAC0980), pyruvate decarboxylase (CAP0025) and ferredoxin oxidoreductase (CAC2229) were identified in *C. acetobutylicum* (Sivagnanam et al., 2011; Sivagnanam et al., 2012). These enzymes are responsible for pyruvate generation and conversion to formic acid, acetyl-CoA and hydrogen (Figure 4.5). Differing from sugar phosphates of PPP and glycolysis, the two peaks of pyruvate (Figure 4.6f) coincided, interestingly, to the two peaks observed for ethanol production, also respectively during acidogenesis and solventogenesis. This result may be expected knowing that PYR and ethanol are linked by the enzymes pyruvate decarboxylase and alcohol dehydrogenase. In acidogenesis, the peak of PYR under high sodium is 22.4 ± 4.35 % lower than in the control (at 48 h), but when cells enter solventogenesis the maximum PYR concentration in NaCl is 27.9 ±

1.92 % higher (at 84 h) than in the control group (at 72 h). However, it remains unclear why PYR shortly re-accumulates during solventogenesis. Indeed, pyruvate kinase activity has been reported to decrease during the transition from acidogenesis to solventogenesis in xylose-feeded *C. acetobutylicum* cultures (Mao et al., 2010). The specific culture conditions in the present study may have caused a different metabolic rearrangement leading to this sudden PYR peak.

In addition to the PPP and the glycolytic pathway, TCA cycle was also analyzed. Six organic acids were quantified in cell extracts, such as (iso)citric, malic, succinic, fumaric, and α-ketoglutaric acid, but these were all under the detection limit: (iso)citric acid (< 0.154 µmol gDW^{-1}); malic acid (< 0.028 µmol gDW^{-1}); succinic acid (< 0.032 µmol gDW^{-1}; fumaric acid (< 0.0064 µmol gDW^{-1}) and α-ketoglutaric acid (< 0.0048 µmol gDW^{-1}) in both the NaCl and the control groups. For comparison, we have reported a concentration of ~ 4 µmol gDW^{-1} of malic acid in Chinese Hamster Ovary (CHO) cells (Robitaille et al., 2015). However, for the solvent-producing *Clostridium* specific species, Crown *et al*. reported a split TCA cycle theory suggesting that α-ketoglutarate is generated from Re-citrate synthase (CS) (Crown et al., 2011). Meanwhile, Amador-Noguez *et al*. elucidated a complete bifurcated TCA cycle for the same strain (Amador-Noguez et al., 2010), and although several proteins were confirmed belonging to the TCA pathway in *C. acetobutylicum (Sivagnanam et al., 2011)*, current data are still making tedious confirming the active part of the TCA cycle for this strict anaerobic bacterium. Indeed, our data at undetectable levels confirm that the potential active TCA enzymes, if expressed, do maintain the associated metabolic intermediates at very low levels. Therefore, if not absent, the TCA cycle shows a very low concentration level, but the reaction rates were not measured in this work.

In the NaCl group, although xylose consumption rate was 31.49 ± 1.18 % lower than in the control culture (Figure 4.2), the ATP level stayed at higher values than in the control group. This result either suggests an increased ATP production rate, but from other pathways than from xylose catabolism (see Figure 4.4), to face a higher demand for cell maintenance and repair, or a decrease of the ATP rate of utilization because of a reduced metabolic activity. The hypothesis of a reduced metabolic activity in acidogenesis is supported by the observed lower (up to 80.73 ± 1.47 %) concentrations in the intermediate metabolites X5P, R5P, F6P, G6P and G1P at high sodium. A global lower cell content in intermediate metabolites of glycolysis at high sodium may result in a low activity of the pentose phosphate pathway (PPP), which explains a lower growth rate.

Therefore, high sodium condition resulted in a postponed lag phase as well as of the timing of acid/solvent phase switch as well as for the cell concentration in most of the intermediate metabolites, but did not result on delayed behaviour for the cell concentrations in ATP and AMP, as well as for the adenylate energy charge (ATP-to-(ATP+ADP+AMP) ratio) (Figure 4.4).

4.5.5 The cell redox state is robustly controlled

The redox shuttles NAD(H) and NADP(H) are known as biomarkers of microbial metabolic activity with NAD(P)H-dependent enzymes playing a key role in butanol biosynthesis (Liu et al., 2013a). In the present work, in the NaCl group, all four redox shuttles increasing phase occurs at 24-36 h, i.e. delayed of 12 h from that in the control culture. This time-profile coincides with the time distribution of biomass growth and xylose consumption rate (Figure 4.2d). Meanwhile, the four redox shuttles accumulated in acidogenesis and then reduced to basic levels in solventogenesis. This result is in agreement with Grupe and Gottschalk who showed that cells start consuming NAD(P)H accumulated in acidogenesis while entering solventogenesis, thus NAD(P)H level serves as an acid stress signal during the shift from acidogenesis to solventogenesis (Grupe & Gottschalk, 1992). In batch culture, Meyer and Papoutsakis (1989) reported NADH accumulation of 2.4 μmol gDW^{-1} in acidogenesis, with a decrease to a stable value of ~ 0.8 μmol gDW^{-1} during solventogensis, in a pH controlled culture with initial 80 mM glucose and fed NH_4^+ (Meyer & Papoutsakis, 1989b). However, in the present study, NADH concentration reached 21.87 ± 0.821 μmol gDW^{-1} and 19.76 ± 0.346 μmol gDW^{-1} in the NaCl and the control groups, respectively, but then decreased in both cultures to 0.052 ± 0.006 when accessing solventogenesis (Figure 4.7a). The severe acidification process in acidogenesis, potentially causing cell proton accumulation, may have affected (or challenged) the cell redox state, triggering a cell resistance phenomenon that may explain NAD(H) and NADP(H) accumulation.

The ratio of NAD to NADH reached about 24 in the acid phase and decreased to a low level in the solvent phase. A key enzyme in the electron transfer system, ferredoxin (Fd) coupled with the H transfer from redox (NADH- Fd), converted from oxidoreductase (Fd Ox) to reductase (Fd Red) by accepting H from NADH. NADH-ferredoxin oxidoreductase specific activity was reported to be five times more active during acidogenesis than in the solvent-producing phase (Gheshlaghi et al., 2009; Vasconcelos et al., 1994), which may partially explain the high ratio of NAD to NADH.

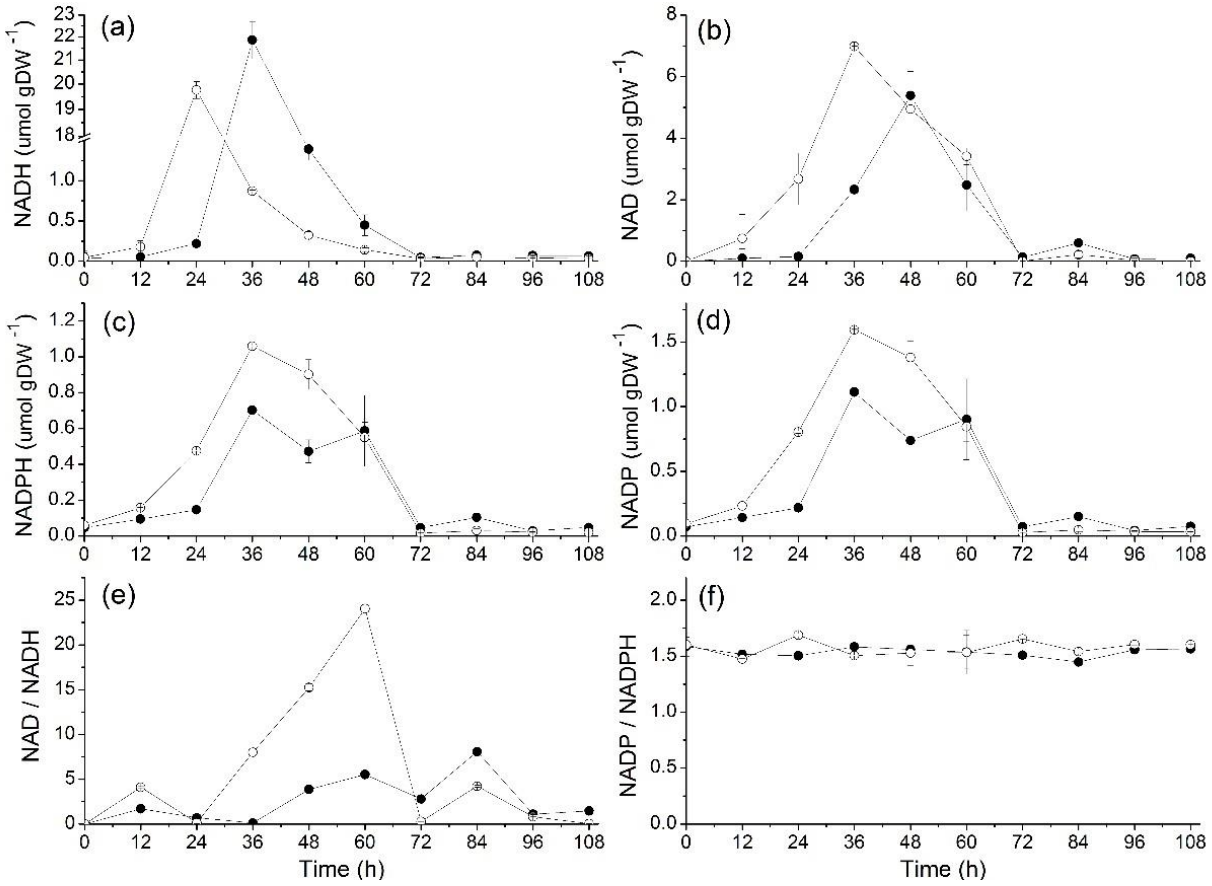

Figure 4. 7 Effect of NaCl addition on redox level and ratio on *C. acetobutylicum* ATCC 824 batch culture on xylose. (a) NADH; (b) NAD^+; (c) NADPH; (d) $NADP^+$; (e) NAD^+-to-NADH ratio; (f) $NADP^+$-to-NADPH ratio. ● 170 mM NaCl addition culture and ○ the control culture. Error bars represent standard deviations from three independent replicates (n=3).

In the present study, NAD(H) and NADP(H) concentrations evolved differently when supplementing sodium (Figure 4.7). The maximum concentration of NADH was about 20- to 30-fold higher than that of NADPH in the control and the NaCl group, respectively, while NAD^+ was about 5-fold $NADP^+$ in both the control and the NaCl groups (see details in Table 4.3). This result agrees with London and Knight's study in which they reported a NAD^+ concentration 10 to 40 folds higher than $NADP^+$ concentration in *Clostridium* species, reaching 8.9 ± 0.56 µmol gDW^{-1} (NAD^+) and 0.87 ± 0.08 µmol gDW^{-1} ($NADP^+$), and 4.91 ± 0.45 (NAD^+) and 0.11 ± 0.01µmol gDW^{-1} ($NADP^+$) in *C. pasteutianum* and *C. welchii*, respectively (London & Knight, 1966). In fact, the NAD(H) redox pair is mainly involved in energy production and NADP(H) in biosynthesis (Liu et al., 2013a; Shuler & Kargi, 1992), while both NADH and NADPH were shown being

involved in butanol and ethanol formation (Meyer & Papoutsakis, 1989b). Therefore, all of the above may explain a higher NADH concentration level than NADPH in ABE culture.

For present study, in control culture, the NAD^+-to-NADH ratio shows a linear increase from 24 h and reached a maximum value of 24.03 ± 0.190 at 60 h (Figure 4.7e), which coincides with production of ABE (Figure 4.3). However, in the same time point of NaCl group, the NAD^+-to-NADH ratio only reached a maximum value of 5.52 ± 0.09 (at 24 h), i.e. 23.0 ± 1.62% that in the control culture, although following a linear increasing trend and correlating with maximum values of solvents as for the control. Apparently, when comparing the maximum value in both NaCl and control groups, high sodium concentration promoted NADH accumulation in acidogenesis in *C. acetobutylicum*. In fact, a non-respiratory metabolism unconditionally requires a redox balance for its management of the primary metabolism (Jones & Woods, 1986). It has been reported that NADH-ferredoxin oxidase activity (0.168 μmol min^{-1} mg^{-1}) is more than five folds higher than ferredoxin-NAD^+ reductase (0.0326 μmol min^{-1} mg^{-1}) in acid-producing culture of *C. acetobutylicum* (Petitdemange et al., 1976). Therefore, our results suggested that either the NAD(H) oxidase is inhibited or the reductase is promoted under NaCl conditions, while NAD(H) concentration and ratio behaviours follow cell proliferation behaviour.

It is conceivable that high sodium affects hydrogenase activity, a key enzyme shown to affect significantly NADH level and further solvents production (Girbal & Soucaille, 1994; Zhang et al., 2014). In CO gassing experiment, inhibited hydrogenase improved NADH concentration as well as the NADH-to-NAD^+ ratio of ~ 400 % compared to initial levels (Meyer & Papoutsakis, 1989b). Meanwhile, Rao and Mutharasan increased NADH concentration as well as promoted butanol production by inducing a competitive inhibition mechanism for hydrogenase while supplementing viologen in a continuous culture (Rao & Mutharasan, 1987). Therefore, in the present study, a high sodium environment, which induced high NADH concentration, may also be related to the regulation of the hydrogenase system complex activity.

As a typical cell signal and an important parameter involved in the regulation of cell metabolism, the behaviour of the redox ratios were further investigated (Lutke-Eversloh, 2014). In addition to literature assessing various carbon sources, CO gassing and viologen induction assays all showed affecting the NAD^+-to-NADH ratio (Girbal & Soucaille, 1994; Meyer & Papoutsakis, 1989b; Rao

& Mutharasan, 1987; Zhang et al., 2014). Wietzke and Bahl reported that a transcriptional repressor (Rex) coupled to butanol production was correlated to the NAD^+-to-NADH ratio in *C. acetobutylicum* (Wietzke & Bahl, 2012). Meanwhile, Zhang *et al*. proposed that Rex affects NADH-depending enzymes, and further enhance butanol production (Zhang et al., 2014). Moreover, Wang, *et al*. found that Rex affinity for NADH was 20,000 times higher than that for NAD^+ in *Bacillus subtilis (*Wang et al., 2008*).* Taken altogether, literature and our results thus suggest that the NAD^+-to-NADH ratio does affect Rex function, which in turn affects the regulation of butanol production.

In the case of the NADP(H) redox pair, both NADPH and $NADP^+$ cell concentrations in high sodium medium were about 68 % that in control group in acidogenesis (Figure 4.7c, d). Interestingly, the $NADP^+$-to-NADPH ratio showed to be similar for both NaCl and control cultures at a constant value throughout acidogenesis and solventogenesis with 1.56 ± 0.013 (Figure 4.7f). Therefore, our results show that the NAD^+-to-NADH ratio is affected at high sodium but not the $NADP^+$-to-NADPH ratio. Indeed, in the *Clostridia* metabolic pathway, $NADP^+$-to-NADPH are mainly involved in the secondary metabolism, managing enzymatic reactions such as from acetaldehyde dehydrogenase, butyraldehyde dehydrogenase, ethanol dehydrogenase and butanol dehydrogenase (Liu et al., 2013a). Therefore, as a significant result, the stable $NADP^+$-to-NADPH ratio may be correlated with the solvents specific productivity, which shows similar levels in both the control and the NaCl groups. Therefore, the cell robustness at maintaining a constant $NADP^+$-to-NADPH ratio, even under high sodium condition, may partly explain a maintained solvents specific productivity, although a large part of the central carbon metabolism shown being affected.

4.6 **Conclusion**

We here studied the effect of high sodium concentration on *Clostridum* ABE fermentation behaviour. High sodium condition showed to affect biomass growth but not the cell specific productivity in solvents. A quantitative metabolomics analysis revealed that the metabolic intermediates related to biomass synthesis are highly inhibited (i.e. sugar phosphates). While the cell energetics showed being stimulated at high sodium, $NADP^+$-to-NADPH exhibited a high robustness that could explain a maintained solvents specific productivity. This work suggests that

rather desalting wood hydrolysates in biorefinery, which is a costly process, similar butanol production can be reached by performing fermentation at high biomass concentration.

4.7 Acknowledgements

The authors thank the BioFuelNet Center of Excellence and the Natural Sciences and Natural Science and Engineering Research Council of Canada for their financial support.

4.8 Authors' contributions

X. Z. designed and performed the experiments; analyzed the data and wrote the manuscript. S. C. contributed performing the experiments. J. C. performed culture sample analysis and quantification on the UPLC-MSMS equipment. Prof. M. J. contributed to the design of the experimental as well as data analysis. He did also participate to the manuscript writing, and he has approved the final version of the manuscript.

CHAPTER 5 ARTICLE 2: A DYNAMIC METABOLIC FLUX ANALYSIS OF CO-PRODUCING RIBOFLAVIN IN ABE (ACETONE-BUTANOL-ETHANOL) FERMENTATION BY *CLOSTRIDIUM ACETOBUTYLICUM* ATCC 824

Xinhe Zhao[1], Mayssa Kasbi[1], Jingkui Chen[1], Sabine Peres[2], Mario Jolicoeur[1*]

[1] Research Laboratory in Applied Metabolic Engineering, Department of Chemical Engineering, École Polytechnique de Montréal, P.O. Box 6079, Centre-Ville Station, Montréal, Québec, H3C 3A7, Canada

[2] LRI, Université Paris-Sud, CNRS, Université Paris-Saclay, 91405 Orsay, France
MaIAGE, INRA, Université Paris-Saclay, 78350 Jouy-en-Josas, France

[*] Corresponding author: Prof. Mario Jolicoeur
École Polytechnique de Montréal, P.O. Box 6079, Centre-ville Station, Montréal, Québec, H3C 3A7, Canada
Phone : (514) 340-4711 ext. 4525
Email : mario.jolicoeur@polymtl.ca
Fax : +1-514-340-4159

(Published in Biotechnology and Bioengineering; doi:10.1002/bit.26393 (2017))

5.1 Abstract

The present study reveals that supplementing sodium acetate (NaAc) strongly stimulates riboflavin production in acetone-butanol-ethanol (ABE) fermentation by *Clostridium acetobutylicum* ATCC 824 with xylose as carbon source. Riboflavin production increased from undetectable concentrations to ~ 0.2 g L^{-1} (0.53 mM) when supplementing 60 mM NaAc. Of interest, solvents production and biomass yield were also promoted with 5-fold acetone, 2.6-fold butanol and 2.4-fold biomass adding NaAc. A kinetic metabolic model was developed and calibrated to simulate an ABE-co-producing riboflavin biosystem using 60 mM acetate culture data. The model could also adequately predict cell behaviour under 0 mM acetate culture condition by being compared with experimental data, especially for substrate utilization, ABE production, as well as riboflavin evolving. An efficient parameter estimation method adapted from Rizzi was developed during model calibration. Meanwhile, an auto-generator was also developed to generate different matlab codes, which accelerated the modelling process. Dynamic metabolic fluxes simulated by the model showed a simultaneous increase of riboflavin (ribA) and GTP (precursor of riboflavin) (PurM) synthesis flux rates under NaAc supplementation, which brought a light on further genetic manipulation strategies. It also suggested that the NaAc condition had first stimulated the accumulation of intracellular metabolite intermediates during the acidogenic phase, which then fed the solventogenic phase leading to increased ABE production. Moreover, lower GTP-to-adenosine phosphates (ATP, ADP, AMP) ratio under NaAc supplemented condition suggests that GTP may have a minor role in the cell energetic metabolism compared to its contribution to riboflavin synthesis. Both the metabolomics and modelling studies gave a clearer view of mechanism on ABE fermentation co-producing riboflavin in acetate condition.

5.2 Key words:

Riboflavin; ABE; *Clostridium*; Dynamic model; Metabolism; Cell energetics

5.3 Introduction

Riboflavin (vitamin B_2) is naturally synthesized intracellularly from the enzymatic reaction involving the precursors flavin mononucleotide (FMN) and flavin adenine dinucleotide (FAD). Considered as a secondary metabolite, it plays a significant role in cell metabolism and its synthesis pathway has been found in plants and in many microorganisms, but not in higher animals. Therefore, a two-milligram dose of vitamin B_2 per day is recommended in human diet. Currently, the global market of riboflavin is estimated at 3,000 tons per year that are produced by chemical and biochemical synthesis as well as from fermentation methods (Lim et al. 2001). Since the 1940s, various microorganisms have been found to constitutively produce riboflavin (Arzberger 1943). Bacteria such as *Clostridium*, yeasts species such as *Candida flareri, Candida guilliermondii, Candida famata* and *Mycobacterium phlei*, fungi species such as *Aspergillus terreus, Eremothecium ashbyii* and *Ashbya gossypii* have all showed producing riboflavin (Lim et al. 2001). Bacteria and yeasts naturally secretes riboflavin but normally at low levels. However, *Clostridium acetobutylicum* led to up to 100 mg L^{-1} riboflavin under bipyrimidine induction (Legg and Beesch 1945), and 600 mg L^{-1} riboflavin were obtained with *Candida flareri* in a culture medium optimized to this end (Lim et al. 2001). However, the fungal specie *Ashbya gossypii*, which leads to high levels of ~ 5 g L^{-1}, is currently used to produce riboflavin industrially (Lim et al. 2001). Riboflavin is thus a by-product of ABE fermentation by *C. acetobutylicum*, a bacteria primary used to produce a mixture of solvents of commercial interest (Burgess et al. 2009). However, after decades of work, the yield in riboflavin remains insufficient in Clostridium, a co-product which could add an extra economic value to ABE bioprocess. As reported, when the riboflavin yield as a by-product reaches 1 g/L, it will be competitive in the current market (Cai and Bennett, 2011).

In this work, we focused on biorefining hemicellulose hydrolysates wastes from the pulp-and-paper industry using black spruce, of which hemicellulose hydrolysates are xylose-rich (up to 80 g L^{-1}) and also contain acetate, a by-product of the hydrolysis process (Alriksson 2006). We thus here report that while assessing sodium acetate as a mean for pH control limiting the acid crash problem in such ABE fermentation bioprocess, using a synthetic medium, we observed by serendipity a net improvement of riboflavin production in *C. acetobutylicum* with xylose as the major carbon source. The riboflavin yield in 60 mM acetate culture could reach 0.2 g L^{-1}. Therefore, improving the riboflavin yield as a by-product of ABE fermentation in acetate culture is quite likely to reach the

industrialization level (1 g L^{-1} yield) in the future. Interestingly, adding acetate was also shown to positively affect butanol production. We have thus investigated the metabolomic response of *C. acetobutylicum* ATCC 824 to sodium acetate to identify the mechanisms leading to the induction of riboflavin synthesis pathway. A dynamic metabolic flux analysis (dMFA) has been performed using an *in silico* platform specifically developed for *C. acetobutylicum*, based on previous works (Ghorbaniaghdam et al. 2013; Robitaille et al. 2015). The metabolic network includes glycolysis, pentose phosphate pathway (PPP), ABE synthesis and purine-related riboflavin metabolism. Experimental data on cell energetic and redox states were also analyzed. Our results thus suggest a low-cost alternative for increasing the commercial value of ABE fermentation bioprocess co-producing butanol and riboflavin.

5.4 Materials and methods

5.4.1 Cell culture

Batch cultures of *Clostridium acetobutylicum* ATCC 824 were performed in a 3.6-L bioreactor (Infors-HT, Bottmingen, Switzerland) with 2 L of medium. Cultures were inoculated at 5 % (v/v), from seed cultures prepared in 0.5-L serum bottles. RCM (reinforce Clostridium medium) was used for seed cultures, but CGM (Clostridium growth medium) was used as fermentation medium in bioreactor cultures (Choi et al. 2012). NaAc was supplied at 60 mM (test) and 0 mM (control) in the CGM culture medium with 230 mM xylose. The test culture bioreactor was run four times independently and only two batches were chosen for the final data analysis, as the sampling time intervals were close between these two batches and easy for error calculation. The other two batches' data was also provided for a clearer view of the repeatable effect of high sodium acetate concentration on cell behaviour at different time points (shown in the Supplementary material 3). The xylose saturated solution was filter sterilized (air vent 0.22 µm, Millipore) and added in sterile (autoclaving at 121 ˚C for 20 min) culture media under a laminar flow hood. Filter sterilized (air vent 0.22 µm, Millipore) 100 % nitrogen gas was sparged in culture serum bottles, as well as from the bottom of the bioreactor, to guarantee anaerobic condition during culture, with resazurin (0.025 %, 4 mL L^{-1}) as oxygen indicator. Seeds cultures were performed in serum bottles at 37 ˚C, and placed in an agitated incubator at 100 rpm. Bioreactor cultures were carried out at 37 ˚C and agitated at 100 rpm with Rushton impellers. Samples were taken every ~ 12 h, and centrifuged at

20,000 *g* for 10 min at 4 ˚C. The supernatant was separated from the cell pallet and stored in - 80 ˚C for further analyses of the media content in ABE, acids and xylose (see below). Cell pallets were washed with 1 mL of PBS (Phosphate buffer solution) two times, then 1 mL of an 80 % methanol-water solution was added, and the mixture was stored in - 80 ˚C for further analyses of intracellular sugar phosphates, nucleotides and redox (see below).

5.4.2 Riboflavin purification and identification

For the yellow sediment, we first did a literature review to find its probability, and found that the *Clostridium* species could generate riboflavin, which is a yellow crystal. Therefore, we compared both the crystal shape and MS/MS of our sediment with standard riboflavin in order to find whether they are the same compound, as follows:

The yellow sediment was collected from the fermentation broth by first centrifuging at 20,000 *g* for 10 min at room temperature, and washed two times by distilled water. Then the yellow-rich sediment was purified as follow, repeating the procedure at least three times. The sediment (~ 0.1 g) was first dissolved in 2 mL 100 % methanol at room temperature and centrifuged at 20,000 *g* (10 min, room temperature), and the supernatant (riboflavin saturated methanol solution) was stored at - 20 ˚C overnight to favour riboflavin crystals precipitation. The purified crystals sample was dissolved in 1 mL 70 % methanol for identification step, comparing to a pure riboflavin standard (Sigma, Oakville, Canada, cat. # 83885) also dissolved in 70 % methanol. The yellow crystal was identified on a 1290 UPLC (G64220A binary pump, G64226A auto sampler and G4212A UV detector, Agilent, Québec, Canada) coupling to a triple quadrupole mass spectrometer (G6460A, Agilent, Québec, Canada), and equipped with an BEH Amide column (100 x 2.1 mm, 1.7 µm) (cat. # 186004801, Waters, Montréal, Canada). 2 µL of cell extract was injected to the column with mobile phase A: 10 mM ammonium acetate and 0.04 % ammonium hydroxide in 50 % acetonitrile (v/v), and mobile phase B: 10 mM ammonium acetate and 0.04 % ammonium hydroxide in 90 % acetonitrile (v/v) at a flow rate of 0.13 mL min^{-1}. The signal was detected by both a UV detector at 265 nm and an MS detector, then compared with pure standard riboflavin (Sigma, Oakville, Canada, cat. # 83885).

Following the quantification of riboflavin was done using a spectrophotometer (UV-2100, UNICO, Canada) under an absorption wavelength of 444 nm (A 444). The concentration was calculated

using a calibration curve established using a pure standard of riboflavin, as described in (Sauer et al. 1996).

5.4.3 Metabolites analysis

Culture samples supernatant were filtered (air vent 0.22 μm, Millipore) to perform extracellular analysis. ABE was analyzed using a GC-FID system (PerkinElmer, Québec, Canada) equipped with the Elite-WAX ETR (30 m, 0.32 mm I.D.) column with a mixed air and hydrogen as mobile phase (Gerchman et al. 2012). Acetic and butyric acid analyses were performed with HPLC system (1525 binary pump, 2777 auto sampler and 996 PDA detector, Waters, Canada) equipped with an Aminex HPX-87H column (300 x 7.8 mm, cat. # 1250140, Bio-Rad, Canada) with a mobile phase of 5 mM H_2SO_4 at flow rate of 0.6 mL min^{-1} (Ahmed et al. 2015; Zhao et al. 2016). The quantification of intracellular metabolites (sugar phosphates, organic acids, energetic nucleotides and redox) was performed using a UPLC/MS/MS system as previously described (Ghorbaniaghdam et al. 2014). Briefly, cell pellets stored in 80 % methanol mixture were ultrasonicated in ice water for 30 min and centrifuged at 20,000 *g* for 10 min at 4 ˚C. Then, the supernatant was filtered (0.22 μm Millipore filter) before injecting into the UPLC system, which was equipped with 6460 triple quadruple mass spectrometer. All the protocols of quantification were described previously by Ghorbaniaghdam et al (Ghorbaniaghdam et al. 2014).

5.4.4 The dynamic metabolic model

A dynamic metabolic model describing the ABE fermentation biosystem, and based on previous works (Ghorbaniaghdam et al. 2013; Robitaille et al. 2015), was used to analyze the metabolic flux network dynamics. The contributions of this work to previous models came from several aspects: present modelling work combined riboflavin generation and ABE production (which is a new interconnected system), and regulation such as butanol inhibition and acetate activation were introduced in the model (which could better explain cell behaviour). Meanwhile, an efficient parameter estimation method adapted from Rizzi's work was developed during model calibration. An auto generator was also developed to generate different matlab codes, which accelerated the modelling process. Details on model development are presented as Supplementary material 1 for space limitation as well as for clarity purposes. Briefly, the model structure includes major central carbon metabolism and pathways related to ABE and riboflavin synthesis such as glycolysis,

pentose phosphate pathway (PPP), acids and solvents synthesis, purine metabolism and riboflavin synthesis. The metabolic network and reactions stoichiometry, as well as parameters value, metabolites initial concentration, flux kinetics and mass balances of the model are also presented in Supplementary material 1. Biochemical reactions are indicated as unidirectional except for rpiA, PTA, PTB, which are defined as reversible according to model simulation results (n.b. flux direction was not imposed in simulations). Finally, each flux kinetic as well as the cells specific growth rate are described by a multi Michaelis-Menten equation. The model structure and kinetic parameters were identified following the method proposed by Rizzi et al. (Rizzi et al. 1997), while minimizing simulation error of experimental data. Therefore, the model was first anchored to experimental data for then being used to perform a dynamic metabolic flux analysis of the biosystem, accessing flux rate values with culture time.

5.5 Results and Discussion

5.5.1 Sodium acetate induces riboflavin production in ABE fermentation

While evaluating the effect of supplementing the culture medium with 60 mM NaAc to limit the acid crash problem in ABE fermentation, with xylose as unique carbon source, a yellowish sediment was observed by serendipity in the culture broth (Figure 5.1). We found that the *Clostridium* species is known to produce riboflavin (Lim et al. 2001), but at concentrations that are close-to-under the detection limit to the best of our knowledge (Arzberger 1943; Hickey 1945; Lim et al. 2001). Various methods have been assessed to improve riboflavin yield in *C. acetobutylicum*. Cai and Bennet obtained 0.07 g L^{-1} of riboflavin by a genetically modified strain of *C. acetobutylicum* ATCC 824 (pJpGN) in a buffered culture medium (Cai and Bennett, 2011), while Hickey reported 0.1 g L^{-1} riboflavin from wild *C. acetobutylicum* ATCC 824 by adding 2, 2-bipyrimidine in the medium (Hickey, 1945). These efforts were interrupted because higher levels of riboflavin were discovered in some fungi species (*Ashbyagossypii*, ~5 g/L), compared to yeast and bacteria. However, the fact that *Clostridum* could produce riboflavin is well-accepted. Thus, we considered the yellowish sediment to be riboflavin, which was stimulated under 60mM NaAc condition and further identified.

The yellow product was extracted from the culture broth and purified, then compared with commercial standard riboflavin (Sigma, Oakville, Canada, cat. # 83885) (Supplementary material

2). The crystal shape of the yellow riboflavin precipitate agrees with Bretzel's previous observation (Bretzel et al. 1999), and the UPLC/MS/MS analysis shows that the mass/z (376) and retention time of this compound were the same as the commercial standard of riboflavin (Sigma, Oakville, Canada, cat. # 83885) (Supplementary material 2). Until now, we had not found another riboflavin isomeride or a component with the same mass/z (376) and retention time as riboflavin. Therefore, by combining the well-known *Clostridum* with riboflavin production and the identification process, we can finally identify the compound as riboflavin.

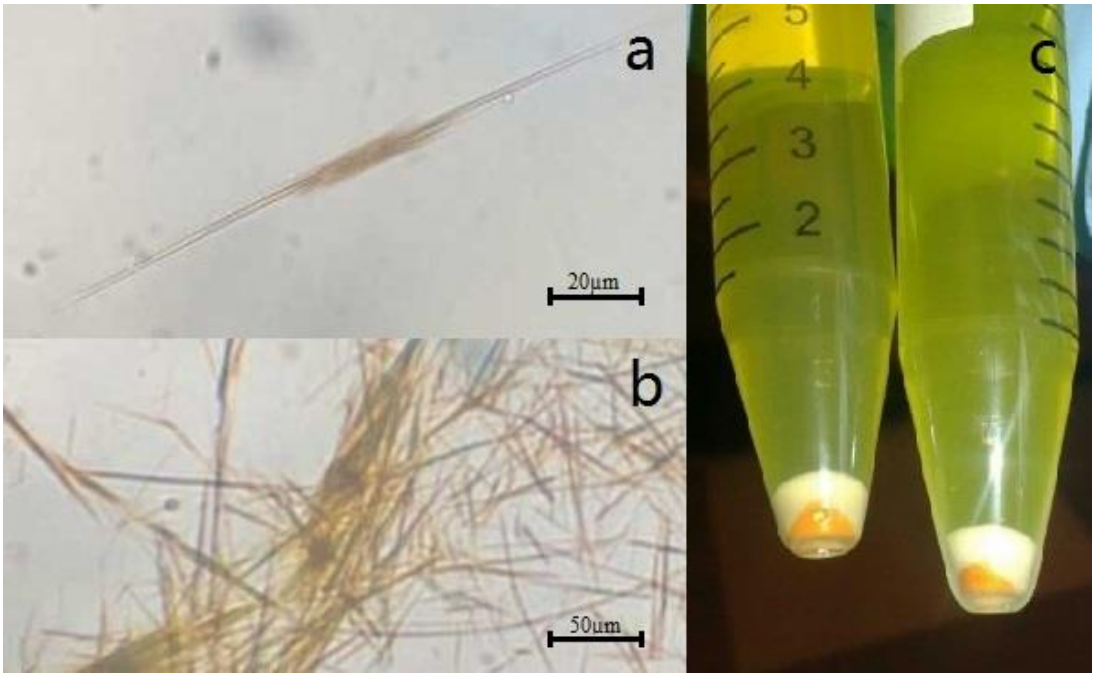

Figure 5. 1 Images of riboflavin obtained in *C. acetobutylicum* ATCC 824 bioreactor culture (56 h) with xylose and 60 mM sodium acetate. (a) Microscopic image of riboflavin crystal: 1000X magnification under bright field optical microscopy (Leitz Laborlux S Microscope); (b) 400X magnification under bright field optical microscopy. (c) Centrifuged fermentation broth: the orange sediment is riboflavin and white sediment is biomass.

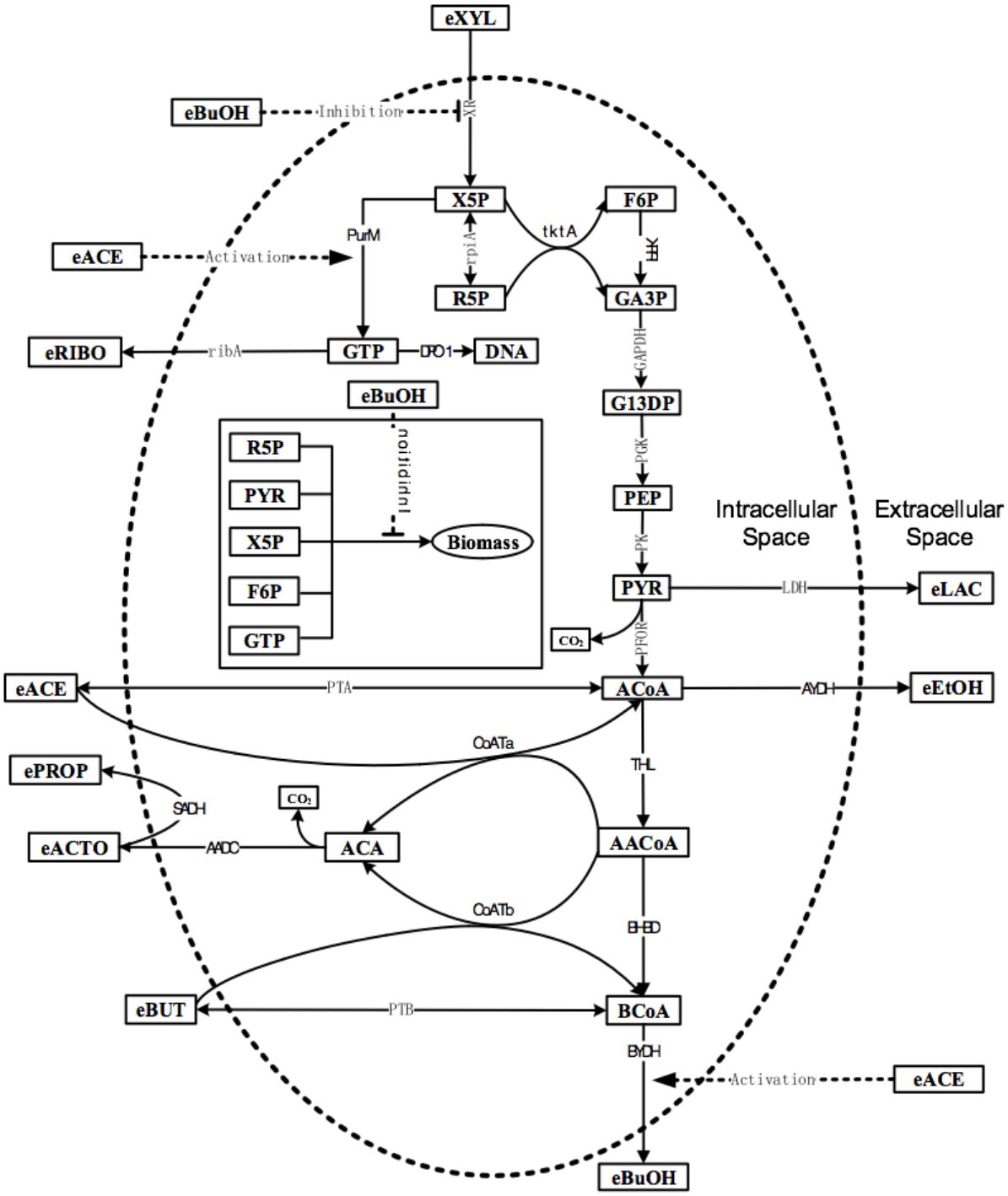

Figure 5. 2 Metabolic pathways described in the model. The dashed line delimits the cell membrane.

In this work, further analysis of bioreactor culture broths and quantification of its riboflavin content revealed a concentration peak of ~ 0.2 g L^{-1} (0.53 mM), clearly evidenced by the orange sediment

shown in Figure 5.1, in the 60 mM NaAc supplemented xylose culture medium, compared to only ~ 0.021 g L^{-1} (0.058 mM) in the control culture (i.e. without NaAc) where no such sediment was visually visible (Figure 5.3a). An initial 60 mM NaAc concentration has thus led to a 10-fold increase of riboflavin production. Interestingly, riboflavin and acetate productions were concurrent in the control culture (0 mM NaAc at t = 0) while riboflavin concentration followed acetate consumption in the 60 mM NaAc supplemented culture, trends that are also described by model simulations (Figure 5.3a, b). Maximal simulated riboflavin concentrations reached 0.38 mM in the 60 mM NaAc culture at 80 h compared to 0.057 mM at 70 h in the control culture. Model simulations are respectively underestimating of 19.5 % (80 h) and overestimating of 8.1 % (70 h) experimental data (Figure 5.3a). Indeed, riboflavin production in the 60 mM NaAc condition ceased 24 h after acetate consumption has ceased, although there was still a non-negligible concentration of xylose (~ 45 mM, Figure 5.4b). Interestingly, acetate concentration followed distinct behaviours in the two cultures, although a net production was observed during acidogenesis in both cultures. However, in solventogenesis acetate consumption has been observed in the 60 mM NaAc culture while it stayed at a relatively constant level in the control culture (Figure 5.3b). At the current stage of development, the model thus led to continuous acetate production in the control culture and acetate consumption in the 60 mM NaAc culture (defined as the difference of PTA and CoATa flux rates) (Figure 5.3d). Of high interest, the 60 mM NaAc culture resulted in higher yield of solvents (Figure 5.4c, d, e). Therefore, results clearly suggest NaAc addition is stimulating end-products accumulation.

The riboflavin synthesis rate (ribA flux rate) was almost 10-fold higher in the 60 mM NaAc culture compared to control, at early in the culture (Figure 5.3c). Although riboflavin accumulated along with exponential growth phase, its synthesis rate decreased continuously, which may be explained by decreasing NaAc concentration so as the associated activation effect. Therefore, these results suggest that NaAc is strongly stimulating ribA activity. Furthermore, the ribA -to- XR flux ratio in the 60 mM NaAc culture was higher than that in control (Figure 5.3e), a coherent result when comparing ribA fluxes (Figure 5.3c). Interestingly, although the cell specific growth rate (μ) and butanol synthesis rate (BYDH) were also stimulated in NaAc culture (not shown data; refer to concentration behaviours in Figure 5.4), higher riboflavin synthesis rate (ribA) -to- specific growth rate ratio (Figure 5.3f) and riboflavin (ribA) -to- butanol synthesis rate (BYDH) ratio (Figure 5.3h) were both higher in the 60 mM NaAc culture. This result suggests that riboflavin productivity was

stimulated at a higher extent compared to cell growth rate and butanol synthesis rate. Furthermore, the ratio of riboflavin (ribA flux) -to- GTP synthesis rate (PurM flux) from the purine pool suggests that half (48 %) of GTP synthesis rate contributes to riboflavin synthesis (Figure 5.3g).

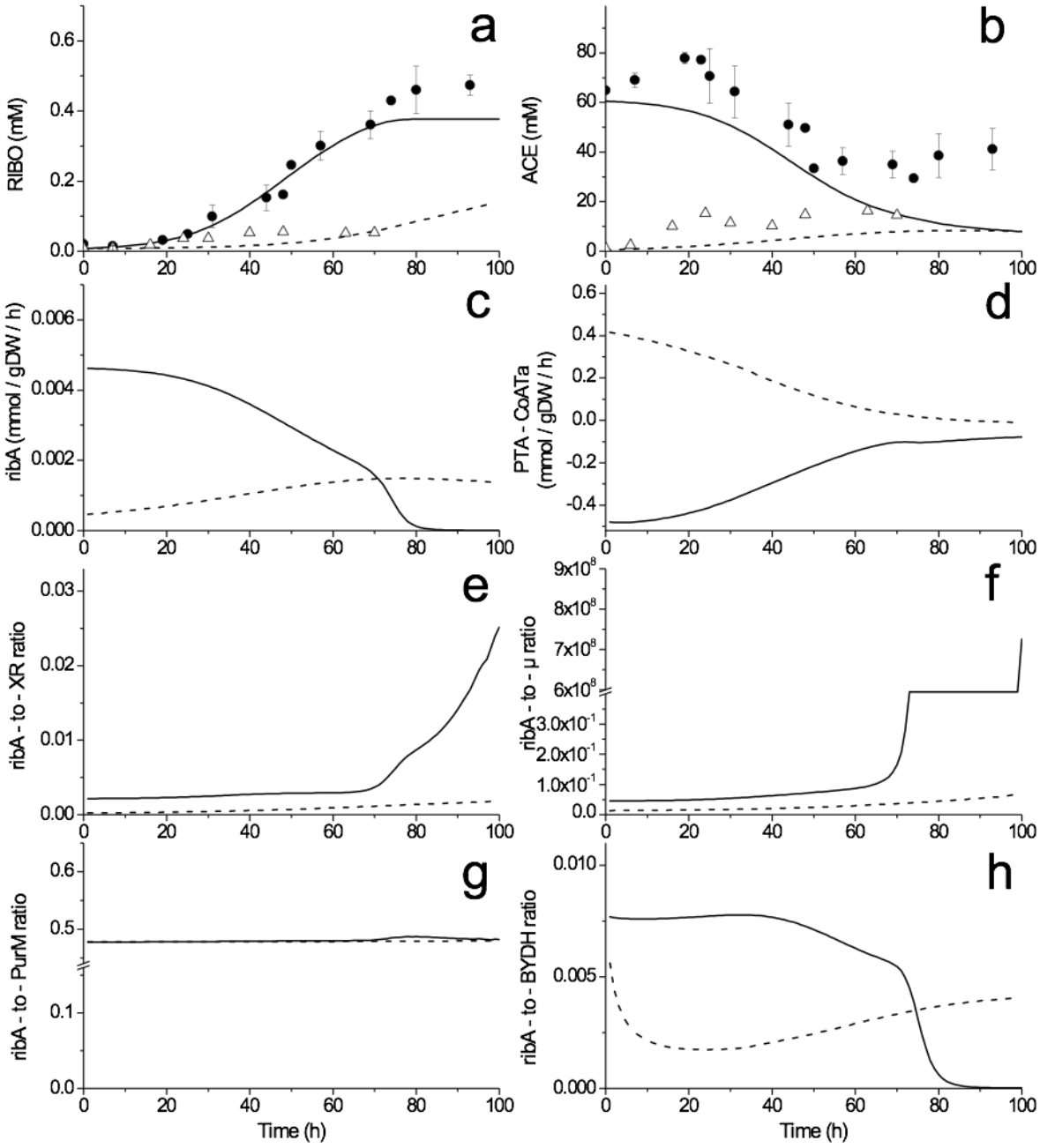

Figure 5. 3 Metabolites concentrations and flux rates simulation results related to riboflavin and acetate metabolisms for a xylose culture of *C. acetobutylicum* ATCC 824. Solid line refers to simulation results for the 60 mM NaAc culture and dashed line to the control culture. Solid circle

is experimental data for 60 mM NaAc; open triangle is experimental data in control culture. Error bars represent standard deviations from two independent bioreactor culture replicates. (a) riboflavin; (b) acetate; (c) ribA flux rate; (d) net acetate productivity (PTA minus CoATa); (e) ribA -to- XR ratio; (f) ribA -to- the specific growth rate (μ) ratio; (g) ribA -to- PurM ratio; (h) ribA -to- BYDH ratio.

5.5.2 Supplementing NaAc promotes ABE fermentation

Bacterial growth as well as solvents production were promoted in the 60 mM NaAc supplemented culture. For instance, butanol and acetone reached maximal values of 144.9 mM and 63.4 mM in the NaAc culture at ~ 50 h, respectively, but in the control culture only 40.1 mM and 9.7 mM were obtained at ~ 40 h, respectively (Figure 5.4c, d). It has been proposed that the buffering effect provided by supplementing NaAc in ABE fermentation could have avoided the "acid crash" while switching from acidogenesis to solventogenesis (Hüsemann and Papoutsakis 1990). Cell growth and solvents accumulation are known being inhibited at low pH values while acids are generated in excess (Maddox et al. 2000; Wang et al. 2011). The pH level in the 60 mM NaAc culture was maintained at a slightly higher value (6.5 to 5.3) than in the control culture (6.5 to 4.5). A lower pH level may partly explain lower cell growth rate and xylose uptake rate in the control culture (Figure 5.4f). The culture broth reached a maximum optical density (OD 600) of 19.2 ± 0.37 (4.04 ± 0.08 gDW L^{-1}) compared to 5.7 ± 0.64 (1.42 ± 0.14 gDW L^{-1}) in control culture (Figure 5.4a). In agreement with a lower cell growth rate, xylose was also consumed at a lower rate in the control culture compared to NaAc supplemented cultures (Figure 5.4b). Model simulation results described the general tendencies for cell growth, xylose and acetate consumption, as well as acids and solvents production (Figure 5.4). The clostridia metabolic network has been highly simplified in this model, which could mainly explain the discrepancies observed between model simulations and some experimental results. However, it offers a reliable platform to perform a dynamic metabolic flux analysis evaluating the effect of supplementing sodium acetate to ABE fermentation process, as well as simulating the significant activation of pathways leading to riboflavin production and secretion. Indeed, the analysis of model simulated flux rates (Figure 5.5h) shows being in agreement with Chen & Blaschek who observed by a proteomic study that coenzyme A transferase (CoATa) is over-expressed in high NaAc supplemented culture of *Clostridium beijerinckii* NCIMB 8052 (Chen and Blaschek 1999). Of interest, acetic acid supplementation was also reported to

promote solvents production in ABE fermentation (Holt et al. 1984), but without reporting any increase of riboflavin production.

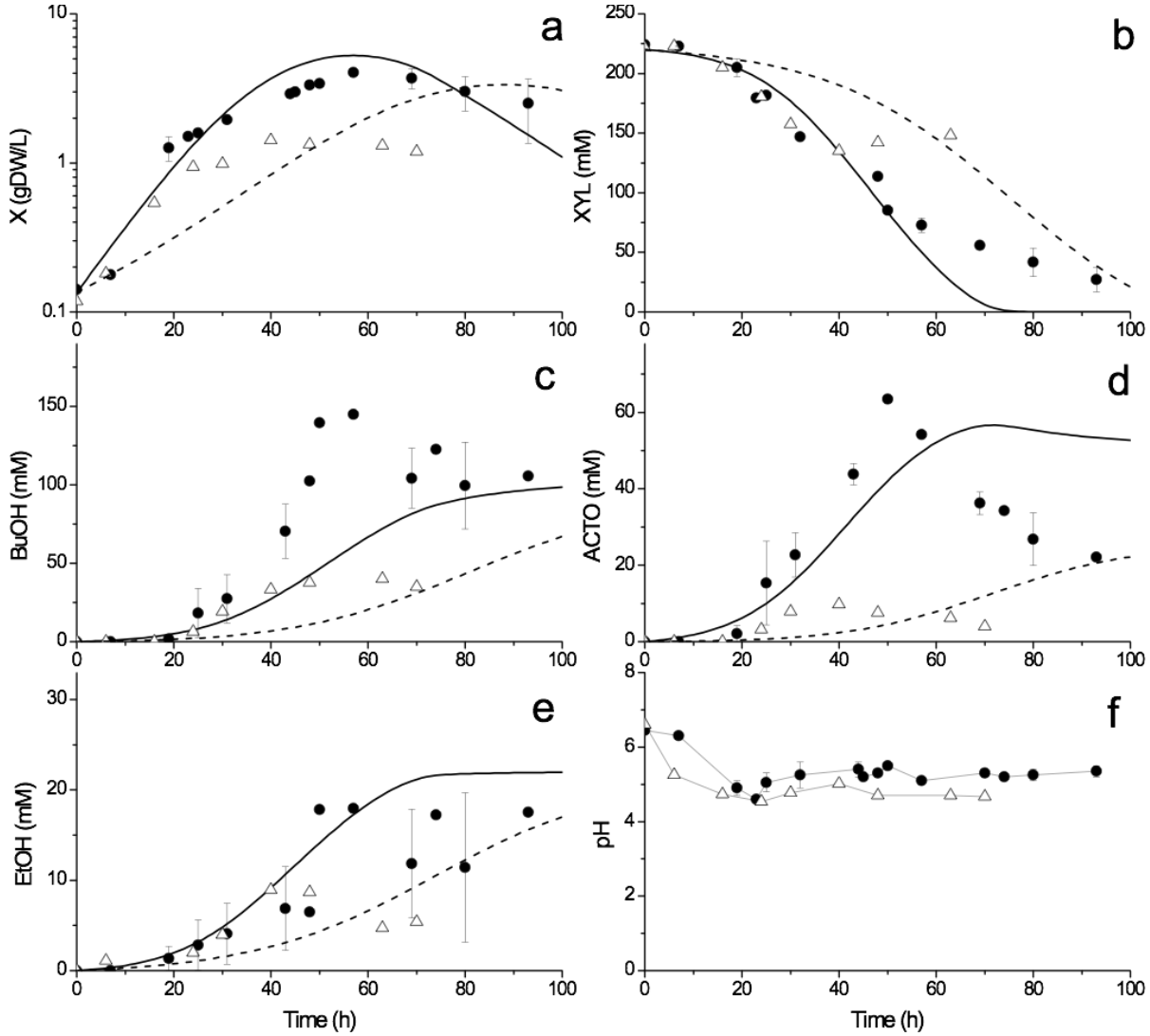

Figure 5. 4 Simulation results of biomass, solvents production and carbon consumption status for a xylose culture of *C. acetobutylicum* ATCC 824. Solid line refers to simulation results for the 60 mM NaAc culture, and dashed line to the control culture. Solid circle is experimental data for 60 mM NaAc, and open triangle is experimental data in control culture. Error bars represent standard deviations from two independent bioreactor culture replicates. (a) biomass; (b) xylose; (c) butanol; (d) acetone; (e) ethanol; (f) pH.

5.5.3 Carbon flux analysis supplementing 60 mM NaAc

5.5.3.1 Evolving from acidogenesis to solventogenesis

The biphasic fermentation of ABE system is well known. Cells need to accumulate acids at a minimal threshold level to stimulate the activation of the solvents synthesis system (Jang et al. 2012), and model simulations suggest being in agreement at describing this phenomenon. Indeed, both the acetate output -to- the input flux (CoATa -to- PTA) ratio and the butyrate output -to- the input flux (CoATb -to- PTB) ratio shortly increase at xylose depletion (~ 70 h in simulation results) for then being negative, a result explained by reversed PTA and PTB fluxes with acids being purely consumed from that time point to generate solvents. However, this phase shift was not observed simulating the control culture, which may explain the lower solvent production yields in control culture. Although these observations are only based on model simulations, which show xylose depletion at ~ 70 h contrarily to experimental data clearly showing remaining xylose, they may reveal a real phenomenon. The CoATa -to- CoATb ratio indicates a higher acetate consumption rate than for butyrate, and especially in the 60 mM NaAc culture (Figure 5.5c). However, comparing these flux rates with xylose uptake rate suggests that acetate plays a secondary role as carbon source in the 60 mM NaAc culture. Interestingly, the xylose (XR) -to- acetate uptake rate ratio, deduced from calculating the difference between CoATa and PTA (i.e. CoATa - PTA), stayed constant the first 45 h, for shortly increasing and then sharply decreasing when xylose consumption has ceased (Figure 5.5d). Solvents generating enzymes activity, such as AYDH (ethanol), BYDH (butanol), CoATa and AADC (acetone) were all higher in the 60 mM NaAc supplemented culture compared to the control for the first 30 h, 37 h, 60 h and 60 h, respectively, for then all decreasing at lower values (Figure 5.5e, f, g, h). These results agree with a proteomic analysis of a xylose culture in *C. acetobutylicum*, with levels of acetyl-CoA acetyltransferase (CoATa) and acetoacetate decarboxylase (AADC) that were reduced of 72.7 % and 77 %, respectively, at the same culture stages (Sivagnanam et al. 2012).

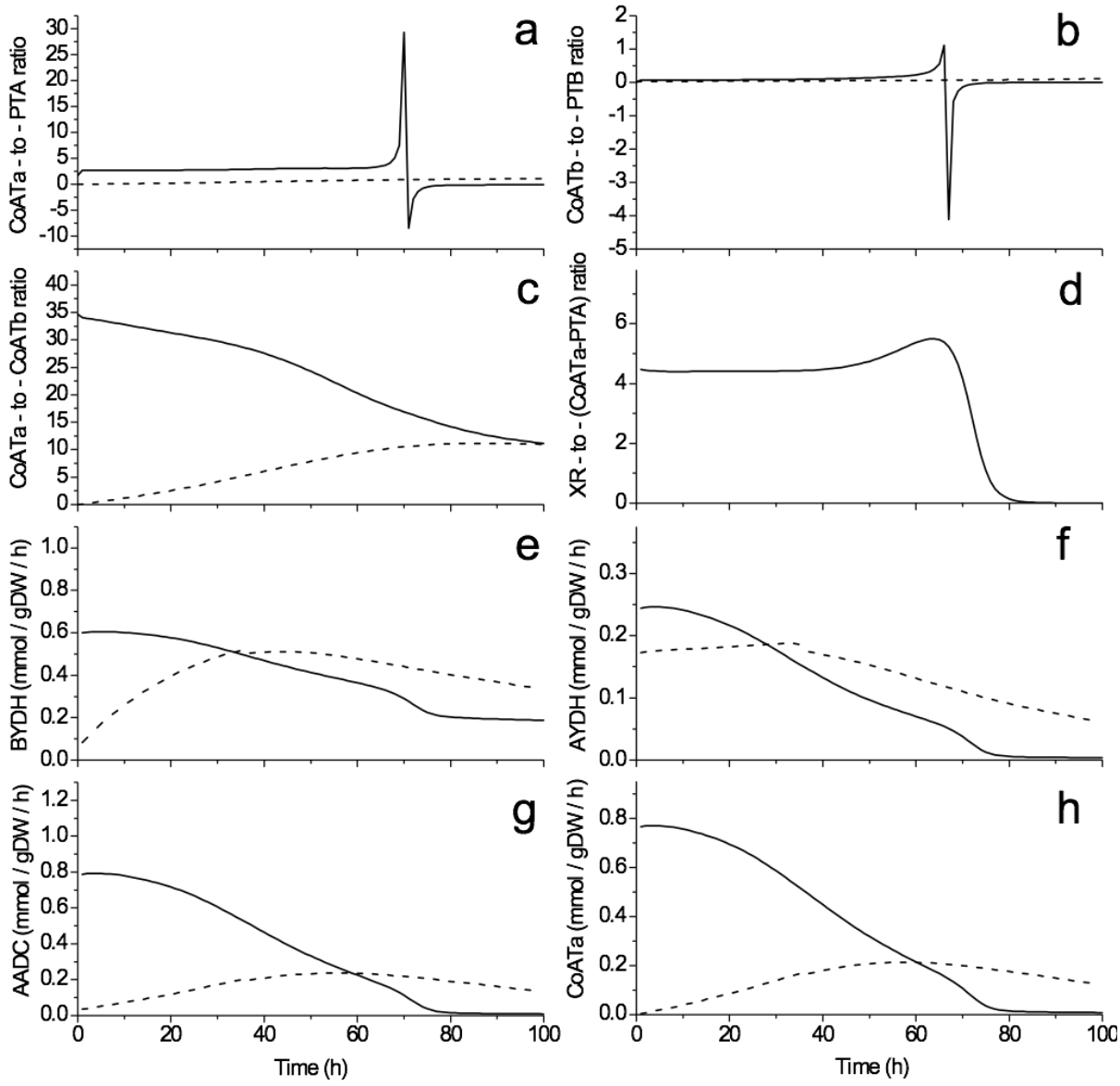

Figure 5. 5 Dynamic metabolic flux analysis results for a xylose culture of *C. acetobutylicum* ATCC 824 from model simulation. Solid line refers to simulation results for the 60 mM NaAc culture and dashed line to the control culture. (a) CoATa -to- PTA ratio; (b) CoATb -to- PTB ratio; (c) CoATa -to- CoATb ratio; (d) XR -to- (CoATa-PTA) ratio; (e) flux rate of BYDH; (f) flux rate of AYDH; (g) flux rate of AADC; (h) flux rate of CoATa.

5.5.3.2 **Central carbon metabolism slightly leaks to riboflavin synthesis**

Intracellular carbon metabolism in clostridia has been widely studied (Gheshlaghi et al. 2009; Jang et al. 2012). However, co-producing riboflavin involves Ru5P for GTP synthesis (Alosta 2007). In NaAc supplemented culture, Ru5P and X5P combined concentrations (Ru5P&X5P) decreased from 1.0E-3 ± 2.9E-4 mmol gDW^{-1} to 8.4E-5 ± 4.6E-5 mmol gDW^{-1} (Figure 5.6a). However, in the control culture, Ru5P&X5P reached a peak of 2.3E-3 mmol gDW^{-1} at 48 h, and stayed at high level until 70 h (1.2E-3 mmol gDW^{-1}). In fact, all quantified intracellular carbon flow metabolites concentration showed globally higher levels in the control culture compared to the NaAc supplemented culture (Figure 5.6). This phenomenon may be attributed to a robust "highway" processing system when cells enter solventogenesis under NaAc supplemented environment, canalizing metabolites accumulated in acidogenesis towards solvents production reactions.

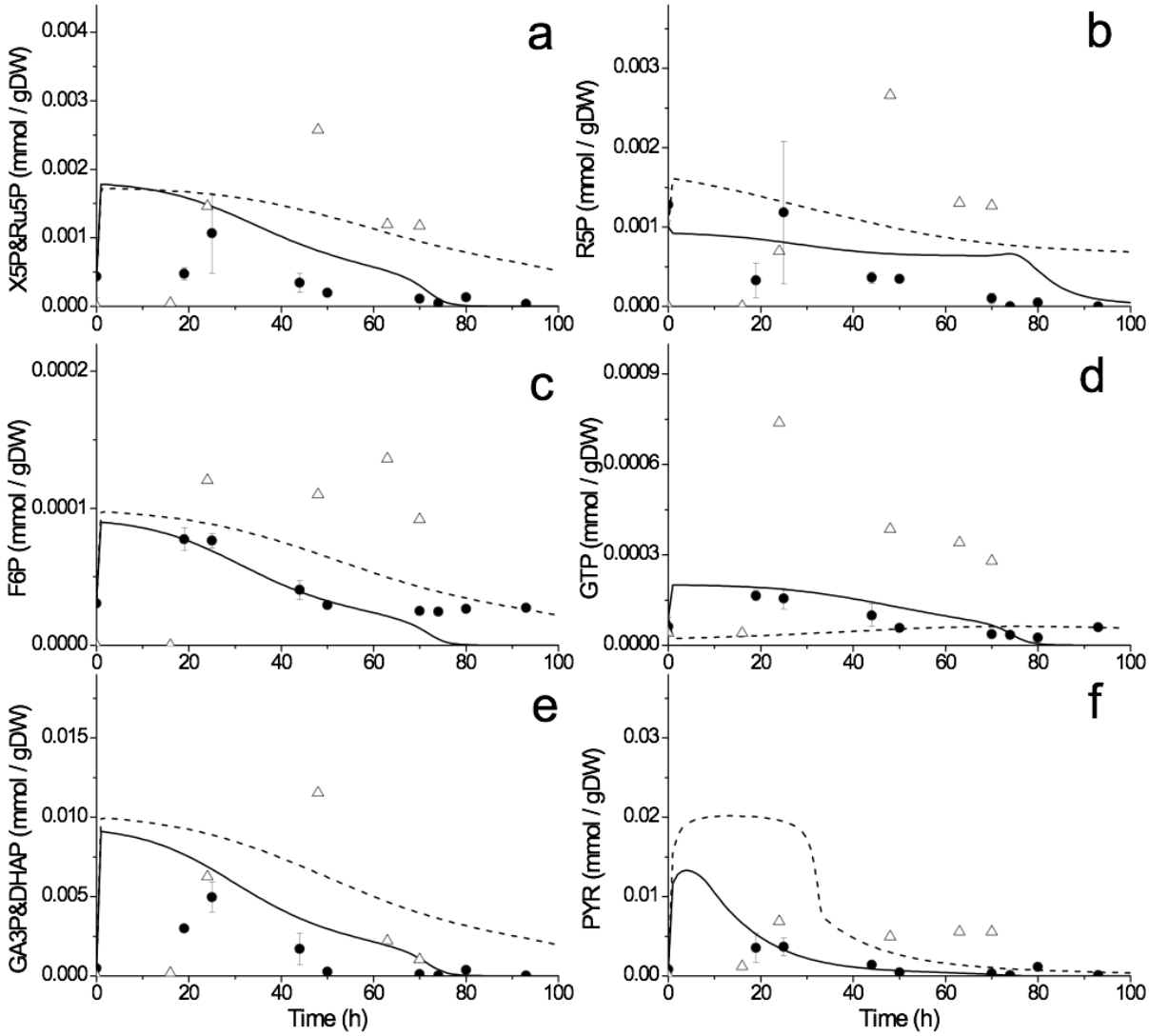

Figure 5. 6 Simulation results of intracellular carbon metabolites for a xylose culture of *C. acetobutylicum* ATCC 824. Solid line refers to simulation results for the 60 mM NaAc culture and dashed line to the control culture. Solid circle is experimental data for 60 mM NaAc; open triangle is experimental data in control culture. Error bars represent standard deviations from two independent culture replicates. (a) X5P&Ru5P; (b) R5P; (c) F6P; (d) GTP; (e) GA3P&DHAP; (f) PYR.

A dynamic model, such as the one developed in this work, also allows drawing a metabolic flux rate map for the network described at specific time points. We have thus taken snapshot images of the cells metabolic state at exponential growth (10 h) and at stationary phase (60 h) in both the control and the 60 mM NaAc supplemented cultures (Figure 5.7). As expected, the central carbon metabolism shows, in all cases, being the major route from the uptake of carbon substrates (i.e. xylose in control; xylose and acetate in 60 mM NaAc culture) to the end-point secreted metabolites. The flux to riboflavin synthesis only accounts for ~ 0.3 % of the xylose uptake flux. There is thus room for improving riboflavin production, adding sodium acetate. Of interest, adding acetate (i.e. a second carbon source) emphasizes the central role of ACoA as a hub for carbon flow between primary metabolism and solvents production oriented metabolism. While the central carbon metabolism is still highly active, solvents synthesis shows reduced rates at stationary growth, looking at PTA (ACoA to eACE), PTB (BCoA to eBUT), AYDH (ACoA to eEtOH), a phenomenon that is more pronounced in the 60 mM NaAc culture. Our observations, obtained *in silico* here, agree with a recently reported transcriptome study in *C. beijerinckii* NCIMB 8052 (Shi and Blaschek 2008), in which the expression of acetate formation genes encoding for phosphotransacetylase (*pta*) and acetate kinase (*ack*), and the butyrate formation gene encoding for butyrate kinase (*buk*), increased up to two-fold during acidogenesis and then declined along with solvents formation.

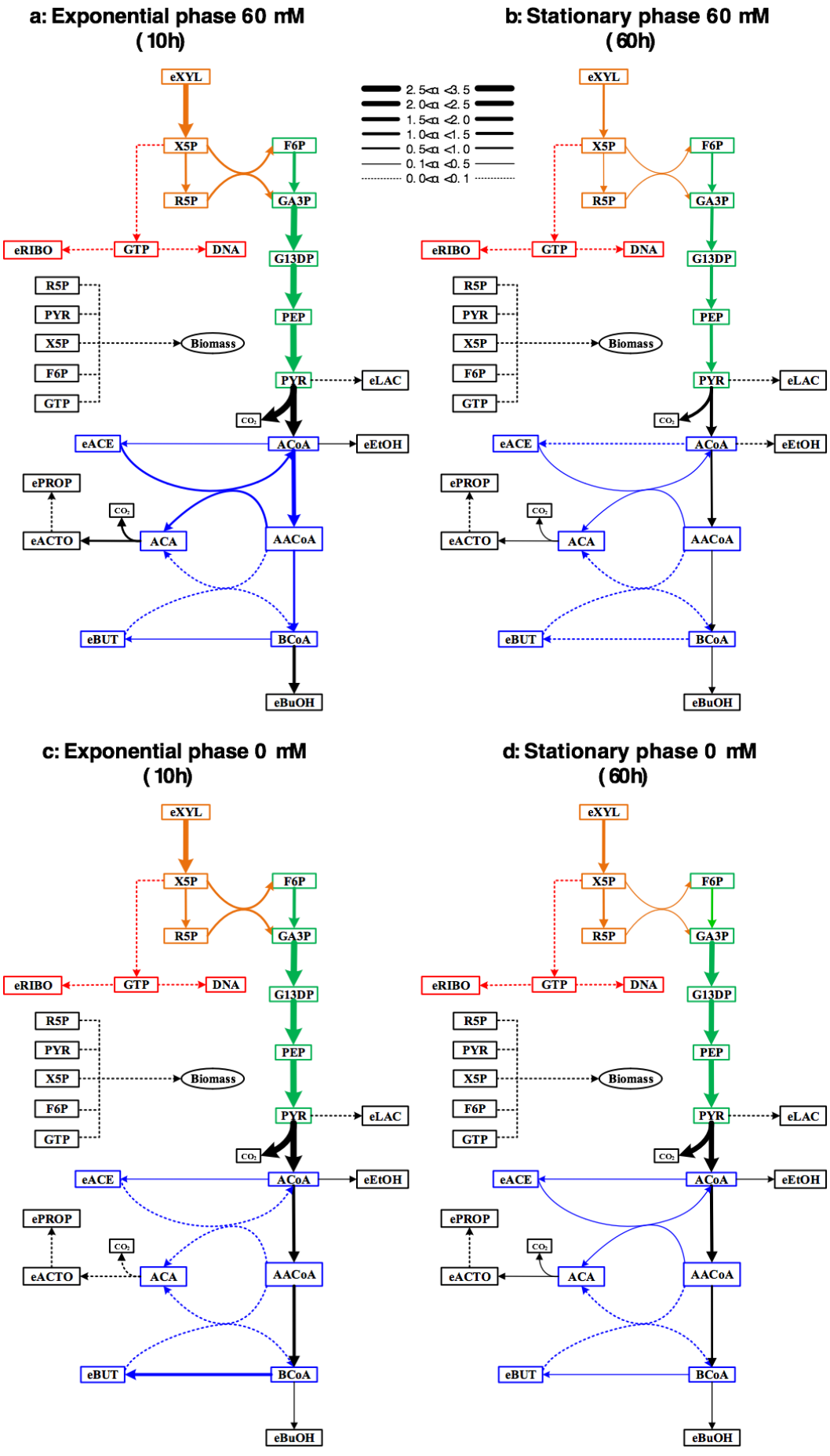
a: Exponential phase 60 mM (10h)
b: Stationary phase 60 mM (60h)
c: Exponential phase 0 mM (10h)
d: Stationary phase 0 mM (60h)
2.5≤ ≤3.5
2.0≤ <2.5
1.5≤ <2.0
1.0≤ <1.5
0.5≤ <1.0
0.1≤ <0.5
0.0≤ <0.1
eXYL
X5P
F6P
R5P
GA3P
eRIBO
GTP
DNA
G13DP
PEP
PYR
eLAC
Biomass
CO2
eACE
ACoA
eEtOH
ePROP
eACTO
ACA
AACoA
eBUT
BCoA
eBuOH

Figure 5. 7 Comparison of *C. acetobutylicum* ATCC 824 metabolic flux distribution at 10 h and 60 h for 60 mM NaAc supplement culture (a, b) and control culture (c, d) from model simulations. Brown colour represents PPP pathway; green colour represents glycolytic pathway; red colour represents riboflavin pathway; and blue colour represents acids to solvents conversion pathway. Flux unit is in mmol gDW^{-1} h^{-1}.

5.5.3.3 **GTP plays a key role in riboflavin production**

In our model, riboflavin is generated from GTP as reported for many microbial species, while GTP generation was simplified to be issued from X5P (Figure 5.2). Lim et al. have summarized three metabolic models of GTP synthesis as found in three representative organisms including *Candida famata*, *Bacillus subtilis* and *Ashbya gossypii*, which belong to yeast, bacteria and fungi, respectively (Lim et al. 2001). In *C. famate*, GTP is directly generated from Ru5P, while in *B. subtilis* it requires going through IMP, XMP and GMP, for then leading to GTP. However, in *A. gossypii*, GTP generation requires a more complex metabolic pathway, which includes glyoxylate reactions in the peroxisome and the citrate cycle in mitochondria from fatty acid catabolism. Here we simplified the reaction to GTP synthesis from X5P, because in the anaerobic clostridia species, TCA cycle activity is close of being negligible compared to other carbon fluxes (Gheshlaghi et al. 2009). In addition, we have included an activation effect of NaAc on riboflavin synthesis rate, using a kinetic representation suggested in literature (Robitaille et al. 2015). This hypothesis stands for either a direct or an indirect activation effect, through enzymatic reactions that are not explicitly described in our simplified model but that are lumped within described pathways.

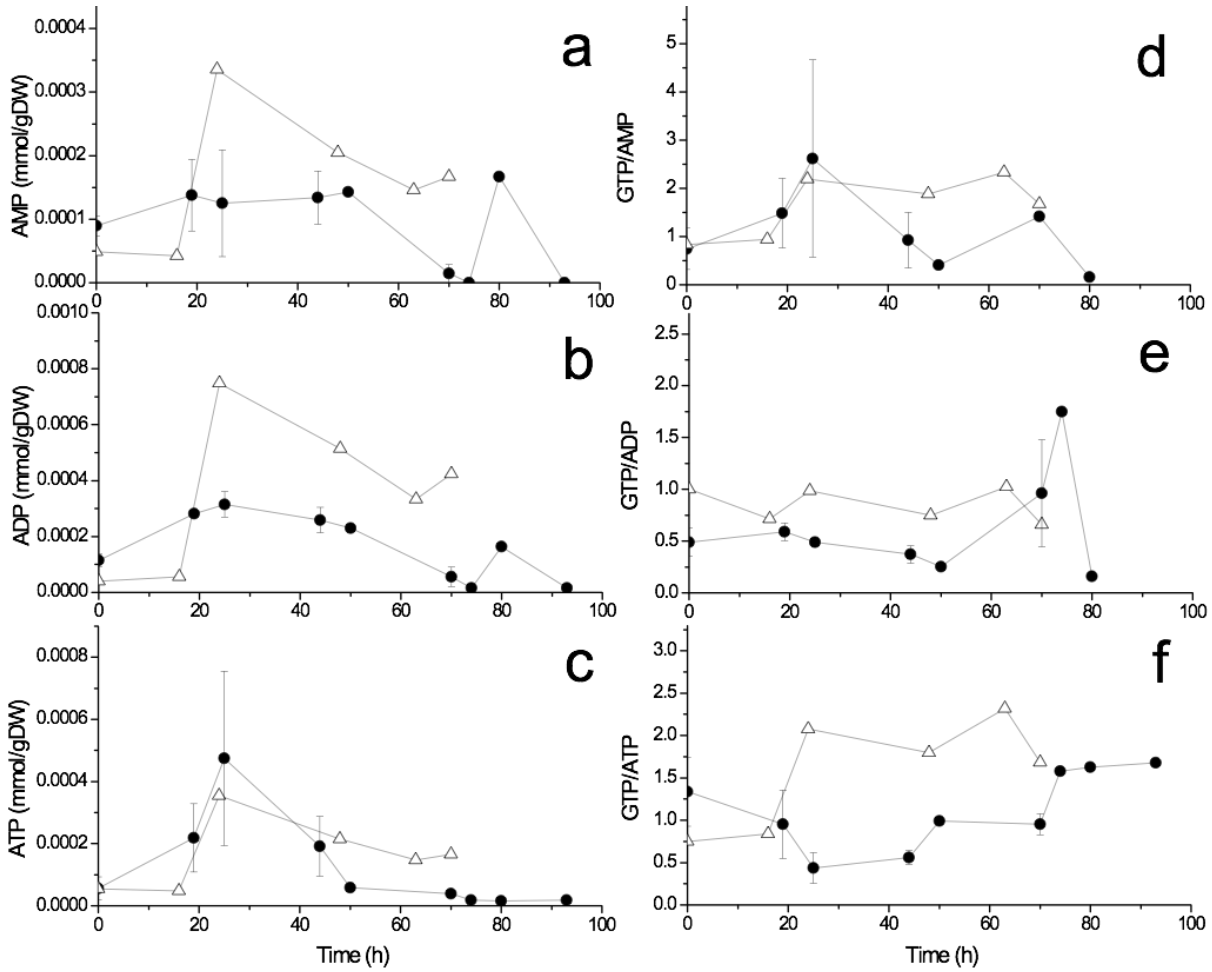

Figure 5. 8 Effect of NaAc on *C. acetobutylicum* ATCC 824 energetic state. Solid circle is experimental data for 60 mM NaAc; open triangle is experimental data in control culture. Error bars represent standard deviations from two independent culture replicates. Error bars represent standard deviations from two independent culture replicates. (a) AMP; (b) ADP; (c) ATP; (d) GTP -to- AMP ratio; (e) GTP -to- ADP ratio; (f) GTP -to- ATP ratio.

As previously mentioned, GTP is a precursor of the riboflavin biosynthesis pathway (Alosta 2007). In the NaAc supplemented culture, GTP concentration reached 1.6E-4 ± 1.6E-5 mmol gDW^{-1} (at 20 h), while a higher value of 7.4E-4 mmol gDW^{-1} at 24 h was observed in control culture, for continuously decreasing thereafter (Figure 5.6d). Therefore, GTP is accumulated in the control culture compared to the NaAc supplemented culture, in which GTP consumption was concurrent to riboflavin synthesis under acetate supplementation condition.

Indeed, GTP plays multiple key roles and for instance, it is the precursor of DNA synthesis by DNA polymerase I. Moreover, GTP energizes the process of AMP synthesis from nucleic acids, and ATP in turn provides energy for GTP and GDP synthesis (Michal 1999). Consequently, GTP and ATP are providing energy for the *de novo* synthesis of each other. Therefore, as a precursor of riboflavin, GTP can be significantly affected by the time-concentration dynamic of the adenosine phosphate groups. We have thus performed the intracellular quantification of the major adenosine phosphates (AMP, ADP and ATP) to learn more on potential limitation effects (Figure 5.8). In the control culture, AMP and ADP reached maximal values of 3.3E-4 mmol gDW^{-1} and 7.5E-4 mmol gDW^{-1} at 24 h, respectively, while lower levels were observed in the NaAc supplemented culture. For instance, AMP reached 1.2E-4 ± 8.4E-5 mmol gDW^{-1} at 25 h in the 60 mM NaAc culture, which is 62.8 % lower than the control. We have then analyzed the concentration ratios behaviours of the energetic nucleotides. Investigating the ratio of GTP to the three adenosine phosphates nucleotides quantified, results show that all these ratios were maintained at higher levels in the control than in the NaAc culture between 20 to 70 h (Figure 5.8d, e, f), corresponding to the higher riboflavin and solvents production period. Then, considering the lower ATP, ADP and AMP values observed in the NaAc culture, together with lower GTP -to- ATP, GTP -to- ADP and GTP -to- AMP ratios in NaAc culture, we can suggest that GTP has a lower role in the energetic metabolism compared to its contribution to riboflavin synthesis under 60 mM NaAc supplemented condition.

5.5.3.4 **Redox nucleotide concentration behaviour was affected by adding acetate**

As main regulators, redox nucleotides play a significant role in cell metabolism. Specifically in ABE fermentation, the NADP(H) redox pair is involved in reactions catalyzed by ethanol/butanol dehydrogenase, and glyceraldehyde-3-phosphate dehydrogenase, lactate dehydrogenase and ferredoxin-NADP reductase (Amador-Noguez et al. 2011; Gheshlaghi et al. 2009). However, one mole of NADPH is converted to NADH in the reaction from Ru5P to GTP, and another one mole of NADPH is converted to NADH by uracil reductase for GTP degradation (Zamboni 2003). Therefore, NADP(H) and NAD(H) pools fluctuation were also investigated along with riboflavin production. The NADPH concentration in control culture reached a maximum value of 9.3E-4 mmol gDW^{-1}, which was higher than that in the NaAc supplemented culture with 2.9E-4 ± 1.3E-4 mmol gDW^{-1}, respectively at 24 h and 25 h (Figure 5.9d). However, NADH shows an inversed trend with culture time, since NaAc supplemented culture reached 1.9E-2 ± 1.0E-2 mmol gDW^{-1}

at 19 h compared to 5.7E-3 mmol gDW^{-1} for the control at 16 h (Figure 5.9b). As mentioned above, two moles of NADPH are converted to two moles of NADH from Ru5P to riboflavin synthesis reaction, which agrees with our results showing lower NADPH and higher NADH concentrations in the 60 mM NaAc culture compared to that in control. NaAc addition may have promoted the conversion of NADPH to NADH, thus stimulating riboflavin synthesis reaction rate (Zamboni 2003). Additionally, we found a higher NADH -to- NAD ratio in the NaAc supplemented culture (9.4 ± 2.6) compared to the control (5.1) (Figure 5.9e). Therefore, NaAc addition have led to NADH accumulation accompanied with riboflavin synthesis.

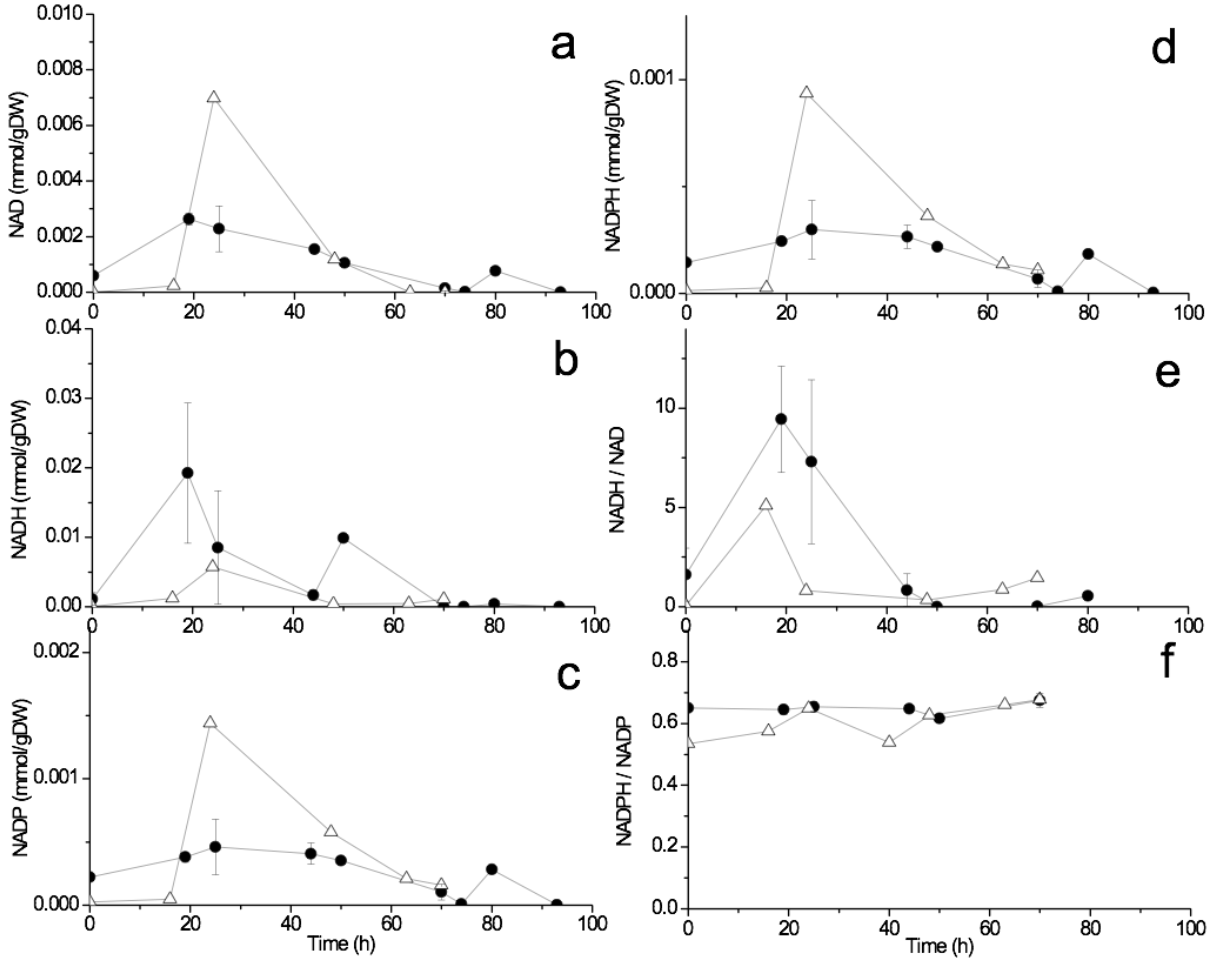

Figure 5. 9 Effect of NaAc on *C. acetobutylicum* ATCC 824 redox states. Solid circle is experimental data for 60 mM NaAc; open triangle is experimental data in control culture. Error bars represent standard deviations from two independent culture replicates. (a) NAD; (b) NADH; (c) NADP; (d) NADPH; (e) NADH -to- NAD ratio; (f) NADPH -to- NADP ratio.

5.5.3.5 **Amino acid metabolic analysis**

Amino acids metabolism is significant to ABE and riboflavin production. Riboflavin production was affected by amino acids has been reported in many microorganisms. For instance, Giri and Krishnaswamy investigated a yeast strain *Saccharomyces Cerevisise* cultivated by various amino acids for riboflavin production. Their results showed methionine, glycine, and arginine employed as the most efficient organic nitrogen sources in sequence, which promoted riboflavin yields of 40.5, 34.8 and 32.8 μg mL^{-1}, respectively (control reached 26.3 μg mL^{-1}) (Giri & Krishnaswamy, 1953). Meanwhile, in *Laciobacillus casei*, asparagine, methionine and glycine effectively promoted riboflavin accumulation as reported by Burkholder (Burkholder, 1943). In present study, 15 amino acids were tracked during NaAc supplemented cultures and the control culture, Figure 5.10 shows various amino acids consumption tendency. In summary, 11 amino acids were consumed obviously (phenylalanine, threonine, isoleucine, leucine, methionine, valine, tyrosine, glycine, serine, arginine, asparagine.), 3 amino acids (proline, histadine and asparatic acid) kept in a stable level. Interestingly, one amino acid (glutamine) accumulated. In fact, this is the first time we found glutamine could be accumulated in clostridia species. With respect to global amino acids metabolism, Fonknechten et al. investigated that in clostridia species (*Clostridium sticklandii*), glycine, serine, arginine and threonine were consumed, which were proved in present work as well. They also found glutamate, aspartate and alanine were accumulated (Fonknechten et al., 2010), however no glutamine accumulation was observed. Mead studied 30 various clostridia species and divided them into four groups depending on their amino acid consumption features, however, all of them only show different priority in utilization, but no amino acid accumulation was discovered (Mead, 1971). In our research, glutamine accumulated from initial 0.12 ± 0.003 mM to 0.27 ± 0.04 mM at ~ 80 h (Figure 5.10i). Glutamine syntheses played the key role on transforming glutamate to glutamine with one mole ATP degradation (Michal, 1999). However, glutamate could be generated by many amino acids through alpha-ketoglutaric acid in citrate cycle, such as asparagine, phenylalanine and tyrosine. Therefore, as the first possibility, accumulated glutamine was converted from other degraded amino acids in present research and may be induced by NaAc supplement.

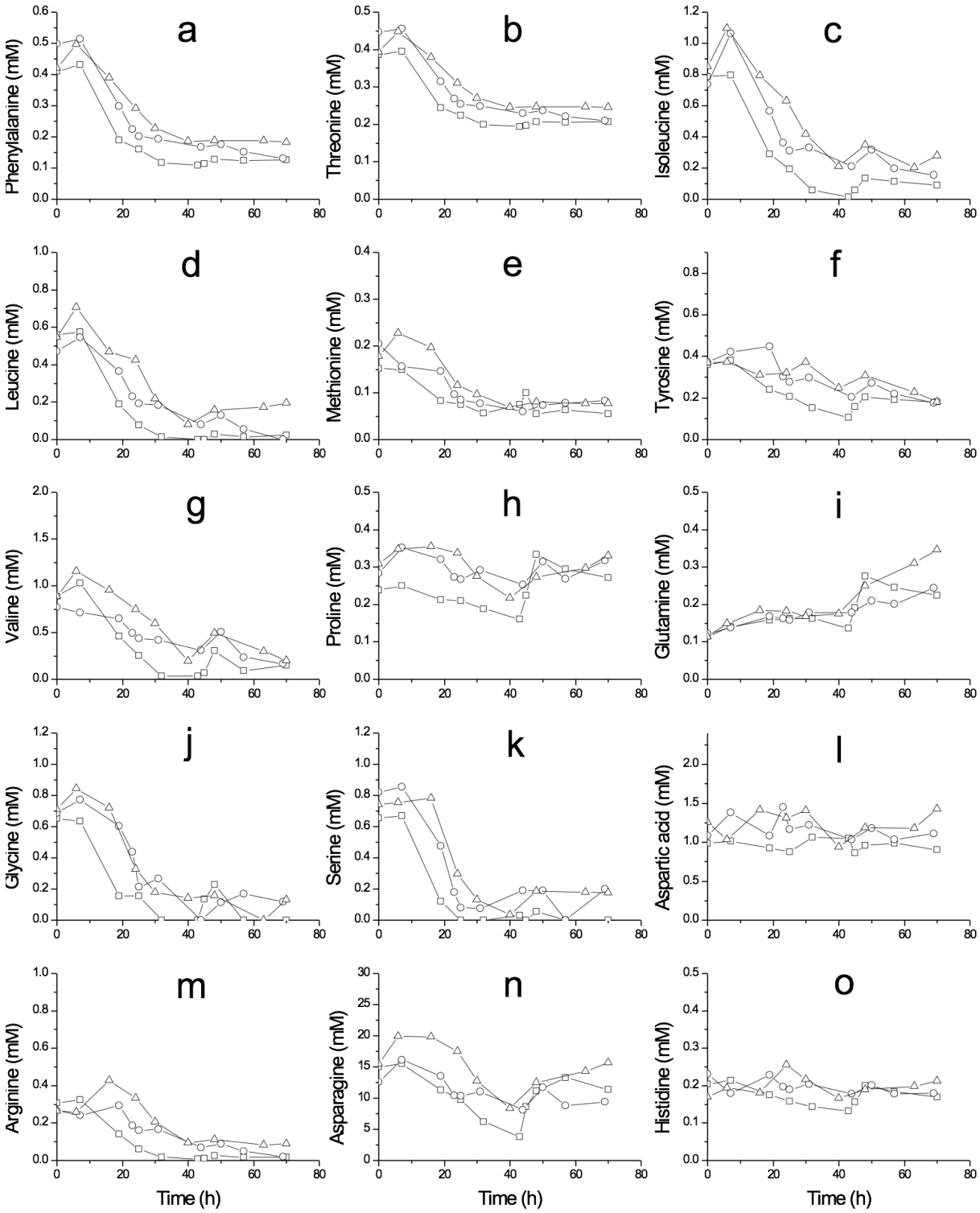
a
Phenylalanine (mM)
b
Threonine (mM)
c
Isoleucine (mM)
d
Leucine (mM)
e
Methionine (mM)
f
Tyrosine (mM)
g
Valine (mM)
h
Proline (mM)
i
Glutamine (mM)
j
Glycine (mM)
k
Serine (mM)
l
Aspartic acid (mM)
m
Arginine (mM)
n
Asparagine (mM)
o
Histidine (mM)
Time (h)
Time (h)
Time (h)

Figure 5. 10 Fifteen amino acids degradation in test and control cultures in xylose by *C. acetobutylicum* ATCC 824. Open square and circle symbols are two parallar test culture in 60 mM NaAc condition, triangle is control.

As previous discussion, GTP is a significant flux joint in riboflavin generation. Amino acids provide carbon and nitrogen resource for its novo synthesis though purine metabolism. Therefore, some amino acids would be related to GTP and riboflavin production when they participated into purine metabolism. For instance, glycine has been proved generating 5C and 7N atoms and glutamine was responsible for 3N and 9N generating in purine ring atoms. (Michal, 1999). Meanwhile, glycine was easily catalyzed to serine by glycine hydroxymethyltransferase and to threonine by L-threonine aldolase. So glycine and glutamine should play a special role in riboflavin generation.

As mentioned above, glycine consumption contributed to a high riboflavin production which is in accordance with our result shown in Figure 5.10j. It reached to trace amount at 32 h and 44 h in both test cultures, but it still remained 0.16 ± 0.01 mM between 30-48h in control group. The similar tendency of consumption also exhibited in arginine (Figure 5.10m), another riboflavin sensitive organic nitrogen source, which was consumed less in control group compared to test culutres (Figure 5.10b). Meanwhile, as one of the main nitrogen source in the present culture, asparagine also showed higher utilization in test groups (Figure 5.10n). Therefore, glycine and arginine and asparagine may be comparably effect to promoted riboflavin accumulation in this research, which is in according with previous reports.

5.6 **Conclusion**

In is clear from this work that supplementing NaAc at 60 mM stimulates riboflavin production in ABE fermentation by *C. acetobutylicum* ATCC 824 with xylose as the carbon source. It thus provides a novel strategy for co-producing riboflavin and ABE solvents, i.e. both products of commercial interest. Investigating central carbon metabolism dynamics using a kinetic metabolic model simulating experimental data, brought insights on how the addition of sodium acetate also activates ABE solvents production. Model simulations also agree with biphasic fermentation from acidogensis to solventogenesis, that occurs in ABE fermentation. This work thus provides a new approach to producing riboflavin as a co-product enhancing the commercial feasibility of ABE

fermentation bioprocesses. Finally, further work implementing the kinetic metabolic model with cell energetics and redox states, as well as cell nutrition states (amino acids), should enhance the model simulation capacity as an *in silico* platform to seek the maximizing of riboflavin-ABE fermentation yields.

5.7 Acknowledgements

The authors thank the BioFuelNet Center of Excellence and the Natural Sciences and Engineering Research Council of Canada for their financial support. All authors declare they have no conflict of interest for the work presented in this manuscript.

5.8 Author Contributions

X.Z. designed and performed the experiments; analyzed the data, processed model and wrote the manuscript. M.K. contributed performing the experiments. J.C. performed culture sample analysis and quantification on the UPLC/MS/MS and the GC-FID equipment. S.P. contributed with a program generating automatically the Matlab code for a specific metabolic network of reactions. M.J. contributed to the design of the experimental, data analysis as well as on model development. He did also participate to the manuscript writing, and he has approved the final version of the manuscript.

5.9 Supplementary material 1

A dynamic metabolic flux analysis of co-producing riboflavin in ABE (acetone-butanol-ethanol) fermentation by *Clostridium acetobutylicum* ATCC 824

Xinhe Zhao[1], Mayssa Kasbi[1], Jingkui Chen[1], Sabine Peres[2], Mario Jolicoeur[1*]

[1] Research Laboratory in Applied Metabolic Engineering, Department of Chemical Engineering, École Polytechnique de Montréal, P.O. Box 6079, Centre-ville Station, Montréal, Québec, H3C 3A7, Canada

[2] LRI, Université Paris-Sud, CNRS, Université Paris-Saclay, 91405 Orsay, France

MaIAGE, INRA, Université Paris-Saclay, 78350 Jouy-en-Josas, France

Title: The dynamic metabolic model

5.9.1 Model hypothesis and description

A kinetic metabolic model was developed to describe ABE fermentation biosystem dynamics, with the aim of performing a dynamic metabolic flux analysis (dMFA) to evaluate the effect of supplementing the culture medium at 60 mM sodium acetate (NaAc) of an ABE fermentation on xylose. The model was developed for Clostridia based on a modelling approach previously developed to describe plant (Cloutier et al. 2008; Cloutier et al. 2007) and Chinese Hamster Ovary cells (CHO) (Ghorbaniaghdam et al. 2013; Robitaille et al. 2015). Details on model development and potentialities of use can be found in the latter cited articles. Briefly, the model structure includes the central carbon metabolism and specific pathways related to ABE and riboflavin synthesis, such as PPP and glycolysis pathways, active parts of tricarboxylic acid cycle (TCA), acids and solvents formation, purine metabolism and riboflavin synthesis. The metabolic network and enzymatic reactions stoichiometry were taken from literature (Gheshlaghi et al. 2009; Hideaki Shinto et al. 2008). Model reaction network is illustrated in Figure 5.2, reactions stoichiometry is presented in Table S1, and flux kinetic equations are presented in Table S2.

Table S 1. Stoichiometric of reactions in the model

Enzyme	Reaction
XR	XYL => X5P
rpiA	X5P = R5P
PurM	X5P => 0.5 GTP
ribA	GTP => 0.6 RIBO
DPO1	GTP => DNA
tktA	2 X5P + R5P => 2 F6P + GA3P
PFK	F6P => 2 GA3P
GA3PDH	GA3P => G13DP
PGK	G13DP => PEP
PK	PEP => PYR
LDH	PYR => LAC
PFOR	PYR => ACoA + CO_2
PTA	ACoA = ACE
AYDH	ACoA => EtOH
THL	2 ACoA => AACoA
CoATa	AACoA + ACE => ACoA + ACA
BHBD	AACoA => BCoA
CoATb	AACoA + BUT => ACA + BCoA
AADC	ACA => ACTO + CO_2
SADH	ACTO => PROP
PTB	BCoA = BUT
BYDH	BCoA => BuOH
growth	X5P + R5P + F6P + PYR + GTP => X

=> unidirectional reaction; = reversible reaction

Table S 2. Kinetic equations of the metabolic fluxes in the model

No.	Kinetics
1	$V\_XR = V_{max\_XR} \bullet \frac{XYL}{K_{m\_XR\_XYL} + XYL} \bullet \frac{k_{i\_XR\_BuOH}}{k_{i\_XR\_BuOH} + XYL}$
2	$V\_rpiA = V_{max\_rpiA} \bullet \frac{X5P}{K_{m\_rpiA\_X5P} + X5P} - V_{maxr\_rpiA} \bullet \frac{R5P}{K_{m\_rpiA\_R5P} + R5P}$
3	$V\_PurM = V_{max\_PurM} \bullet \frac{X5P \bullet (1 + \frac{ACE}{k_{a\_PurM\_ACE}} \bullet \frac{\beta_{PurM\_ACE}}{\alpha_{PurM\_ACE}})}{K_{m\_PurM\_X5P} \bullet \left(1 + \frac{ACE}{k_{a\_PurM\_ACE}}\right) + X5P \bullet (1 + \frac{ACE}{k_{a\_PurM\_ACE}} \bullet \frac{1}{\alpha_{PurM\_ACE}})}$
4	$V\_ribA = V_{max\_ribA} \bullet \frac{GTP}{K_{m\_ribA\_GTP} + GTP}$
5	$V\_DPO1 = V_{max\_DPO1} \bullet \frac{GTP}{K_{m\_DPO1\_GTP} + GTP}$
6	$V\_tktA = V_{max\_tktA} \bullet \frac{X5P}{K_{m\_tktA\_X5P} + X5P} \bullet \frac{R5P}{K_{m\_tktA\_R5P} + R5P}$
7	$V\_PFK = V_{max\_PFK} \bullet \frac{F6P}{K_{m\_PFK\_F6P} + F6P}$
8	$V\_GAPDH = V_{max\_GAPDH} \bullet \frac{GA3P}{K_{m\_GAPDH\_GA3P} + GA3P}$
9	$V\_PGK = V_{max\_PGK} \bullet \frac{G13DP}{K_{m\_PGK\_G13DP} + G13DP}$
10	$V\_PK = V_{max\_PK} \bullet \frac{PEP}{K_{m\_PK\_PEP} + PEP}$
11	$V\_LDH = V_{max\_LDH} \bullet \frac{PYR}{K_{m\_LDH\_PYR} + PYR}$
12	$V\_PFOR = V_{max\_PFOR\_PYR} \bullet \frac{PYR}{K_{m\_PFOR\_PYR} + PYR}$
13	$V\_THL = V_{max\_THL\_ACoA} \bullet \frac{ACoA}{K_{m\_THL\_ACoA} + ACoA}$

14 $$V\_PTA = V_{max\_PTA} \bullet \frac{ACoA}{K_{m\_PTA\_ACoA} + ACoA} - V_{maxr\_PTA} \bullet \frac{ACE}{K_{m\_PTA\_ACE} + ACE}$$

15 $$V\_CoATa = V_{max\_CoATa} \bullet \frac{ACE}{K_{m\_CoATa\_ACE} + ACE} \bullet \frac{AACoA}{K_{m\_CoATa\_AACoA} + AACoA}$$

16 $$V\_AYDH = V_{max\_AYDH\_ACoA} \bullet \frac{ACoA}{K_{m\_AYDH\_ACoA} + ACoA}$$

17 $$V\_AADC = V_{max\_AADC} \bullet \frac{ACA}{K_{m\_AADC\_ACA} + ACA}$$

18 $$V\_SADH = V_{max\_SADH} \bullet \frac{ACTO}{K_{m\_SADH\_ACTO} + ACTO}$$

19 $$V\_CoATb = V_{max\_CoATb} \bullet \frac{BUT}{K_{m\_CoATb\_BUT} + BUT} \bullet \frac{AACoA}{K_{m\_CoATb\_AACoA} + AACoA}$$

20 $$V\_BHBD = V_{max\_BHBD} \bullet \frac{AACoA}{K_{m\_BHBD\_AACoA} + AACoA}$$

21 $$V\_PTB = V_{max\_PTB} \bullet \frac{BCoA}{K_{m\_PTB\_BCoA} + BCoA} - V_{maxr\_PTB} \bullet \frac{BUT}{K_{m\_PTB\_BUT} + BUT}$$

22 $$V\_BYDH = V_{max\_BYDH} \bullet \frac{BCoA \bullet (1 + \frac{ACE}{k_{a\_BYDH\_ACE}} \bullet \frac{\beta_{BYDH\_ACE}}{\alpha_{BYDH\_ACE}})}{K_{m\_BYDH\_X5P} \bullet \left(1 + \frac{ACE}{k_{a\_BYDH\_ACE}}\right) + BCoA \bullet (1 + \frac{ACE}{k_{a\_BYDH\_ACE}} \bullet \frac{1}{\alpha_{BYDH\_ACE}})}$$

23 $$V\_growth = V_{max\_growth} \bullet \frac{R5P}{K_{m\_growth\_R5P} + R5P} \bullet \frac{X5P}{K_{m\_growth\_X5P} + X5P} \bullet \frac{F6P}{K_{m\_growth\_F6P} + F6P} \bullet \frac{PYR}{K_{m\_growth\_PYR} + PYR} \bullet \frac{GTP}{K_{m\_growth\_GTP} + GTP}$$

Reactions direction illustrated in Figure 5.2 and in Table S1 were either determined from literature or from model simulation results, although each flux sign was not constrained while performing model simulations. Overall, three reactions (rpiA, PTA, PTB) exhibited reversibility in simulations and were thus illustrated accordingly. Multi Michaelis-Menten equations were developed to describe each reaction kinetics (Equation 1):

$V_i = V_{i,max} \left[\prod_{i=1}^{n} \frac{S_i}{K_{mi}+S_i}\right]$ Equation 1.

Where V_i is the specific flux rate (mmol gDW^{-1} h^{-1}), $V_{i,max}$ the maximum specific flux rate (mmol gDW^{-1} h^{-1}) and S_i is substrate "*i*" specific concentration (mmol gDW^{-1}). Intracellular concentrations and fluxes are normalized to the bacterial cell mass since it is the most precise data in hand, i.e. with no data on the cell intracellular volume. This description approach forces a flux being modulated from the concentration of each single substrate involved. Mass balances were developed on each intracellular metabolite (in mmol gDW^{-1}), which resulted in a set of 24 ordinary differential equations system (Table S3). The general mass balance equation is described as follows:

$$\frac{dM}{dt} = S \bullet -\mu \bullet M - \mu \bullet \varepsilon \qquad \text{Equation 2.}$$

where S is the stoichiometric matrix of the network fluxes, is the vector of the reaction flux (mmol gDW^{-1} h^{-1}), μ is the specific growth rate (h^{-1}), and *M* is the vector of the 24 metabolites concentration. The cell dilution term ($\mu \bullet M$) describes the dilution of intracellular metabolites from cell division of a mother cell into two daughter cells, each with similar final volume. Moreover, the consumption of intracellular metabolites into cell material for growth is also described with $\mu \bullet \varepsilon$, where $\varepsilon$is the stoichiometric coefficient of the "*i*" metabolite integrated into biomass (i.e. not available to reactions).

Table S 3. Mass balances equations of the model

No.	Mass balance
1	$\frac{dAACoA}{dt} = V\_THL - V\_CoATa - V\_BHBD - V\_CoATb - (V\_growth \bullet AACoA)$
2	$\frac{dACA}{dt} = V\_CoATa + V\_CoATb - V\_AADC - (V\_growth \bullet ACA)$
3	$\frac{dACoA}{dt} = V\_PFOR - V\_PTA - V\_AYDH - (2 \bullet V\_THL) + V\_CoATa - (V\_growth \bullet ACoA)$
4	$\frac{dBCoA}{dt} = V\_BHBD + V\_CoATb - V\_PTB - V\_BYDH - (V\_growth \bullet BCoA)$
5	$\frac{dDNA}{dt} = V\_DPO1 - (V\_growth \bullet NDA)$
6	$\frac{dF6P}{dt} = 2 \bullet V\_tktA - V\_PFK - (V\_growth \bullet F6P) - (V\_growth\_F6P \bullet V\_growth)$
7	$\frac{dG13DP}{dt} = V\_GAPDH - V\_PGK - (V\_growth \bullet G13DP)$
8	$\frac{dGA3P}{dt} = V\_tktA + (2 \bullet V\_PFK) - V\_GAPDH - (V\_growth \bullet GA3P)$
9	$\frac{dGTP}{dt} = (0.5 \bullet V\_purM) - V\_ribA - V\_DPO1 - (V\_growth \bullet GTP) - (V\_growth\_GTP \bullet V\_growth)$
10	$\frac{dPEP}{dt} = V\_PGK - V\_PK - (V\_growth \bullet PEP)$
11	$\frac{dPYR}{dt} = V\_PK - V\_LDH - V\_PFOR - (V\_growth \bullet PYR) - (V\_growth\_PYR \bullet V\_growth)$
12	$\frac{dR5P}{dt} = V\_rpiA - V\_tktA - (V\_growth \bullet R5P) - (V\_growth\_R5P \bullet V\_growth)$

13	$\frac{dX5P}{dt} = V\_XR - V\_rpiA - V\_purM - (2 \bullet V\_tktA) - (V\_growth \bullet X5P) - (V\_growth\_X5P \bullet V\_growth)$
14	$\frac{dXYL}{dt} = -V\_XR \bullet X$
15	$\frac{dRIBO}{dt} = (0.6 \bullet V\_ribA) \bullet X$
16	$\frac{dLAC}{dt} = V\_LDH \bullet X$
17	$\frac{dACE}{dt} = (V\_PTA - V\_CoATa) \bullet X$
18	$\frac{dACTO}{dt} = (V\_AADC - V\_SADH) \bullet X$
19	$\frac{dBUT}{dt} = (V\_CoATb + V\_PTB) \bullet X$
20	$\frac{dEtOH}{dt} = V\_AYDH \bullet X$
21	$\frac{dBuOH}{dt} = V\_BYDH \bullet X$
22	$\frac{dCO2}{dt} = (V\_PFOR + V\_AADC) \bullet X$
23	$\frac{dPROP}{dt} = V\_SADH \bullet X$
24	$\frac{dX}{dt} = X \bullet V\_growth - a \bullet X \bullet \frac{BuOH}{ki\_growth\_BuOH}$

Biomass growth is assumed to be supported by the consumption of precursors of biomass macromolecules such as R5P, X5P and Ru5P (all contributing to (deoxy) ribonucleic acid, and nucleotides), PYR (cell wall polysaccharide formation (Schaffer and Messner 2005)) and F6P

(phospholipids formation); with the specific growth rate being described as equation 23 in Table S2. In addition, growth rate inhibition by butanol was considered by including a specific cell death term simply detailed as an inhibition constant term (Equation 3) as proposed by (Bouville 2007).

$$\frac{dX}{dt} = \mu X - aX\frac{C\_BuOH}{K_{i\_BuOH}} \quad \text{Equation 3.}$$

where "μ" is the specific growth rate (h^{-1}), "a" is a proportionality constant describing cell death rate (h^{-1}), C_BuOH is the butanol concentration in the medium (mM) and K_{i_BuOH} is the inhibition constant describing butanol inhibition on cell viability (mM). All intracellular metabolites were referred as mmol per gram dry cell weight (mmol gDW^{-1}) while extracellular metabolites were taken as in mM. For simplification purposes, all extracellular metabolites were hypothesized moving freely, without any transport delay nor concentration gradients between cell volume and external medium. Enzymes activation (Equation 4) or inhibition (Equation 5) were considered in the flux rate equations, as proposed in (Segel 1975).

$$V = \frac{S_i \bullet (1+\frac{A_i}{k_{activation}} \bullet \frac{\beta}{\alpha})}{K_m \bullet \left(1+\frac{A}{k_{activation}}\right) + S_i \bullet (1+\frac{A}{k_{activation}} \bullet \frac{1}{\alpha})} \quad \text{Equation 4.}$$

$$V = V_{initial} \bullet \frac{K_{inhibition}}{K_{inhibition}+S_i} \quad \text{Equation 5.}$$

The list of metabolites considered in the model network and their initial values are presented in Table S4 and the flux kinetic parameters in Table S5. All parameters were initially determined from experimental data (when possible) and from literature (when available), and finally determined minimizing an objective function defining simulation error as detailed below. The model structure, with ordinary differential equations system, was written in Matlab code (The MathWorks Inc., Natick, MA, USA). Since the model is a simplified representation of the complete cell network of biochemical reactions, enzymes described in each reaction thus represent lumped sets of reactions. Consequently, the kinetic parameters also represent lumped information from any other reactions and regulatory mechanisms involved in a flux and that are not considered in the model. However, since model structure and kinetic description rely on experimental data information, the output results interpretation stay reliable, when limiting the study to the actual experimental space.

Table S 4. State variables initial values

Component	Initial value	Unit
AACoA	3.0E-08	mmol gDW^{-1}
ACA	3.0E-07	mmol gDW^{-1}
ACoA	5.0E-05	mmol gDW^{-1}
BCoA	3.0E-08	mmol gDW^{-1}
F6P	3.3E-05	mmol gDW^{-1}
G13DP	3.0E-05	mmol gDW^{-1}
GA3P	4.6E-04	mmol gDW^{-1}
GTP	9.2E-05	mmol gDW^{-1}
PEP	3.0E-05	mmol gDW^{-1}
PYR	7.7E-04	mmol gDW^{-1}
R5P	1.0E-03	mmol gDW^{-1}
X5P	4.0E-04	mmol gDW^{-1}
DNA	2.0E-03	mmol gDW^{-1}
eXYL	2.2E+02	mM
eRIBO	8.2E-03	mM
eLAC	6.1E-01	mM
eACE	6.1E+01	mM
eACTO	1.0E-03	mM
eBUT	1.6E+00	mM
eEtOH	0.0E+00	mM
eBuOH	0.0E+00	mM
eCO2	1.0E+00	mM
ePRPO	1.0E-01	mM
X	1.4E-01	gDW L^{-1}

Table S 5. Parameters values

Parameters	Value	Units	Parameters	Value	Units
vmax_XR	2.2	mmol gDW^{-1} h^{-1}	km_XR_XYL	5	mM
vmax_rpiA	5	mmol gDW^{-1} h^{-1}	km_rpiA_X5P	0.01	mmol gDW^{-1}
vmaxr_rpiA	0.02	mmol gDW^{-1} h^{-1}	km_rpiA_R5P	0.015	mmol gDW^{-1}
vmax_PurM	0.001	mmol gDW^{-1} h^{-1}	km_ribA_GTP	0.005	mmol gDW^{-1}
vmax_ribA	0.12	mmol gDW^{-1} h^{-1}	km_DPO1_GTP	0.006	mmol gDW^{-1}
vmax_DPO1	0.006	mmol gDW^{-1} h^{-1}	km_TKTa_R5P	0.00015	mmol gDW^{-1}
vmax_TKTa	3	mmol gDW^{-1} h^{-1}	km_TKTa_X5P	0.005	mmol gDW^{-1}
vmax_PFK	3.4	mmol gDW^{-1} h^{-1}	km_PFK_F6P	0.00014	mmol gDW^{-1}
vmax_GAPDH	7	mmol gDW^{-1} h^{-1}	km_GAPDH_GA3P	0.01	mmol gDW^{-1}
vmax_PGK	4	mmol gDW^{-1} h^{-1}	km_PGK_G13DP	0.001	mmol gDW^{-1}
vmax_PK	3.35	mmol gDW^{-1} h^{-1}	km_PK_PEP	0.003	mmol gDW^{-1}
vmax_LDH	0.06	mmol gDW^{-1} h^{-1}	km_LDH_PYR	0.00006	mmol gDW^{-1}
vmax_PFOR	3.4	mmol gDW^{-1} h^{-1}	km_PFOR_PYR	0.0008	mmol gDW^{-1}
vmax_PTA	1	mmol gDW^{-1} h^{-1}	km_PTA_ACoA	0.00005	mmol gDW^{-1}
vmaxr_PTA	0.3	mmol gDW^{-1} h^{-1}	km_PTA_ACE	20	mM
vmax_AYDH	4	mmol gDW^{-1} h^{-1}	km_THL_ACoA	0.0001	mmol gDW^{-1}
vmax_THL	5	mmol gDW^{-1} h^{-1}	km_AYDH_ACoA	0.0008	mmol gDW^{-1}
vmax_CoATa	22	mmol gDW^{-1} h^{-1}	km_CoATa_ACE	24	mM
vmax_BHBD	19	mmol gDW^{-1} h^{-1}	km_CoATa_AACoA	0.000001	mmol gDW^{-1}
vmax_CoATb	2	mmol gDW^{-1} h^{-1}	km_BHBD_AACoA	0.000001	mmol gDW^{-1}
vmax_AADC	18	mmol gDW^{-1} h^{-1}	km_CoATb_AACoA	0.000004	mmol gDW^{-1}
vmax_PTB	25	mmol gDW^{-1} h^{-1}	km_CoATb_BUT	0.2	mM
vmaxr_PTB	0.5	mmol gDW^{-1} h^{-1}	km_AADC_ACA	0.00001	mmol gDW^{-1}
vmax_BYDH	8	mmol gDW^{-1} h^{-1}	km_PTB_BCoA	0.0000005	mmol gDW^{-1}
vmax_SADH	0.1	mmol gDW^{-1} h^{-1}	km_PTB_BUT	0.1	mM
vmax_growth	0.28	h^{-1}	km_SADH_ACTO	10	mM
V_growth_F6P	0.26	mmol gDW^{-1}	km_growth_F6P	0.00008	mmol gDW^{-1}
V_growth_R5P	0.76	mmol gDW^{-1}	km_growth_R5P	0.00005	mmol gDW^{-1}
V_growth_X5P	0.26	mmol gDW^{-1}	km_growth_X5P	0.0001	mmol gDW^{-1}
V_growth_GTP	0.000025	mmol gDW^{-1}	km_growth_GTP	0.00006	mmol gDW^{-1}

V_growth_PYR	0.26	mmol gDW^{-1}	km_growth_PYR	0.00008	mmol gDW^{-1}
ka_PurM_ACE	10	mM	ka_BYDH_ACE	3	mM
alpha_PurM_ACE	5	/	alpha_BYDH_ACE	1.5	/
beta_PurM_ACE	20	/	beta_BYDH_ACE	35	/
km_PurM_X5P	0.0001	mmol gDW^{-1}	km_BYDH_BCoA	0.000005	mmol gDW^{-1}
ki_growth_BuOH	20	mM	ki_XR_BuOH	45	mM

5.9.2 Model calibration and parameters sensitivity analysis

The objective function is defined as the sum of weighted square residues between experimental data ($X_{n,t}^{exp}$) and model simulated values ($X_{n,t}^{sim}$), and this form allows normalizing each data range, thus avoiding effect from large differences in data values.

$$\min\left(\sum_{n=1}^{N}\sum_{t=1}^{T}\left(\frac{X_{n,t}^{exp}-X_{n,t}^{sim}}{X_{n,t}^{exp}}\right)^2\right) \quad \text{Equation 6.}$$

We then proceed by unlocking the subsets of measured metabolites until all related kinetic parameters value are determined. Parameter optimization step is performed by minimizing the objective function using the Matlab "lsqcurvefit" sub-routine. Model parameters sensitivity analysis was performed to confirm the optimization step, and identify sensitive parameters, i.e. the candidates for a refined optimization process. A sensitivity analysis on model parameters value was performed with each parameter value changed, one by one, over a range of - 50 % to + 100 % around its initial (or optimized) value, while keeping all others constant. The value of the objective function was evaluated assessing each parameter, one at the time, for detecting significant parameters and avoid over-parameterization, with a criterion of 10 % deviation of the objective function value when changing parameters value.

In this work, sensitivity analysis resulted in the identification of 26 parameters thus revealed to be sensitive from the 72 parameters of the model (Figure S1). Then, the model was tested by validating the parameters value optimization process discriminating with the confidence interval of each parameter. 95 % confidence interval for highly sensitive parameters were determined using the Matlab sub-routine "alparci" (Figure S2).

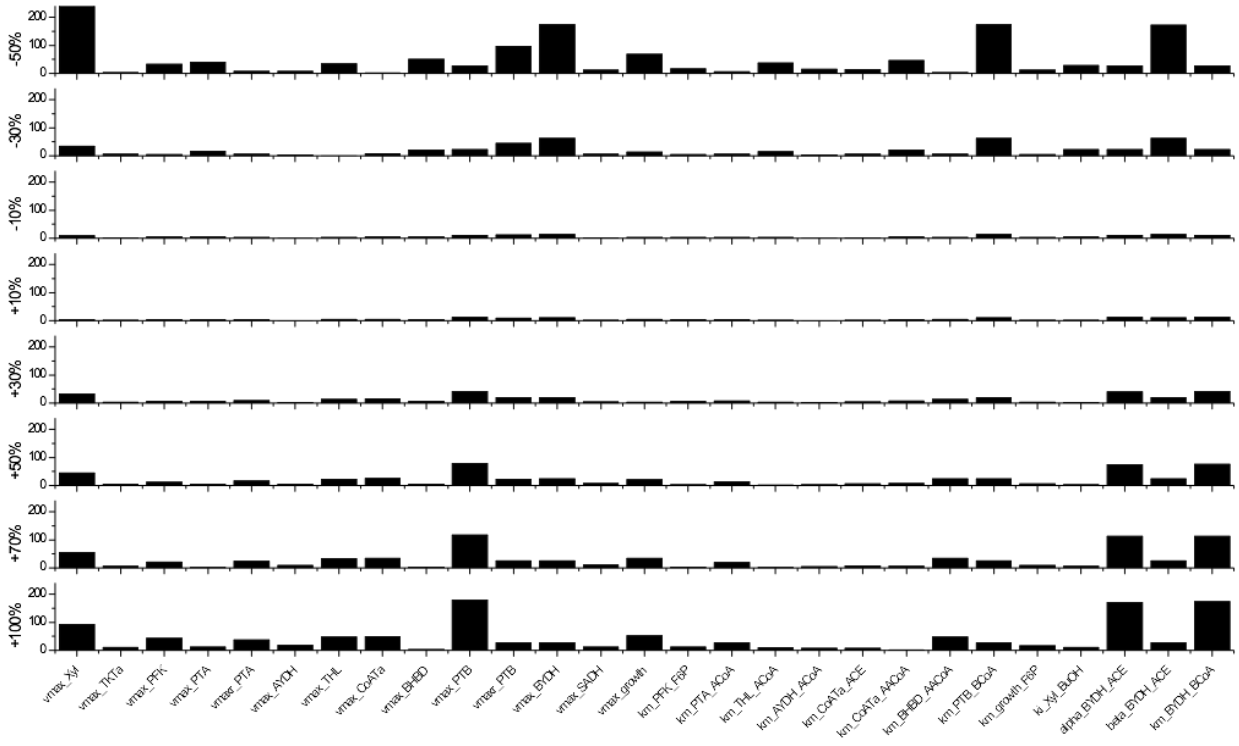

Figure S 1. Sensitivity analysis of model parameters for 60 mM NaAc supplemented culture. Vertical axis value represents percentage change in the objective function for parameter change from - 50 % to + 100 % around the optimized value. Parameters not shown have percentage changes less than 10 %.

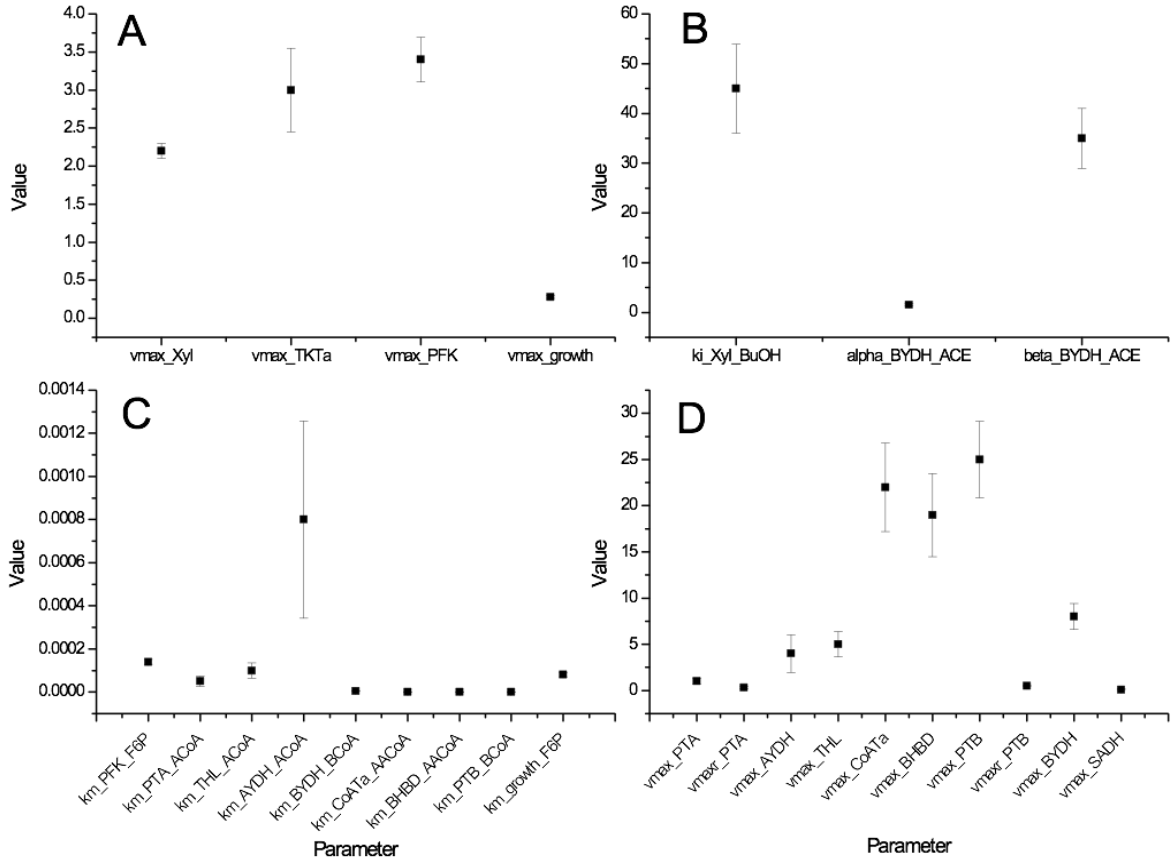

Figure S 2. Parameter estimates with error bars representing 95 % confidence intervals for highly sensitive parameters of (a) PPP pathway and growth; (b) solvents production; (c) km values; (d) acids and solvents conversion.

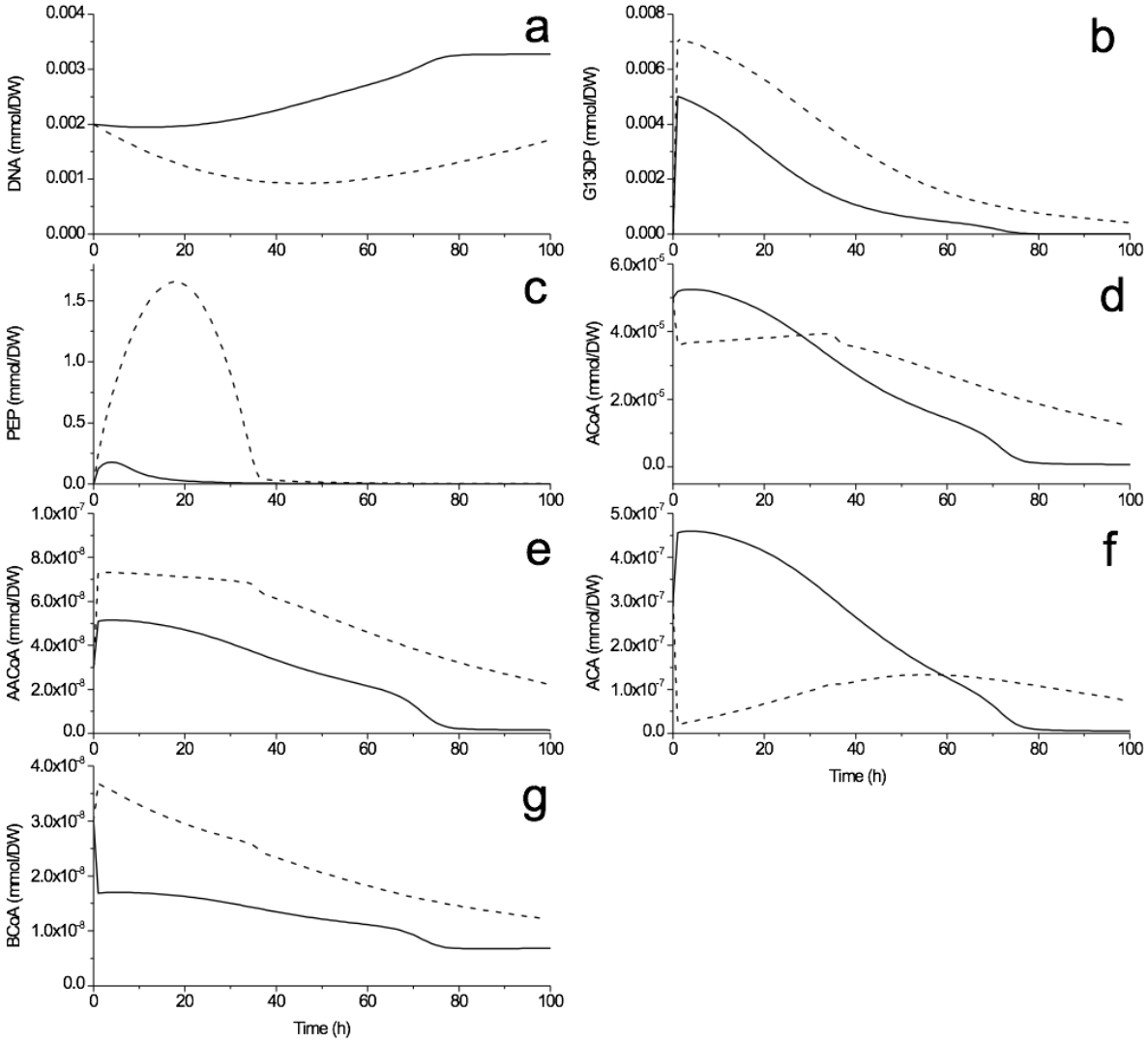

Figure S 3. Model simulation results of intracellular metabolites for which no experimental data were available. Solid line is for the 60 mM NaAc supplementation culture, dashed line is for the control culture without NaAc addition. (a) DNA; (b) G13DP; (c) PEP; (d) ACoA; (e) AACoA; (f) ACA; (g) BCoA.

5.10 **Supplementary material 2**

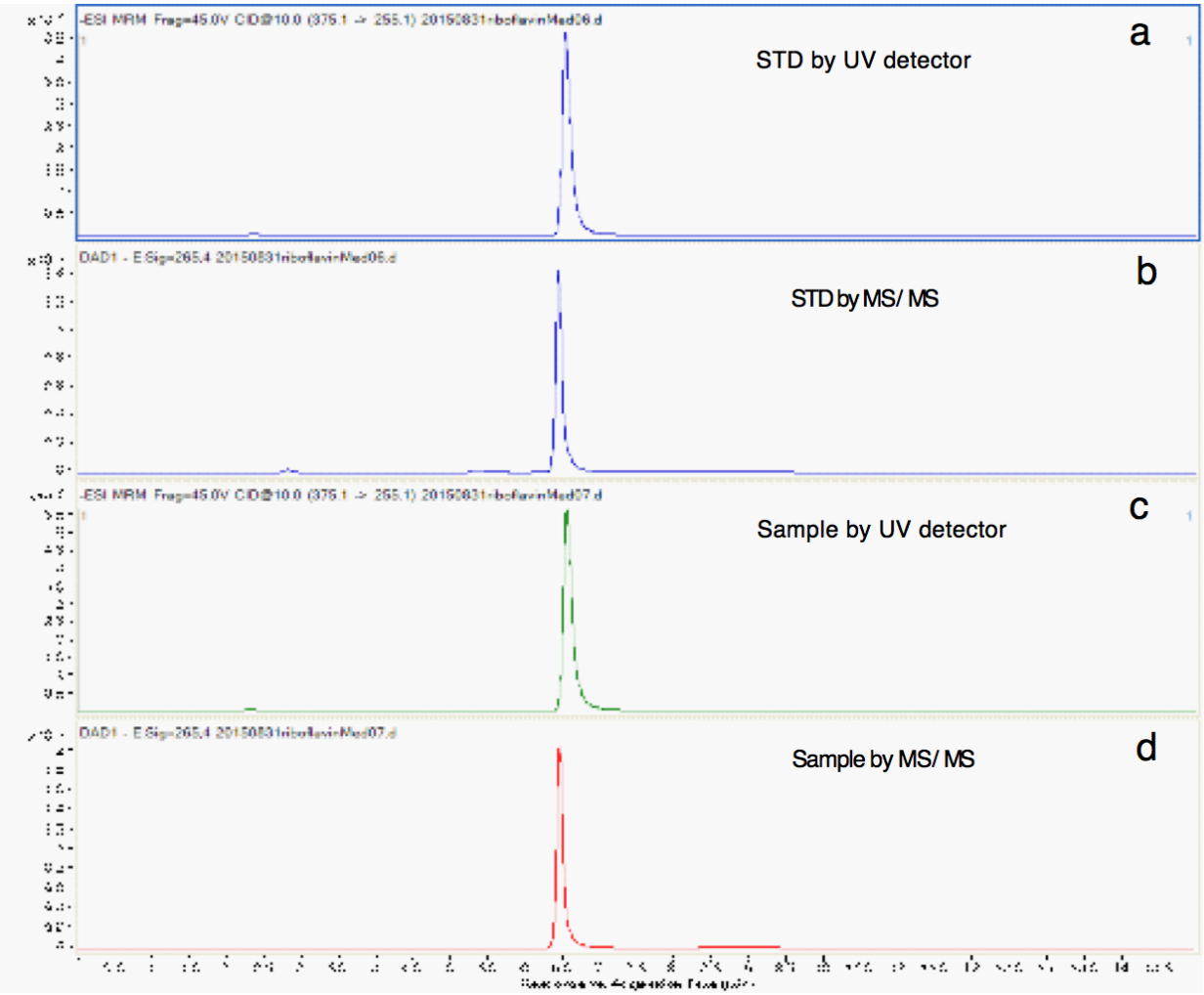

Figure S 4. Riboflavin identification by comparing 60 mM sodium acetate bioreactor culture sample to pure riboflavin standard by HPLC/MS/MS analysis. Riboflavin standard analysis by (a) UV detector and (b) MS/MS, and sample analysis by (c) UV detector and (d) MS/MS.

5.11 Supplementary material 3

Another two batches of test cultures in a 60 mM sodium acetate condition are shown below. Although the sampling times were different from the previous two batches, the results all showed the same trends as the two batches chosen in the article section.

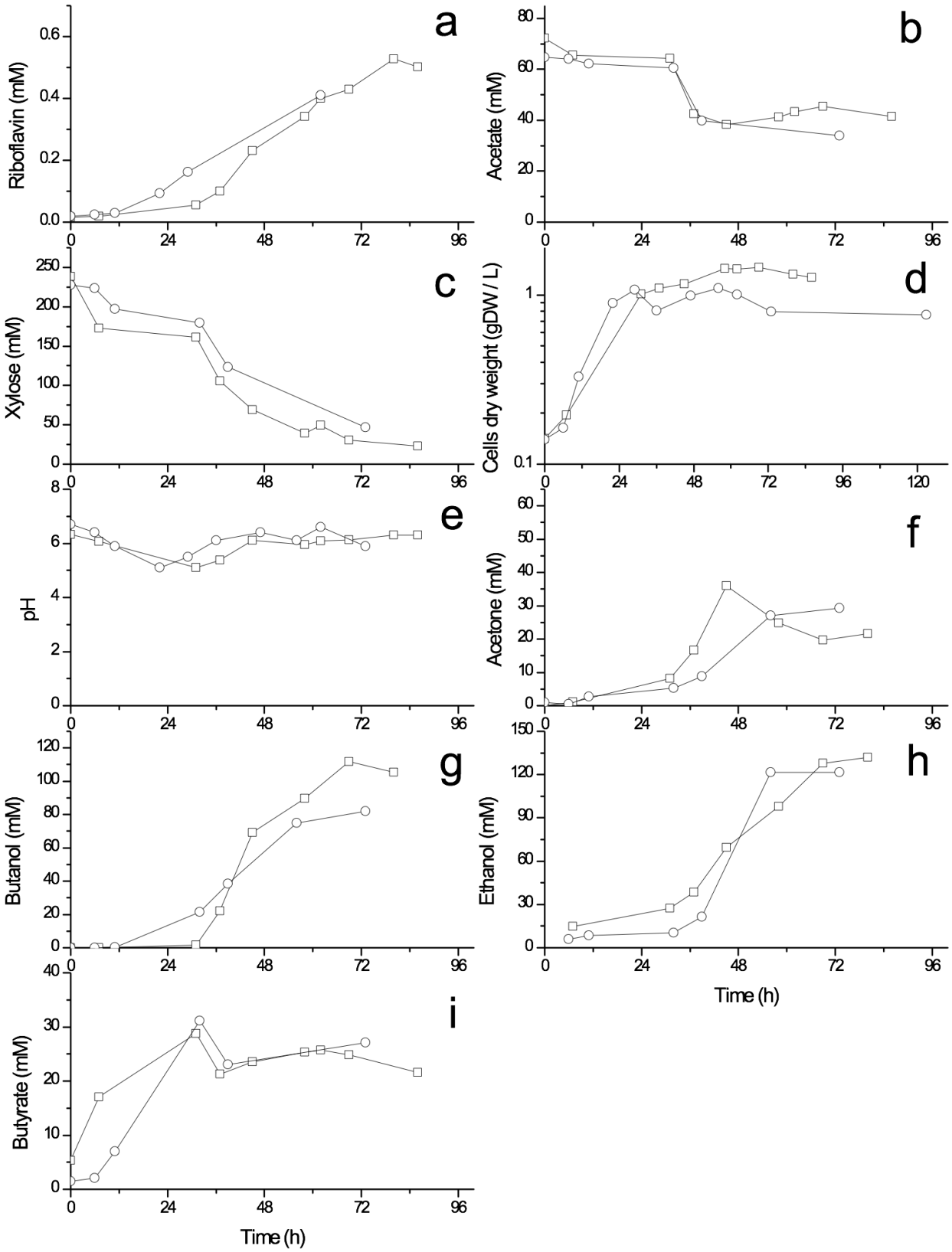
a
Riboflavin (mM)
0.0
0.2
0.4
0.6
0
24
48
72
96
b
Acetate (mM)
0
20
40
60
80
c
Xylose (mM)
0
50
100
150
200
250
d
Cells dry weight (gDW / L)
0.1
1
0
24
48
72
96
120
e
pH
0
2
4
6
8
f
Acetone (mM)
0
10
20
30
40
50
60
g
Butanol (mM)
0
20
40
60
80
100
120
h
Ethanol (mM)
0
30
60
90
120
150
i
Butyrate (mM)
0
10
20
30
40
Time (h)
Time (h)

Figure S 5. Main products, biomass, pH, and xylose consumption in two parallel batches in a 60 mM NaAc condition for the xylose culture of *C. acetobutylicum* ATCC 824. (a) riboflavin; (b) acetate; (c) xylose; (d) cell dry weight; (e) pH; (f) acetone; (g) butanol; (h) ethanol; (i) butyrate.

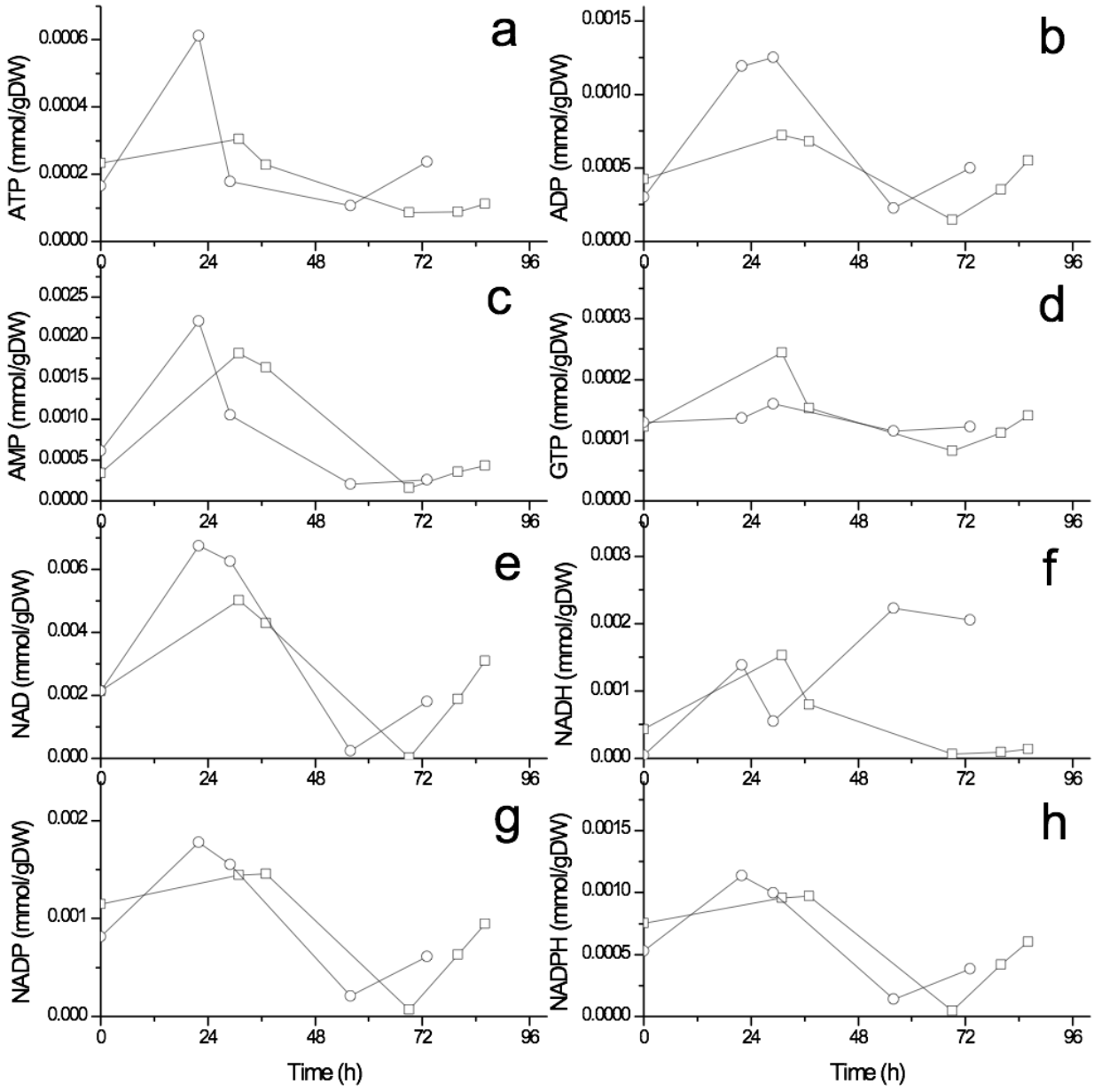

Figure S 6. Energy and redox status in two parallel batches in a 60 mM NaAc condition for a xylose culture of *C. acetobutylicum* ATCC 824. (a) ATP; (b) ADP; (c) AMP; (d) GTP; (e) NAD; (f) NADH; (g) NADP; (h) NADPH.

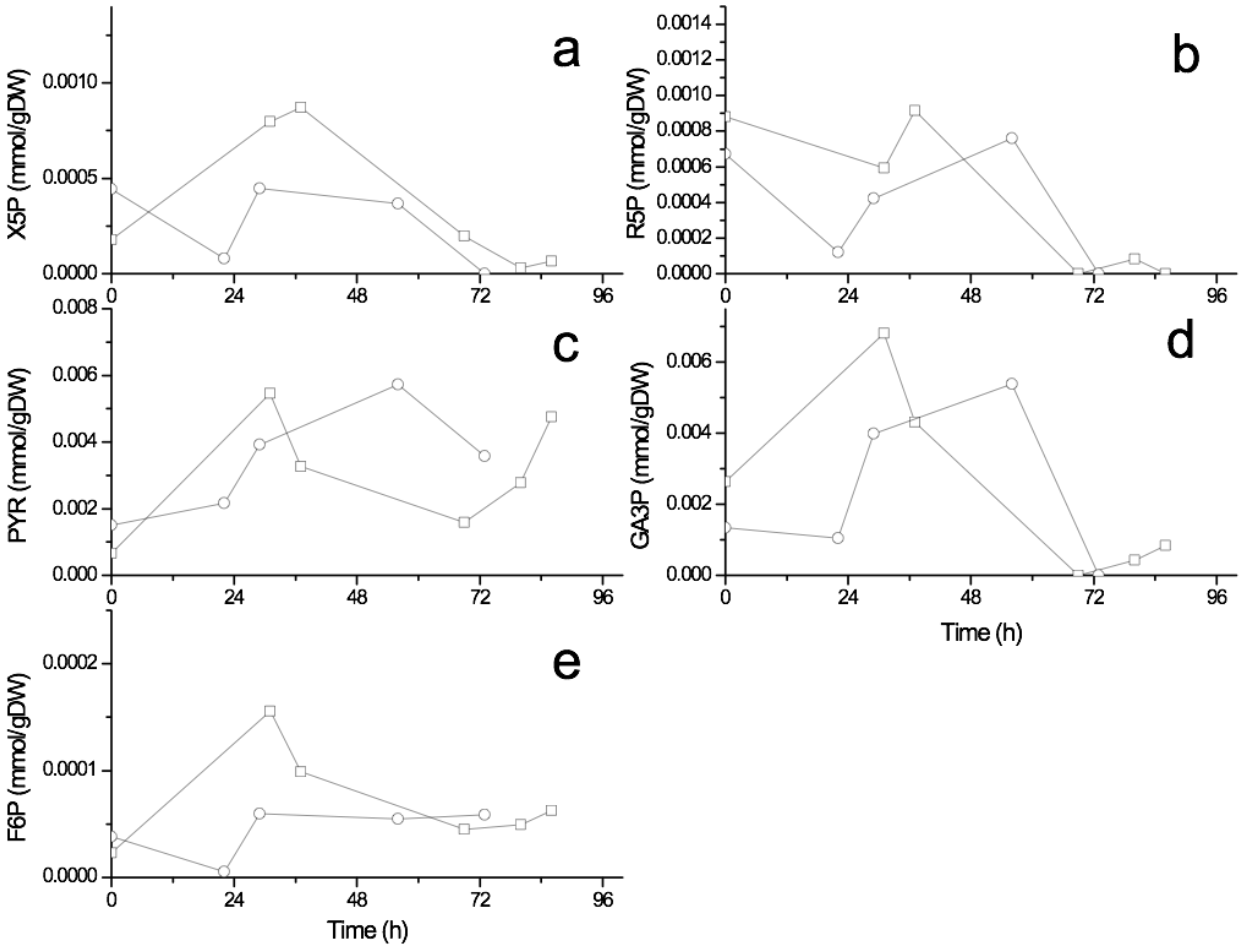

Figure S 7. Main carbon metabolites in two parallel batches in a 60 mM NaAc condition for a xylose culture of *C. acetobutylicum* ATCC 824. (a) X5P; (b) R5P; (c) PYR; (d) GA3P; (e) F6P.

CHAPTER 6 GENERAL DISCUSSION

Butanol applied in the biofuel market remains in a fluctuating status. The world's largest bio-butanol producer, Cathay Biotech., had an active production capacity of 100,000 tons per year in 2011 (reported from consulting firm CMAI in 2011, Chemical Market Associates, Inc.), when the biobutanol market price was in competition with gasoline. However, the company is currently closed due to the world crude oil price consistently decreasing from about $100 in 2011 to the current price of about $40. As we know, corn starch was used as a raw material in the current ABE fermentation system, which is attributed to a high production cost. Therefore, considering the cost of raw materials and the fluctuation of crude oil prices, finding a competitive raw material and promoting ABE productivity would be a potential way of developing the biobutanol industry. Meanwhile, byproducts of acetone and ethanol are also impacted by the global oil price. In particular, ethanol is already being used in the current gasoline system with a 10 % addition, and *Saccharomyces cerevisiae* has expressed a high ethanol yield (120 g L^{-1}), which is still competitive to biobutanol. Therefore, promoting cheaper feasible raw materials used in biobutanol production (ABE fermentation) and improving cell productivity from a mechanism study are viable and significant methods of bringing biobutanol in competition with the current gasoline and biofuel market.

The main objective of this research was to investigate the potential use of hemicellulose hydrolysates obtained from the Canadian pulp and paper industry's waste water, i.e. black liquor, to produce biobutanol by ABE fermentation. A synthetic medium was used and supplemented with xylose as the unique carbon source, as it is the main sugar found in the hemicellulose hydrolysates. Other compounds specifically found in the hydrolysates (i.e. high sodium or acetate) and which can affect the performance of the fermentation process were added to the synthetic culture medium in order to evaluate their effects. Briefly, sodium comes from the chemicals used in the hydrolysis process as well as in the cleaning procedures, and acetate is a by-product of the hydrolysis process. Although some studies have already been published assessing these compounds, our aim was to evaluate the effects at the metabolic level, including performing a dynamic metabolic flux analysis.

Supplementing 200 mM of sodium chloride clearly inhibited cell growth in *C. acetobutylicum* ATCC 824, and resulted in the inhibition of the pentose phosphate and glycolytic pathways. The

hypothesis of a reduced metabolic activity, in the acidogenesis phase, is also supported by lower cell concentrations in X5P, R5P, F6P, G6P, and G1P at high sodium. In fact, high sodium influence may act in many ways, such as challenging membrane electronegativity potential regulation, which affects cell membrane dynamics and cell volume, which in turn can affect enzymes kinetics, etc. Meanwhile, ATP was accumulated at a high sodium concentration - another important factor that may affect metabolism. Indeed, the ATP accumulation phenomenon at high sodium suggested either an increase of the ATP production rate to face a higher demand in ATP for cell maintenance and repair, or a decrease of its utilization rate because of an induced reduction in metabolic activity. Moreover, a high salt condition induces a high osmotic pressure which challenges cell homeostasis. High sodium thus diverts cell metabolism and resources towards the management of membrane integrity, as well as its transporters and channels. The cell therefore invests a significant amount of resources to remain functional, and this adaptation phenomenon may explain, in part, why these cells exhibit a lag phase and lower biomass yield. The lower metabolic state under a high sodium condition may thus be attributed to a shortage in resources, as well as a possible increase of the intracellular salt content, which affects enzyme functions. In general, a high sodium condition was shown to affect biomass growth, but not the cell-specific productivity in solvents. A quantitative metabolomics analysis revealed that the metabolic intermediates related to biomass synthesis are highly inhibited (i.e. sugar phosphates). While cell energetics were shown to be stimulated at high sodium, the $NADP^+$-to-NADPH ratio exhibited a high stability level that could explain a robust solvent-specific productivity. This work suggests that rather than desalting wood hydrolysates in a biorefinery, which is a costly process, similar butanol production can be reached by performing fermentation at a high biomass concentration.

As a second objective, we investigated the metabolomic response of *C. acetobutylicum* ATCC 824 to a 60 mM sodium acetate (NaAc) supplement, in order to simulate hemicellulose hydrolysates. Since we observed the production of riboflavin by serendipity, we implemented our study to unravel how the metabolic pathways leading to riboflavin were induced by adding acetate. As described in literature, GTP plays a key role in the riboflavin synthesis pathway. Our results showed a decreased GTP concentration in NaAc-supplemented culture, and even the ratio of GTP-to-adenosine phosphates (AMP, ADP and ATP) was lower than in the control culture during the main production period (20-70 h). Although the GTP concentration is not a clear indication of the GTP-to-riboflavin flux, it still indicates some correlation between GTP concentration behaviour

and riboflavin synthesis overexpression under NaAc supplementation. However, compared to the high riboflavin producers' industrial use, the culture conditions assessed in this work still led to a significant riboflavin production and suggested that there is room for improvement. Indeed, integrating the various successful ideas reported in literature such as inducing adding bipyrimidine, as well as applying genetic engineering work and then performing culture medium composition and management optimization work, can lead to maximal butanol production and productivity. Moreover, the present study clearly showed that NaAc supplementation promotes a riboflavin yield, as well as ABE solvent production levels. Of interest, obtaining riboflavin as a by-product, in addition to ABE solvents, contributes to the enhancement of the economic feasibility of a bio-refinery process valourizing a waste stream of the pulp and paper industry. However, further research is necessary to maximize the potential of this bioprocess.

A dynamic model was then set forth, based on the approach developed in the laboratory during the past decade, and showed a simulation of the main carbon flow metabolism and cell growth in xylose batch ABE fermentation co-producing riboflavin under 60 mM of NaAc induction. An adequate metabolic model not only characterizes cell behaviour, but also offers a prediction capacity to prospectively observe biosystem capacity (Jolicoeur, 2014). In fact, various metabolic models have been proposed for clostridia, but these required being implemented to describe our experimental data kinetically, while our model included 23 reactions involving 24 metabolites, as well as 72 kinetic parameters. Butanol inhibition of biomass growth and xylose uptake, as well as acetate activation of riboflavin and butanol synthesis were considered. The model was calibrated on experimental data of extracellular and intracellular metabolite concentration as well as biomass, solvent, and riboflavin concentrations with culture time under 60 mM of sodium acetate, and was also shown to adequately predict cell behaviour under a 0 mM acetate culture condition (with the same model structure and parameter system) when compared with experimental data, especially for substrates utilization, ABE production, and riboflavin evolution. As a significant result, the riboflavin metabolic pathway was combined with the ABE fermentation network and simulated by the model. Performing a dynamic metabolic flux analysis using the model revealed that acetate supplementation upregulates the enzyme reaction rate of acetoacetyl-CoA-acetate-CoA-transferase, which further affects acetate metabolism. In addition, solvent synthesis enzymes are stimulated at different degrees at high acetate. The model also revealed a simultaneous increase of riboflavin (ribA) and GTP (precursor of riboflavin) (PurM) synthesis flux rates under NaAc

supplementation, which led to a high riboflavin production. These findings brought insight on further genetic manipulation strategies. Therefore, the present dynamic model provides a useful platform not only for simulating cell behaviour under various conditions, but also for estimating enzyme reaction rates, and thus guiding optimizing work. Therefore, the present work provides a dynamic model shown as being adequate in simulating the ABE fermentation bioprocess co-producing riboflavin, as well as beneficial for process control.

Focusing on the production yield, acetate had a positive effect on butanol production, which improved the maximum butanol concentration from 50 to 150 mM when adding 60 mM of acetate. While in the presence of 200 mM of NaCl, the butanol concentration dropped from 250 to 75 mM. The difference between the two control groups in acetate culture (50 mM butanol) and NaCl culture (250 mM) is due to the effect of calcium carbonate in the NaCl control group, which we added to maintain the culture pH - a higher pH level (5-6.5 vs. 4.7-6) may reduce the acidogenic phenomenon and lead to a higher butanol production yield in the NaCl control group. As a specific term in ABE fermentation, “acid crash” is a phenomenon which occurs in pH-uncontrolled culture, resulting in the premature cessation of ABE (butanol) production. "Acidogenesis", which occurs when cultures are performed at pH values close to neutrality, is due to the rapid production of acids (butyrate and acetate) followed by the inhibition of solventogenesis. Therefore, by combining the positive effects of calcium carbonate on pH control and acetate on butanol production and riboflavin stimulation, the potential of ABE production with hemicellulose hydrolysate will be greatly improved for industrialization.

With respect to the co-product riboflavin, we know that the current riboflavin market is only 3000 tons per year - a low market capacity compared to 350 million gallons per year for biobutanol. Therefore, when riboflavin is by-produced with biobutanol production, it would be obtained with a large quantity. With the present producing ratio of butanol to riboflavin (100:1), assuming half of the biobutanol enterprises are co-producing riboflavin, it still can produce 5000 tons of riboflavin per year, which would bring a huge shock for the global riboflavin market and even the vitamin market. Therefore, promoting the development of the riboflavin market plays a key role in riboflavin consumption. In fact, the price of riboflavin is still very high for many developing countries - in Africa and Asia, many people have no economic ability to support a daily vitamin supplement, so increasing riboflavin productivity and decreasing its market price is an effective

approach. Meanwhile, enlarging riboflavin’s application scope is another approach which could promote its global market. After many years of application research, riboflavin has already been widely used in human supplements, food coloring, clinical treatment, fodder, and even the cosmetics industry, so with the improvement of living standards and the development of technology, we strongly believe that the demand for riboflavin in various fields would increase rapidly. Our founding of biobutanol co-producing riboflavin would thus be a booster used to stimulate another research field, as well as for the biobutanol industry.

CHAPTER 7 CONCLUSION

This PhD thesis has investigated the effects of sodium ion and acetate supplementation on *Clostridium acetobutylicum* ATCC 824 metabolism in xylose culture, which are the expected culture medium conditions using hemicellulose hydrolysates obtained from black liquor, a waste water stream of the pulp and paper industry. The main research objective aims to characterize the effects of these medium additives on central carbon metabolism, cell energetic state, redox, as well as main products and by-products.

First, the results confirmed that a high sodium ion concentration in a xylose culture inhibited biomass growth as well as solvent production yield, but did not affect solvent-specific productivity. This was an unexpected result because people always believe that high sodium toxicity both relies on biomass and solvent metabolism. A quantitative metabolomics analysis revealed that the metabolic intermediates related to biomass synthesis were highly inhibited (i.e. sugar phosphates). The main effects of high sodium on cell metabolism were observed in acidogenesis, during which we observed the accumulation of ATP and NADH, as well as the inhibition of the pentose phosphate (PPP) and the glycolytic pathways. However, the $NADP^+$-to-NADPH ratio exhibited a high robustness for the entire culture duration, which could explain the robustness of solvent-specific productivities. Additionally, in this study, calcium carbonate was added to the culture medium to maintain the culture's pH, which led to a higher pH level than the other control group without calcium carbonate (in chapter 5), and a maximum of 250 mM of butanol was obtained, which is quite compatible with the highest value reported in the literature (270 mM).

Acetate was supplemented in ABE fermentation to simulate the hydrolysate component, which unexpectedly resulted in the stimulation of riboflavin production, increasing it from undetectable concentrations to ~ 0.2 g L^{-1} (0.53 mM) when supplementing 60 mM of NaAc. Of interest, solvent production and biomass yield were also greatly promoted**.** Compared with the previous genetic strategy, using an acetate supplement is a quite simple and efficient method which leads to the highest riboflavin production yield in the clostridia species. A kinetic metabolic model under an acetate culture condition (60 mM) was developed to simulate an ABE-co-producing riboflavin biosystem, which was also shown to adequately predict culture nutritional states and production without acetate addition by comparing with 0 mM acetate culture data. An efficient parameter estimation method adapted from Rizzi was developed during model calibration, while an auto

generator was also developed to generate different Matlab codes which accelerated the modelling process. It was found that riboflavin (ribA) and GTP (precursor of riboflavin) (PurM) synthesis fluxes were stimulated by the NaAc supplement, while, a lower GTP-to-adenosine phosphate (ATP, ADP, AMP) ratio under a NaAc-supplemented condition suggested that the GTP may have played a minor role in the cell energetic metabolism compared to its contribution to riboflavin synthesis. This method has not only allowed higher production levels of riboflavin to be reached than other induction or genetic engineering strategies reported in literature, but it has also led to enhanced ABE solvent production and productivity. Solvent production and biomass yield were promoted with 5-fold acetone, 2.6-fold butanol, and 2.4-fold biomass adding NaAc. A metabolomics study suggested that a NaAc condition first stimulated the accumulation of intracellular metabolite intermediates during the acidogenic phase, which then fed the solventogenic phase, leading to increased ABE production.

From an overview, both the metabolomics and modelling study gave a clearer view of the ABE fermentation mechanism in a high sodium condition and ABE co-producing riboflavin in an acetate condition. Therefore, by combining the positive effects of calcium carbonate on pH control and those of acetate on butanol production and riboflavin stimulation, the potential of ABE production with hemicellulose hydrolysate will be greatly improved for industrialization in the near future. Finally, this project will benefit both Canada’s paper-making industry and energetic sustainability, which is in perfect accordance with solutions contributing to the fight against the global warming problem.

CHAPTER 8 RECOMMENDATIONS

Biobutanol production is more than just a trendy idea, but once its economic feasibility is demonstrated, the industry will no longer have the choice to change their paradigm.

The use of low-cost and renewable agricultural and industrial waste biomasses as feedstock is the preferred solution to help biobutanol become an economically feasible biofuel. Particularly in Canada, the use of waste from the pulp and paper industry benefits both the production of biobutanol and the environment. However, to efficiently use this cheap feedstock and manage the bioprocess, there is still a lot of work to be done.

1. As various by-products exist in the hemicellulose hydrolysates, the effect of these compounds on ABE fermentation should be clearly investigated. For example, except for sodium ion and acetic acids, there are also high concentration of furans such as HMF, furfural, and phenolic. Other weak acids such as levulinic acid and formic acid also exist. In fact, we tried using hemicellular hydrolysate as a unique nutrient medium or combined with other carbon (xylose) and nitrogen sources (NH_4^+, asparagine, etc.) for ABE fermentation (data showed in Appendix C), but the results were unsatisfactory due to various individual or synergistic inhibition effects from multiple combined compounds involved. Although previous research found that these compounds could inhibit ABE fermentation in different levels, the effect of these chemicals on cell enzyme and metabolism are not clear, which fundamentally affects ABE production. Therefore, further study investigating cell central metabolism and ABE metabolism should be carried out in order to find the mechanism of inhibition and help us to further design strategies from genetic engineering to obtain more toxic/inhibition tolerance strains.

2. In our study, we unexpectedly found that acetic acid could stimulate riboflavin production during ABE fermentation - this is a great chance to further reduce the cost of ABE fermentation by improving the riboflavin production yield. Further investigation on medium and culture management strategies should be carried out in order to optimize riboflavin production. Meanwhile, although the positive effect of acetic acid on riboflavin production is quite obvious, and we have already deeply studied its role at the metabolic level, the mechanism of activation on enzymes is still not clear. Further proteomic and enzymatic study should be carried out to bring light on this potential improvement.

3. Further developing the metabolic model could become a predictive tool to support the development and the management of cell behaviour. In our study, we have calibrated the metabolic model for both ABE and riboflavin production under a 60 mM acetate condition, and validated it using experimental data from a 0 mM acetate condition. In order to make this model more accurate, cell energetic and redox metabolisms should be involved - since ATP is a cofactor in acidogenic reactions, and redox is a co-factor in solventogenesis, these cofactors could directly affect ABE metabolism. These cofactors also largely contribute to central metabolism regulation, so it is very important to make the model more robust under different culture conditions. In addition, we also need to further expand the model metabolic reaction by including key nutrients, such as a nitrogen source, which is also important for cell behaviour. As in Chapter 5, amino acids evolving in a culture medium have been already followed, and the addition of these elements in the model could help us to develop a more detailed culture strategy based on the model prediction. Finally, we need to apply the metabolic model in process control. It will be of ultimate interest to evaluate the model capacity to support directed manipulation of the carbon flow favouring biobutanol and riboflavin production under different culture conditions.

BIBLIOGRAPHY

Ahmed, O.M., Pangloli, P., Hwang, C.-A., Zivanovic, S., Wu, T., D'Souza, D., Draughon, F.A. 2015. The occurrence of *Listeria monocytogenes* in retail ready-to-eat meat and poultry products related to the levels of acetate and lactate in the products. Food Control, 52, 43-48.

Al-Shorgani, N.K., Kalil, M.S., Yusoff, W.M. 2012. Biobutanol production from rice bran and de-oiled rice bran by *Clostridium saccharoperbutylacetonicum* N1-4. Bioprocess Biosyst Eng, 35(5), 817-26.

Al-Shorgani, N.K.N., Ali, E., Kalil, M.S., Yusoff, W.M.W. 2011. Bioconversion of Butyric Acid to Butanol by *Clostridium saccharoperbutylacetonicum* N1-4 (ATCC 13564) in a Limited Nutrient Medium. BioEnergy Research, 5(2), 287-293.

Almaas, E., Kovacs, B., Vicsek, T., Oltvai, Z.N., Barabasi, A.-L. 2004. Global organization of metabolic fluxes in the bacterium *Escherichia coli*. Nature, 427.

Alosta, H. 2007. Riboflavin production by encapsulated *Candida flareri*. in: Faculty of the Graduate College, Vol. Doctor of Philosophy, Oklahoma State University.

Alriksson, B. 2006. Ethanol from lignocellulose: Alkali detoxification of dilute-acid spruce hydrolysates. in: Faculty of Technology and Science Biochemistry, Karlstad University.

Alriksson, B., Sjode, A., Nilvebrant, N.-O., Jonsson, L.J. 2006. Optimal conditions for alkaline detoxification of dilute-acid lignocellulose hydrolysates. Appl Biochem Biotechnol, 129-132(06), 599-611.

Amador-Noguez, D., Brasg, I.A., Feng, X.J., Roquet, N., Rabinowitz, J.D. 2011. Metabolome remodeling during the acidogenic-solventogenic transition in *Clostridium acetobutylicum*. Appl Environ Microbiol, 77(22), 7984-97.

Amador-Noguez, D., Feng, X.J., Fan, J., Roquet, N., Rabitz, H., Rabinowitz, J.D. 2010. Systems-level metabolic flux profiling elucidates a complete, bifurcated tricarboxylic acid cycle in *Clostridium acetobutylicum*. J Bacteriol, 192(17), 4452-61.

Arzberger, C.F. 1943. Production of riboflavin by butyl alcohol producing bacteria. in: 2326425, (Ed.) U.S.P. Office, Vol. 2326425, Google Patents. United States, pp. 2326425.

Atsumi, S., Cann, A.F., Connor, M.R., Shen, C.R., Smith, K.M., Brynildsen, M.P., Chou, K.J., Hanai, T., Liao, J.C. 2008. Metabolic engineering of Escherichia coli for 1-butanol production. Metab Eng, 10(6), 305-11.

Awes, L.A., Felipe, M.G.A., Silva, J.B.A.E., Silvio S, S., Prata, A.M.R. 1998. Pretreatment of sugarcane bagasse hemicellulose hydrolysate for xylitol production by *Candida guilliermondii*. Applied Biochemist and Biotechnology, 70-72, 89-98.

Bankar, S.B., Survase, S.A., Ojamo, H., Granström, T. 2013. Biobutanol: the outlook of an academic and industrialist. RSC Advances, 3(47), 24734.

Bankar, S.B., Survase, S.A., Singhal, R.S., Granstrom, T. 2012. Continuous two stage acetone-butanol-ethanol fermentation with integrated solvent removal using *Clostridium acetobutylicum* B 5313. Bioresour Technol, 106, 110-6.

Bao, G., Dong, H., Zhu, Y., Mao, S., Zhang, T., Zhang, Y., Chen, Z., Li, Y. 2014. Comparative genomic and proteomic analyses of *Clostridium acetobutylicum* Rh8 and its parent strain DSM 1731 revealed new understandings on butanol tolerance. Biochem Biophys Res Commun, 450(4), 1612-8.

Barth-Jr., V.C., Cattani, F., Ferreira, C.A.S., Oliveira, S.D.d. 2012. Sodium chloride affects propidium monoazide action to distinguish viable cells. Anal Biochem, 428(2), 108-10.

Blaschek, H. P, Ezeji, T. C. 2010. Butanol production from lignocellulosic biomass. in: Biofuels from agricultural wastes and byproducts, (Ed.) Wiley-Blackwell.

Bouville, M. 2007. Fermentation kinetics including product and substrate inhibitions plus biomass death: a mathematical analysis. Biotechnol. Lett., 29, 737-741.

Bretzel, W., Schurter, W., Ludwig, B., Kupfer, E., Doswald, S., Pfister, M., Loon, A.v. 1999. Commercial riboflavin production by recombinant Bacillus subtilis: down-stream processing and comparison of the composition of riboflavin produced by fermentation or chemical synthesis. Journal of Industrial Microbiology & Biotechnology, 22, 19–26.

Brown, R. 2003. Biorenewable resources. Blackwell Publishing Co., Iowa State Press, Iowa.

Buehler, E.A., Mesbah, A. 2016. Kinetic Study of Acetone-Butanol-Ethanol Fermentation in Continuous Culture. PLoS One, 11(8), e0158243.

Burgess, C.M., Smid, E.J., van Sinderen, D. 2009. Bacterial vitamin B2, B11 and B12 overproduction: An overview. Int J Food Microbiol, 133(1-2), 1-7.

Burkholder, P.R. 1943. Synthesis of riboflavin by a yeast. Proc. Natl. Acad. Sci. U S A., 29(6), 166-172.

Cai, X., Bennett, G.N. 2011. Improving the *Clostridium acetobutylicum* butanol fermentation by engineering the strain for co-production of riboflavin. J Ind Microbiol Biotechnol, 38(8), 1013-25.

Chen, C.-K., Blaschek, H.P. 1999a. Acetate enhances solvent production and prevents degeneration in *Clostridium beijerinckii* BA101. Appl Microbiol Biotechnol, 52(170-173).

Chen, C.-K., Blaschek, H.P. 1999b. Effect of acetate on molecular and physiological aspects of *Clostridium beijerinckii* NCIMB 8052 solvent production and strain degeneration. Appl Environ Microbiol, 65(2), 499–505.

Choi, S.J., Lee, J., Jang, Y.S., Park, J.H., Lee, S.Y., Kim, I.H. 2012. Effects of nutritional enrichment on the production of acetone-butanol-ethanol (ABE) by *Clostridium acetobutylicum*. J Microbiol, 50(6), 1063-6.

Claassen, P.A.M., Lier, J.B.v., Contreras, A.M.L., Niel, E.W.J.v., Sijtsma, L., Stams, A.J.M., Vries, S.S.d., Weusthuis, R.A. 1999. Utilisation of biomass for the supply of energy carriers. Appl Microbiol Biotechnol, 52(6), 741-755.

Cloutier, M., Bouchard-Marchand, E., Perrier, M., Jolicoeur, M. 2008. A predictive nutritional model for plant cells and hairy roots. Biotechnol Bioeng, 99(1), 189-200.

Cloutier, M., Perrier, M., Jolicoeur, M. 2007. Dynamic flux cartography of hairy roots primary metabolism. Phytochemistry, 68(16-18), 2393-404.

Crown, S.B., Indurthi, D.C., Ahn, W.S., Choi, J., Papoutsakis, E.T., Antoniewicz, M.R. 2011. Resolving the TCA cycle and pentose-phosphate pathway of *Clostridium acetobutylicum* ATCC 824: Isotopomer analysis, in vitro activities and expression analysis. Biotechnol.J., 6(3), 300-305.

DA, F. 1998. Increasing the flux in metabolic pathways: A metabolic control analysis perspective. Biotechnol Bioeng, 58(2-3), 121-4.

Ezeji, T., Blaschek, H.P. 2008. Fermentation of dried distillers' grains and solubles (DDGS) hydrolysates to solvents and value-added products by solventogenic clostridia. Bioresour Technol, 99(12), 5232-42.

Ezeji, T.C., Qureshi, N., Blaschek, H.P. 2007. Production of acetone butanol (AB) from liquefied corn starch, a commercial substrate, using *Clostridium beijerinckii* coupled with product recovery by gas stripping. J Ind Microbiol Biotechnol, 34(12), 771-7.

Fonknechten, N., Chaussonnerie, S., Tricot, S., Lajus, A., Andreesen, J.R., Perchat, N., Pelletier, E., Gouyvenoux, M., Barbe, V., Salanoubat, M., Paslier, D.L., Weissenbach, J., Cohen, G.N., Kreimeyer, A. 2010. *Clostridium sticklandii*, a specialist in amino acid degradation: revisiting its metabolism through its genome sequence. BMC Genomics, 11(555), 1471-2164.

Formanek, R.M., H P Blaschek. 1997. Enhanced butanol production by *Clostridium beijerinckii* BA101 grown in semidefined P2 medium containing 6 percent maltodextrin or glucose. Appl. Environ. Microbiol., 63(6), 2306-2310.

Gabriel, C.L. 1928. Butanol Fermentation Process. Industrial and engineering chemistry 20(10).

George W. Huber, S.I., Avelino Corma. 2006. Synthesis of transportation fuels from biomass : Chemistry, catalysts, and engineering. Chem. Rev, 106, 4044-4098.

Gerchman, Y., Schnitzer, A., Gal, R., Mirsky, N., Chinkov, N. 2012. A simple rapid gas-chromatography flame-ionization-detector (GC-FID) method for the determination of ethanol from fermentation processes. Afr. J. Biotechnol, 11(15).

Gheshlaghi, R., Scharer, J.M., Moo-Young, M., Chou, C.P. 2009. Metabolic pathways of clostridia for producing butanol. Biotechnol Adv, 27(6), 764-81.

Ghorbaniaghdam, A., Chen, J., Henry, O., Jolicoeur, M. 2014. Analyzing clonal variation of monoclonal antibody-producing CHO cell lines using an *in silico* metabolomic platform. PLoS One, 9(3), e90832.

Ghorbaniaghdam, A., Henry, O., Jolicoeur, M. 2013. A kinetic-metabolic model based on cell energetic state: study of CHO cell behavior under Na-butyrate stimulation. Bioprocess Biosyst Eng, 36(4), 469-87.

Girbal, L., Soucaille, P. 1994. Regulation of *Clostridium acetobutylicum* metabolism as revealed by mixed-substrate steady-state continuous cultures: role of NADH/NAD ratio and ATP pool. J. Bacteriol., 176(21), 6433-6438.

Giri, K.V., Krishnaswamy, P.R. 1953. Studies on the synthesis of riboflavin by a mutant yeast, *Saccharomyces cerevisiae*. J Bacteriol., 67(3), 309-313.

Gottwald, M., Gottschalk, G. 1985. The internal pH of *Clostridium acetobutylicum* and its effect on the shift from acid to solvent formation. Arch. Microbiol, 143, 42-46.

Grupe, H., Gottschalk, G. 1992. Physiological events in *Clostridium acetobutylicum* during the shift from acidogenesis to solventogenesis in continuous culture and presentation of a model for shift induction. Appl Environ Microbiol, 58(12), 3896-3902.

Gu, Y., Hu, S., Chen, J., Shao, L., He, H., Yang, Y., Yang, S., Jiang, W. 2009. Ammonium acetate enhances solvent production by *Clostridium acetobutylicum* EA 2018 using cassava as a fermentation medium. J Ind Microbiol Biotechnol, 36(9), 1225-32.

Guo, T., He, A.Y., Du, T.F., Zhu, D.W., Liang, D.F., Jiang, M., Wei, P., Ouyang, P.K. 2013. Butanol production from hemicellulosic hydrolysate of corn fiber by a *Clostridium beijerinckii* mutant with high inhibitor-tolerance. Bioresour Technol, 135, 379-85.

Guo, T., Tang, Y., Xi, Y.-l., He, A.-y., Sun, B.-j., Wu, H., Liang, D.-f., Jiang, M., Ouyang, P.-k. 2011. *Clostridium beijerinckii* mutant obtained by atmospheric pressure glow discharge producing high proportions of butanol and solvent yields. Biotechnology Letters, 33(12), 2379-2383.

Hüsemann, M.H.W., Papoutsakis, E.T. 1990. Effects of propionate and acetate additions on solvent production in batch cultures of *Clostridium acetobutylicum*. Appl Environ Microbiol., 56(5), 1497-1500.

Han, B., Ujor, V., Lai, L.B., Gopalan, V., Ezeji, T.C. 2013. Use of proteomic analysis to elucidate the role of calcium in acetone-butanol-ethanol fermentation by *Clostridium beijerinckii* NCIMB 8052. Appl Environ Microbiol, 79(1), 282-93.

Harris, L.M., Welker, N.E., Papoutsakis, E.T. 2002. Northern, Morphological, and Fermentation Analysis of spo0A Inactivation and Overexpression in *Clostridium acetobutylicum* ATCC 824. Journal of Bacteriology, 184(13), 3586-3597.

Hartmanis, M.G.N., Gatenbeck, S. 1984. Intermediary metabolism in *Clostridium acetobutylicum*: levels of enzymes involved in the formation of acetate and butyrate. Appl Environ Microbiol, 47(6), 1277–1283.

Hartmanis, M.G.N., Klason, T., Gatenbeck, S. 1984. Uptake and activation of acetate and butyrate in *Clostridium acetobutylicum*. Applied Microbiology and Biotechnology, 20(1), 66-71.

He, Q., Chen, H. 2013. Improved efficiency of butanol production by absorbed lignocellulose fermentation. J Biosci Bioeng, 115(3), 298-302.

Hess, G. 2006. BP and dupont plan 'biobutanol'. Chem Eng News 84(26), 9.

Hickey, R.J. 1945. The inactivation of iron by 2, 2-bipyrimidine and its effect on riboflavin synthesis by *Clostridium acetobutylicum*. Arch. Biochem., 8, 439-447.

Hideaki Shinto, Yukihiro Tashiro, Genta Kobayashi, Tatsuya Sekiguchi, Taizo Hanai, Yuki Kuriya, Masahiro Okamotod, Sonomoto, K. 2008. Kinetic study of substrate dependency for higher butanol production in acetone–butanol–ethanol fermentation. Process Biochemistry 43, 1452–1461.

Hipolito, C.N., Crabbe, E., Badillo, C.M., Zarrabal, O.C., Morales Mora, M.A., Flores, G.P., Hernández Cortazar, M.d.A., Ishizaki, A. 2008. Bioconversion of industrial wastewater from palm oil processing to butanol by *Clostridium saccharoperbutylacetonicum* N1-4 (ATCC 13564). Journal of Cleaner Production, 16(5), 632-638.

Holt, R.A., Stephens, G.M., Morris, J.G. 1984. Production of Solvents by *Clostridium acetobutylicum* cultures maintained at neutral pH. Appl Environ Microbiol., 48(6), 1166-1170.

Hu, S., Zheng, H., Gu, Y., Zhao, J., Zhang, W., Yang, Y., Wang, S., Zhao, G., Yang, S., Jiang, W. 2011. Comparative genomic and transcriptomic analysis revealed genetic characteristics related to solvent formation and xylose utilization in *Clostridium acetobutylicum* EA 2018. BMC Genomics, 12, 93.

Huesemann, M.H., Kuo, L.J. 2012. Acetone-butanol fermentation of marine macroalgae. Bioresour Technol, 108, 305-9.

Husemann, M.H.W., Papoutsakis, E.T. 1990. Effects of propionate and acetate additions on solvent production in batch cultures of *Clostridium acetobutylicum*. Applied and Environmental Microbiology, 56(5), 1497-1500.

Inui, M., Suda, M., Kimura, S., Yasuda, K., Suzuki, H., Toda, H., Yamamoto, S., Okino, S., Suzuki, N., Yukawa, H. 2008. Expression of *Clostridium acetobutylicum* butanol synthetic genes in Escherichia coli. Appl Microbiol Biotechnol, 77(6), 1305-16.

Isar, J., Rangaswamy, V. 2012. Improved n-butanol production by solvent tolerant *Clostridium beijerinckii*. Biomass and Bioenergy, 37, 9-15.

Jang, Y.S., Lee, J., Malaviya, A., Seung do, Y., Cho, J.H., Lee, S.Y. 2012. Butanol production from renewable biomass: rediscovery of metabolic pathways and metabolic engineering. Biotechnol J, 7(2), 186-98.

Jang YS, M.A., Lee SY. 2013. Acetone–butanol–ethanol production with high productivity using *Clostridium acetobutylicum* BKM19. Biotechnol Bioeng, 110(6), 1646-1653.

Jolicoeur, M. 2014. Modeling cell behavior: moving beyond intuition. AIMS Bioengineering, 1(1), 1-12.

Jones, D.T., Woods, D.R. 1986. Acetone-Butanol Fermentation Revisited. American Society for Microbiology, 50(4), 484-524.

Jurgens, G., Survase, S., Berezina, O., Sklavounos, E., Linnekoski, J., Kurkijarvi, A., Vakeva, M., van Heiningen, A., Granstrom, T. 2012. Butanol production from lignocellulosics. Biotechnol Lett, 34(8), 1415-34.

Kao, W.C., Lin, D.S., Cheng, C.L., Chen, B.Y., Lin, C.Y., Chang, J.S. 2013. Enhancing butanol production with *Clostridium pasteurianum* CH4 using sequential glucose-glycerol addition and simultaneous dual-substrate cultivation strategies. Bioresour Technol, 135, 324-30.

Kim, B.H., Bellows, P., Datta, R., Zeihusi, J.G. 1984. Control of carbon and electron flow in *Clostridium acetobutylicum* fermentations: utilization of carbon monoxide to inhibit hydrogen production and to enhance butanol yields. Appl. Environ. Microbiol., 48, 764-770.

Kovárová-Kovar, K., Egli, T. 1998. Growth kinetics of suspended microbial cells: From single-substrate-controlled growth to mixed-substrate kinetics. Microbiol Mol Biol Rev, 62(3), 646–666.

Leduc, M., Tikhomiroff, C., Cloutier, M., Perrier, M., Jolicoeur, M. 2006. Development of a kinetic metabolic model: application to Catharanthus roseus hairy root. Bioprocess Biosyst Eng, 28(5), 295-313.

Lee, J. 2009. Fermentation of Rice Bran and Defatted Rice Bran for Butanol ProductionUsing *Clostridium beijerinckii* NCIMB 8052. Journal of Microbiology and Biotechnology, 19(5), 482-490.

Lee, J., Jang, Y.S., Choi, S.J., Im, J.A., Song, H., Cho, J.H., Seung do, Y., Papoutsakis, E.T., Bennett, G.N., Lee, S.Y. 2012. Metabolic engineering of *Clostridium acetobutylicum* ATCC 824 for isopropanol-butanol-ethanol fermentation. Appl Environ Microbiol, 78(5), 1416-23.

Lee, S.Y., Park, J.H., Jang, S.H., Nielsen, L.K., Kim, J., Jung, K.S. 2008. Fermentative butanol production by Clostridia. Biotechnol Bioeng, 101(2), 209-28.

Legg, D.A., Beesch, S.C. 1945. Production of substances rich in riboflavin, Google Patents.

Li, Q., Cai, H., Hao, B., Zhang, C., Yu, Z., Zhou, S., Chenjuan, L. 2010. Enhancing clostridial acetone-butanol-ethanol (ABE) production and improving fuel properties of ABE-enriched biodiesel by extractive fermentation with biodiesel. Appl Biochem Biotechnol, 162(8), 2381-6.

Li, R.D., Li, Y.Y., Lu, L.Y., Ren, C., Li, Y.X., Liu, L. 2011. An improved kinetic model for the acetone-butanol-ethanol pathway of Clostridium acetobutylicum and model-based perturbation analysis. BMC Syst Biol, 5 Suppl 1, S12.

Li, X., Li, Z., Zheng, J., Shi, Z., Li, L. 2012. Yeast extract promotes phase shift of bio-butanol fermentation by *Clostridium acetobutylicum* ATCC824 using cassava as substrate. Bioresour Technol, 125, 43-51.

Lim, S.H., Choi, J.S., Park, E.Y. 2001. Microbial Production of Riboflavin Using Riboflavin Overproducers, *Ashbya gossypii*, *Bacillus subtilis*, and *Candida famate*: An Overview. Biotechnol. Bioprocess Eng., 6, 14.

Liu, C.-G., Xue, C., Lin, Y.-H., Bai, F.-W. 2013a. Redox potential control and applications in microaerobic and anaerobic fermentations. Biotechnol Adv, 31(2), 257-265.

Liu, C., Zuo, W., Pang, H., Pei, J., Huang, Z., Huang, R. 2011. *Clostridium acetobutylicum* for producing butanol by utilizing manihot as raw materials and application thereof. in: CN102417888 B, (Ed.) Guangxi Academy of Sciences. China.

Liu, D., Chen, Y., Li, A., Ding, F., Zhou, T., He, Y., Li, B., Niu, H., Lin, X., Xie, J., Chen, X., Wu, J., Ying, H. 2013b. Enhanced butanol production by modulation of electron flow in *Clostridium acetobutylicum* B3 immobilized by surface adsorption. Bioresour Technol, 129, 321-8.

Liu, X.B., Gu, Q.Y., Yu, X.B., Luo, W. 2012. Enhancement of butanol tolerance and butanol yield in *Clostridium acetobutylicum* mutant NT642 obtained by nitrogen ion beam implantation. J Microbiol, 50(6), 1024-8.

Liu, Z., Ying, Y., Li, F., Ma, C., Xu, P. 2010. Butanol production by *Clostridium beijerinckii* ATCC 55025 from wheat bran. J Ind Microbiol Biotechnol, 37(5), 495-501.

London, J., Knight, M. 1966. Concentrations of nicotinamide nucleotide coenzymes inmicro-organisms. J. Gen. Microbial., 44, 241-254.

Loyarkat, S., Cheirsilp, B., Umsakul, K. 2013. Direct conversion of sugars and organic acids to biobutanol by non-growing cells of *Clostridium* spp. incubated in a nitrogen-free medium. Appl Biochem Biotechnol, 171(7), 1726-38.

Lutke-Eversloh, T. 2014. Application of new metabolic engineering tools for *Clostridium acetobutylicum.* Appl Microbiol Biotechnol, 98(13), 5823-37.

Lutke-Eversloh, T., Bahl, H. 2011. Metabolic engineering of *Clostridium acetobutylicum*: recent advances to improve butanol production. Curr Opin Biotechnol, 22(5), 634-47.

Maddox, I.S., Qureshi, N., Roberts-Thomson, K. 1995. Production of acetone-butanol-ethanol from concentrated substrates using *Clostridium acetobutylicum* in an integrated fermentation-product removal process. Process Biochemistry, 30(3), 209-215.

Maddox, I.S., Steiner, E., Hirsch, S., Wessner, S., Gutierrez, N.A., Gapes, J., Schuster, K. 2000. The cause of "acid crash" and "acidogenic fermentations" during the batch acetone-butanol-ethanol (ABE-) fermentation process. J Mol Microbiol Biotechnol, 2(1), 95-100.

Malaviya, A., Jang, Y.S., Lee, S.Y. 2012. Continuous butanol production with reduced byproducts formation from glycerol by a hyper producing mutant of *Clostridium pasteurianum*. Appl Microbiol Biotechnol, 93(4), 1485-94.

Mann, M.S., Lutke-Eversloh, T. 2013. Thiolase engineering for enhanced butanol production in *Clostridium acetobutylicum*. Biotechnol Bioeng, 110(3), 887-97.

Mao, S., Luo, Y., Bao, G., Zhang, Y., Li, Y., Ma, Y. 2011. Comparative analysis on the membrane proteome of *Clostridium acetobutylicum* wild type strain and its butanol-tolerant mutant. Mol Biosyst, 7(5), 1660-77.

Mao, S., Luo, Y., Zhang, T., Li, J., Bao, G., Zhu, Y., Chen, Z., Zhang, Y., Li, Y., Ma, Y. 2010. Proteome reference map and comparative proteomic analysis between a wild type mutant with enhanced butanol tolerance and butanol yield. Journal of Proteome research, 9, 3046–3061.

Mayank, R., Ranjan, A., Moholkar, V.S. 2013. Mathematical models of ABE fermentation: review and analysis. Crit Rev Biotechnol, 33(4), 419-47.

Mead, G.C. 1971. The amino acid-fermenting Clostridia. Journal of General Microbiology, 67, 47-56.

Mermelstein, L.D., Welker, N.E. 1994. Genetic and metabolic engineering of *Clostridium acetobutylicum* ATCC 824. Annals of the New York Academy of Sciences, 721, 54-68.

Meyer, C.L., Papoutsakis, E.T. 1989a. Continuous and biomass recycle fermentations of *Clostridium acetobutylicum*. Part 1: ATP supply and demand determines product selectivity. Bioprocess Eng., 4, 1-10.

Meyer, C.L., Papoutsakis, E.T. 1989b. Increased levels of ATP and NADH are associated with increased solvent production in continuous cultures of *Clostridium acetobutylicum*. Appl. Microbiol. Biotechnol., 30, 450-459.

Meyer, C.L., Roos, J.W., Papoutsakis, E.T. 1986. Carbon monoxide gasing leads to alcohol production and butyrate uptake without acetone formation in continuous cultures of *Clostridium acetobutylicum*. Appl. Microbiol. Biotechnol., 24, 159-167.

Michal, G. 1999. Biochemical pathways : An atlas of biochemistry and molecular biology. Spektrum Akademischer Verlag, Germany.

Mitchell, W.J. 1997. Physiology of carbohydrate to solvent conversion by Clostridia. Advances in Microbial Physiology, 39, 31-130.

Murray, W. 1992. Pulp and Paper: The Reduction of Toxic Effluents.

N Qureshi, H.B. 2001. Recent advances in ABE fermentation: hyper-butanol producing *Clostridium beijerinckii* BA101. Journal of Industrial Microbiology & Biotechnology, 27, 287-291.

Nair, R.V., Papoutsakis, E.T. 1994. Expression of plasmid-encoded aad in *Clostridium acetobutylicum* M5 restores vigorous butanol production. J Bacteriol, 176(18), 5843–5846.

Ni, Y., Wang, Y., Sun, Z. 2012. Butanol production from cane molasses by *Clostridium saccharobutylicum* DSM 13864: batch and semicontinuous fermentation. Appl Biochem Biotechnol, 166(8), 1896-907.

Ni, Y., Xia, Z., Wang, Y., Sun, Z. 2013. Continuous butanol fermentation from inexpensive sugar-based feedstocks by *Clostridium saccharobutylicum* DSM 13864. Bioresour Technol, 129, 680-5.

Nielsen, J. 1998. Metabolic Engineering: Techniques for Analysis of Targets for Genetic Manipulations. Biotechnolgy and Bioengineering, 58, 125-132.

Nolling, J., Breton, G., Omelchenko, M.V., Makarova, K.S., Zeng, Q., Gibson, R., Lee, H.M., Dubois, J., Qiu, D., Hitti, J., Wolf, Y.I., Tatusov, R.L., Sabathe, F., Doucette-Stamm, L., Soucaille, P., Daly, M.J., Bennett, G.N., Koonin, E.V., Smith, D.R. 2001. Genome sequence and comparative analysis of the solvent-producing bacterium *Clostridium acetobutylicum*. J Bacteriol, 183(16), 4823-38.

Orth, J.D., Thiele, I., Palsson, B.O. 2010. What is flux balance analysis? Nat Biotechnol, 28(3), 245-8.

Papoutsakis, E.T. 1984. Equations and Calculations for Fermentations of Butyric Acid Bacteria. Biotechnolgy and Bioengineering, 26, 174-187.

Peterson, W.H., Fred, E.B. 1932. Butyl-Acetone fermentation of corn meal. Industry and engineering chemistry, 24(2).

Petitdemange, H., Cherrier, C., Raval, G., Gay, R. 1976. Regulation of the NADH and NADPH-ferredoxin oxidoreductases in Clostridia of the butyric group. Biochimica et Biophysica Acta (BBA) - General Subjects, 421(2), 334-347.

Popp, J., Lakner, Z., Harangi-Rákos, M., Fári, M. 2014. The effect of bioenergy expansion: Food, energy, and environment. Renewable and Sustainable Energy Reviews, 32, 559-578.

Qureshi, N., Dien, B.S., Nichols, N.N., Saha, B.C., Cotta, M.A. 2006. Genetically Engineered Escherichia Coli for Ethanol Production from Xylose. Food and Bioproducts Processing, 84(2), 114-122.

Qureshi, N., Ezeji, T.C., Ebener, J., Dien, B.S., Cotta, M.A., Blaschek, H.P. 2008a. Butanol production by *Clostridium beijerinckii*. Part I: use of acid and enzyme hydrolyzed corn fiber. Bioresour Technol, 99(13), 5915-22.

Qureshi, N., Lolas, A., Blaschek, H. 2001. Soy molasses as fermentation substrate for production of butanol using *Clostridium beijerinckii* BA101. J Ind Microbiol Biotechnol, 26(5), 290-295.

Qureshi, N., Saha, B.C., Cotta, M.A. 2008b. Butanol production from wheat straw by simultaneous saccharification and fermentation using *Clostridium beijerinckii:* Part II—Fed-batch fermentation. Biomass and Bioenergy, 32(2), 176-183.

Qureshi, N., Saha, B.C., Cotta, M.A. 2007. Butanol production from wheat straw hydrolysate using *Clostridium beijerinckii.* Bioprocess Biosyst Eng, 30(6), 419-27.

Qureshi, N., Saha, B.C., Dien, B., Hector, R.E., Cotta, M.A. 2010a. Production of butanol (a biofuel) from agricultural residues: Part I – Use of barley straw hydrolysate☆. Biomass and Bioenergy, 34(4), 559-565.

Qureshi, N., Saha, B.C., Hector, R.E., Cotta, M.A. 2008c. Removal of fermentation inhibitors from alkaline peroxide pretreated and enzymatically hydrolyzed wheat straw: Production of

butanol from hydrolysate using Clostridium beijerinckii in batch reactors. Biomass and Bioenergy, 32(12), 1353-1358.

Qureshi, N., Saha, B.C., Hector, R.E., Dien, B., Hughes, S., Liu, S., Iten, L., Bowman, M.J., Sarath, G., Cotta, M.A. 2010b. Production of butanol (a biofuel) from agricultural residues: Part II – Use of corn stover and switchgrass hydrolysates. Biomass and Bioenergy, 34(4), 566-571.

Raganatia, F., Curthb, S., Götzb, P., Olivieria, G., Marzocchellaa, A. 2012. Butanol Production from Lignocellulosic-based Hexoses and Pentoses by Fermentation of *Clostridium Acetobutylicum*. Chemical Engineering Transactions, 27, 6.

Rajagopalan, G., He, J., Yang, K.-L. 2012. A Highly Efficient NADH-dependent Butanol Dehydrogenase from High-butanol-producing Clostridium sp. BOH3. Bioenerg. Res., 6(1), 240-251.

Ranad Shaheen, M.S., David T. Jones. 2000. Comparative Fermentation Studies of Industrial Strains Belonging to Four Species of Solvent-Producing Clostridia. J. Mol. Microbiol. Biotechnol., 2(1), 115-124.

Ranjan, A., Moholkar, V.S. 2012. Biobutanol: science, engineering, and economics. International Journal of Energy Research, 36(3), 277-323.

Rao, G., Mutharasan, R. 1987. Altered electron flow in continuous cultures of *Clostridium acetobutylicum* induced by viologen dyes. Appl. Microbiol. Biotechnol., 53, 1232-1235.

Richmond, C., Han, B., Ezeji, T.C. 2011. Stimulatory effects of calcium carbonate on butanol production by solventogenic *Clostridium* species. Continental J. Microbiology, 5(1), 11.

Rizzi, M., Baltes, M., Theobald, U., Reuss, M. 1997. In vivo analysis of metabolic dynamics in *Saccharomyces cerevisiae*: II. Mathematical model. Biotechnol Bioeng, 55(4).

Robitaille, J., Chen, J., Jolicoeur, M. 2015. A single dynamic metabolic model can describe mAb producing CHO cell batch and fed-batch cultures on different culture media. PLoS One, 10(9), e0136815.

Roels, J.A. 1983. Energetics and kinetics in biotechnology. Elseveier Biomedical Press, Amsterdam.

Sauer, U., Hatzimanikatis, V., Hohmann, H.-P., Manneberg, M., Loon, A.P.G.M.v., Bailey, J.E. 1996. Physiology and metabolic fluxes of wild-type and riboflavin-producing Bacillus subtilis. Applied and enviromental microbiology, 62(10), 3687–3696.

Schaffer, C., Messner, P. 2005. The structure of secondary cell wall polymers: how Gram-positive bacteria stick their cell walls together. Microbiology, 151(Pt 3), 643-51.

Segel, I.H. 1975. Enzyme kinetics: Behavior and analysis of rapid equilibrium and steady-state enzyme systems. John Wiley & Sons, New York.

Shaoming Mao, Yuanming Luo, Tianrui Zhang, Jinshan Li, Guanhui Bao, Yan Zhu, Zugen Chen, Yanping Zhang, Yin Li, Ma, Y. 2010. Proteome reference map and comparative proteomic analysis between a wild type *Clostridium acetobutylicum* DSM 1731 and its mutant with enhanced butanol tolerance and butanol yield. Journal of Proteome Research, 9, 3046-3061.

Shi, H., Xu, W., Luo, Y., Chen, L., Liang, Z., Zhou, X., Huang, K. 2011. The effect of various environmental factors on the ethidium monazite and quantitative PCR method to detect viable bacteria. J Appl Microbiol, 111(5), 1194-204.

Shi, Z., Blaschek, H.P. 2008a. Transcriptional analysis of Clostridium beijerinckii NCIMB 8052 and the hyper-butanol-producing mutant BA101 during the shift from acidogenesis to solventogenesis. Appl. Environ. Microbiol., 74(24), 7709–7714.

Shi, Z., Blaschek, H.P. 2008b. Transcriptional analysis of *Clostridium beijerinckii* NCIMB 8052 and the hyper-butanol-producing mutant BA101 during the shift from acidogenesis to solventogenesis. Appl Environ Microbiol, 74(24), 7709-14.

Shinto, H., Tashiro, Y., Kobayashi, G., Sekiguchi, T., Hanai, T., Kuriya, Y., Okamoto, M., Sonomoto, K. 2008. Kinetic study of substrate dependency for higher butanol production in acetone–butanol–ethanol fermentation. Process Biochemistry, 43(12), 1452-1461.

Shinto, H., Tashiro, Y., Yamashita, M., Kobayashi, G., Sekiguchi, T., Hanai, T., Kuriya, Y., Okamoto, M., Sonomoto, K. 2007. Kinetic modeling and sensitivity analysis of acetone-butanol-ethanol production. J Biotechnol, 131(1), 45-56.

Shuler, M.L., Kargi, F. 1992. Bioprocess engineering - basic concepts. Prentice Hall P T R, New Jersey.

Sivagnanam, K., Raghavan, V.G., Shah, M., Hettich, R.L., Verberkmoes, N.C., Lefsrud, M.G. 2011. Comparative shotgun proteomic analysis of *Clostridium acetobutylicum* from butanol fermentation using glucose and xylose. Proteome Science, 9(66).

Sivagnanam, K., Raghavan, V.G., Shah, M., Hettich, R.L., Verberkmoes, N.C., Lefsrud, M.G. 2012. Shotgun proteomic monitoring of *Clostridium acetobutylicum* during stationary phase of butanol fermentation using xylose and comparison with the exponential phase. J Ind Microbiol Biotechnol, 39(6), 949-55.

Sousa, S.F.d., Bastin, G., Jolicoeur, M., Wouwer, A.V. 2016. Dynamic metabolic flux analysis using a convex analysis approach: application to hybridoma cell cultures in perfusion. Biotechnology and Bioengineering, 113(5), 1102-1112.

Steen, E.J., Chan, R., Prasad, N., Myers, S., Petzold, C.J., Redding, A., Ouellet, M., Keasling, J.D. 2008. Metabolic engineering of Saccharomyces cerevisiae for the production of n-butanol. Microb Cell Fact, 7, 36.

Stephanopoulos, G. 1999. Metabolic Fluxes and Metabolic Engineering. metabolic engineering, 1, 1-11.

Stephanopoulos, G.N., Aristidou, A.A., Nielsen, J. 1998. Metabolic Engineering - Principles and Mwthodologies. Academic Press, California USA.

Stubblefield, E., Mueller, G.C. 1960. Biochemical Composition and Metabolism of HeLa Cells Effects of Sodium Chloride Concentration on Growth. Cancer Research 20, 1646-1655.

Sullivan, L., Bennett, G.N. 2006. Proteome analysis and comparison of *Clostridium acetobutylicum* ATCC 824 and Spo0A strain variants. J Ind Microbiol Biotechnol, 33(4), 298-308.

Sun, Z., Liu, S. 2012. Production of n-butanol from concentrated sugar maple hemicellulosic hydrolysate by Clostridia acetobutylicum ATCC824. Biomass and Bioenergy, 39, 39-47.

Survase, S.A., Heiningen, A., Granstrom, T. 2012. Continuous bio-catalytic conversion of sugar mixture to acetone-butanol-ethanol by immobilized *Clostridium acetobutylicum* DSM 792. Appl Microbiol Biotechnol, 93(6), 2309-16.

Survase, S.A., Sklavounos, E., Jurgens, G., van Heiningen, A., Granstrom, T. 2011. Continuous acetone-butanol-ethanol fermentation using SO2-ethanol-water spent liquor from spruce. Bioresour Technol, 102(23), 10996-1002.

Survase, S.A., van Heiningen, A., Granstrom, T. 2013. Wood pulp as an immobilization matrix for the continuous production of isopropanol and butanol. J Ind Microbiol Biotechnol, 40(2), 209-15.

Thang, V.H., Kanda, K., Kobayashi, G. 2010. Production of Acetone–Butanol–Ethanol (ABE) in Direct Fermentation of Cassava by *Clostridium saccharoperbutylacetonicum* N1-4. Appl Biochem Biotechnol 161, 157-170.

Thauer, R.K., Jungermann, K., Henninger, H., Wenning, J. 1968. The Energy Metabolism of Clostridium kluyveri. European J. Biochem., 4, 173-180.

Tomas, C.A., Beamish, J., Papoutsakis, E.T. 2004. Transcriptional analysis of butanol stress and tolerance in *Clostridium acetobutylicum.* Journal of Bacteriology, 186(7), 2006-2018.

Van der Wal, H., Sperber, B.L., Houweling-Tan, B., Bakker, R.R., Brandenburg, W., Lopez-Contreras, A.M. 2013. Production of acetone, butanol, and ethanol from biomass of the green seaweed Ulva lactuca. Bioresour Technol, 128, 431-7.

Vasconcelos, I., Girbal, L., Soucaille, P. 1994. Regulation of carbon and electron flow in *Clostridium acetobutylicum* grown in chemostat culture at neutral pH on mixtures of gucose and glycerolt. Journal of Bacteriology, 176(3), 1443-1450.

Votruba, J., Volesky, B., Yerushalmi, L. 1986. Mathematical model of a batch acetone-butanol fermentation. Biotechnology and Bioengineering, 28, 247-255.

Wang, E., Bauer, M.C., Rogstam, A., Linse, S., Logan, D.T., von Wachenfeldt, C. 2008. Structure and functional properties of the Bacillus subtilis transcriptional repressor Rex. Mol Microbiol, 69(2), 466-78.

Wang, S., Zhang, Y., Dong, H., Mao, S., Zhu, Y., Wang, R., Luan, G., Li, Y. 2011. Formic acid triggers the "Acid Crash" of acetone-butanol-ethanol fermentation by *Clostridium acetobutylicum*. Appl Environ Microbiol, 77(5), 1674-80.

Wang, Y., Blaschek, H.P. 2011. Optimization of butanol production from tropical maize stalk juice by fermentation with *Clostridium beijerinckii* NCIMB 8052. Bioresour Technol, 102(21), 9985-90.

Wang, Y., Janssen, H., Blaschek, H.P. 2014. Fermentative Biobutanol Production: An Old Topic with Remarkable Recent Advances. John Wiley & Sons.

Wang, Y., Li, X., Blaschek, H.P. 2013. Effects of supplementary butyrate on butanol production and the metabolic switch in *Clostridium beijerinckii* NCIMB 8052: genome-wide transcriptional analysis with RNA-Seq. Biotechnology for Biofuels, 6(138).

Wietzke, M., Bahl, H. 2012. The redox-sensing protein Rex, a transcriptional regulator of solventogenesis in *Clostridium acetobutylicum*. Appl Microbiol Biotechnol, 96(3), 749-61.

Wiselogel, A., Tyson, J., Johnsson, D. 1996. Biomass feedstock resources and composition. Taylor and Francis, Washington, DC.

Xue, C., Zhao, J., Liu, F., Lu, C., Yang, S.T., Bai, F.W. 2013. Two-stage in situ gas stripping for enhanced butanol fermentation and energy-saving product recovery. Bioresour Technol, 135, 396-402.

Yen, H.W., Wang, Y.C. 2013. The enhancement of butanol production by in situ butanol removal using biodiesel extraction in the fermentation of ABE (acetone-butanol-ethanol). Bioresour Technol, 145, 224-8.

Yousheng, L. 2009. Study on Enzymatic Hydrolysis of Corn Straw and Butanol ermentation. in: environmnet engineering, Vol. Master, Dalian University of Technology.

Yu, M., Du, Y., Jiang, W., Chang, W.L., Yang, S.T., Tang, I.C. 2012. Effects of different replicons in conjugative plasmids on transformation efficiency, plasmid stability, gene expression and n-butanol biosynthesis in *Clostridium tyrobutyricum*. Appl Microbiol Biotechnol, 93(2), 881-9.

Yu, M., Zhang, Y., Tang, I.C., Yang, S.-T. 2011. Metabolic engineering of Clostridium tyrobutyricum for n-butanol production. Metabolic Engineering, 13(4), 373-382.

Zaldivar, J., Nielsen, J., Olsson, L. 2001. Fuel ethanol production from lignocellulose: a challenge for metabolic engineering and process integration. Appl Microbiol Biotechnol, 56(1-2), 17-34.

Zamboni, N. 2003. Metabolic engineering of respiration for improved riboflavin production and elucidation of NADPH metabolism in Bacillus subtilis. in: Swiss Federal Institute of Technology Zürich, Vol. Doctor of Natural Science.

Zhang, L., Nie, X., Ravcheev, D.A., Rodionov, D.A., Sheng, J., Gu, Y., Yang, S., Jiang, W., Yang, C. 2014. Redox-responsive repressor Rex modulates alcohol production and oxidative stress tolerance in *Clostridium acetobutylicum*. J. Bacteriol., 196(22), 3949–3963.

Zhang, W.L., Liu, Z.Y., Liu, Z., Li, F.L. 2012. Butanol production from corncob residue using *Clostridium beijerinckii* NCIMB 8052. Lett Appl Microbiol, 55(3), 240-6.

Zhao, X., Condruz, S., Chen, J., Jolicoeur, M. 2016. A quantitative metabolomics study of high sodium response in *Clostridium acetobutylicum* ATCC 824 acetone-butanol-ethanol (ABE) fermentation. Sci Rep, 6, 28307.

Zheng, J., Tashiro, Y., Yoshida, T., Gao, M., Wang, Q., Sonomoto, K. 2013. Continuous butanol fermentation from xylose with high cell density by cell recycling system. Bioresour Technol, 129, 360-5.

Zheng, Y.N., Li, L.Z., Xian, M., Ma, Y.J., Yang, J.M., Xu, X., He, D.Z. 2009. Problems with the microbial production of butanol. J Ind Microbiol Biotechnol, 36(9), 1127-38.

APPENDIX A CORRELATION OF CELLS DRY WEIGHT AND OPTICAL DENSITY

The relation between optical density (OD600) and cells dry weight (gDW) is determined as $y = 0.2182x + 0.0873$.

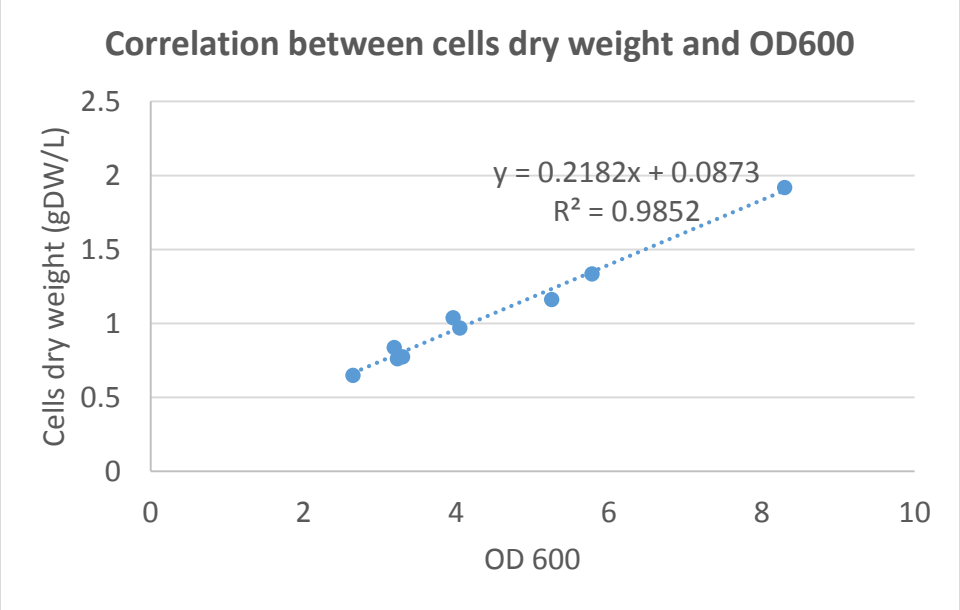

y represents cells dry weight (gDW L^{-1}); x represents OD600 value; R-squared value is 0.9852.

APPENDIX B CULTURE MEDIUM

Seed medium: Modified Reinforced Clostridial broth (MRC) medium (ATCC Medium No. 2107).

Peptone……...10.0 g

Beef Extract……10.0 g

Yeast Extract……...3.0 g

Xylose…….5.0 g

NaCl……5.0 g

Soluble Starch……...1.0 g

L-Cysteine HCl……...0.5 g

Sodium Acetate…….3.0 g

Resazurin (0.025%)……...4 ml

DI Water……...1000 ml

Combine ingredients and dissolve. Adjust pH to 6.8. Dispense and autoclave at 121ºC.

Production medium: The modified Clostridial Growth Medium (CGM) (Choi et al., 2012).

K_2HPO_4……. 0.75 g

KH_2PO_4……0.75 g

$MgSO_4 \cdot 7H_2O$……... 0.7 g

$MnSO_4 \cdot 5H_2O$……. 0.017 g

$FeSO_4 \cdot 7H_2O$……0.01 g

$(NH_4)_2SO_4$……... 2 g

NaCl……... 1g

L-asparagine……. 2 g

ρ- aminobenzoic acid…….. 0.004 g

$CH_3COONa \cdot 3H_2O$……... 30 mmol

Xylose ……... 80g

DI Water……...1000 ml

Adjust pH to 6.8. Dispense and autoclave at 121ºC. Xylose is filtered to sterilize. Based on regular CGM medium, xylose instead of glucose.

APPENDIX C EXPLORATION ON ABE CULTURE WITH HYDROLYSATE AND PRETREATMENT LIQUOR

The hydrolysate and pretreatment liquor were cultured in 500ml anaerobic bottle with 5g/L $CaCO_3$ as buffer by Clostridium acetobutylicum ATCC 824.

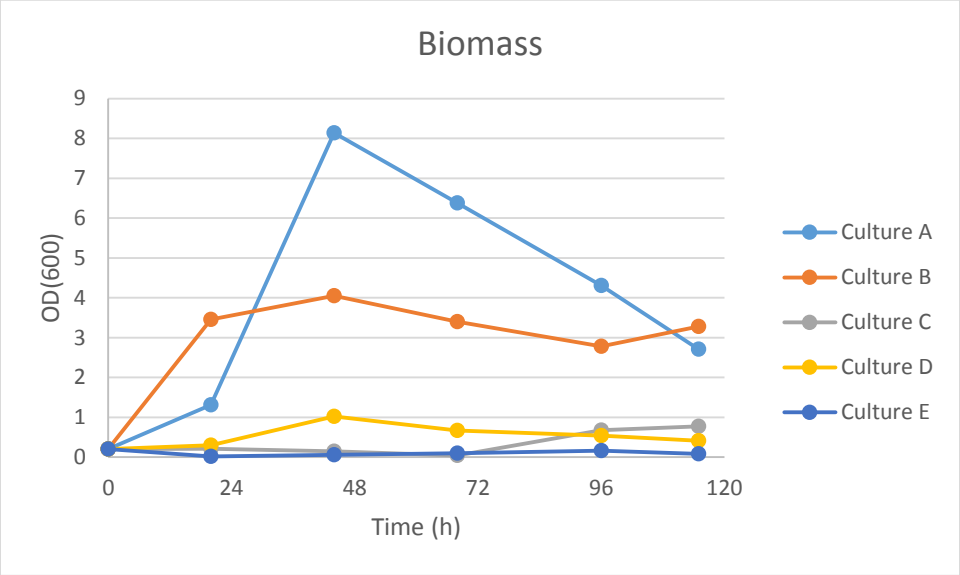

Figure C1. Biomass growth in different medium condition by *C. acetobutylicum* ATCC 824. Culture A used standard CGM medium (xylose as unique carbon source); Culture B is the hydrolysate and standard medium used in medium A (1:1, v/v); Culture C is the hydrolysate medium; Culture D is the pretreatment liquor and standard medium used in medium A (1:1, v/v); Culture E is the pretreatment liquor medium.

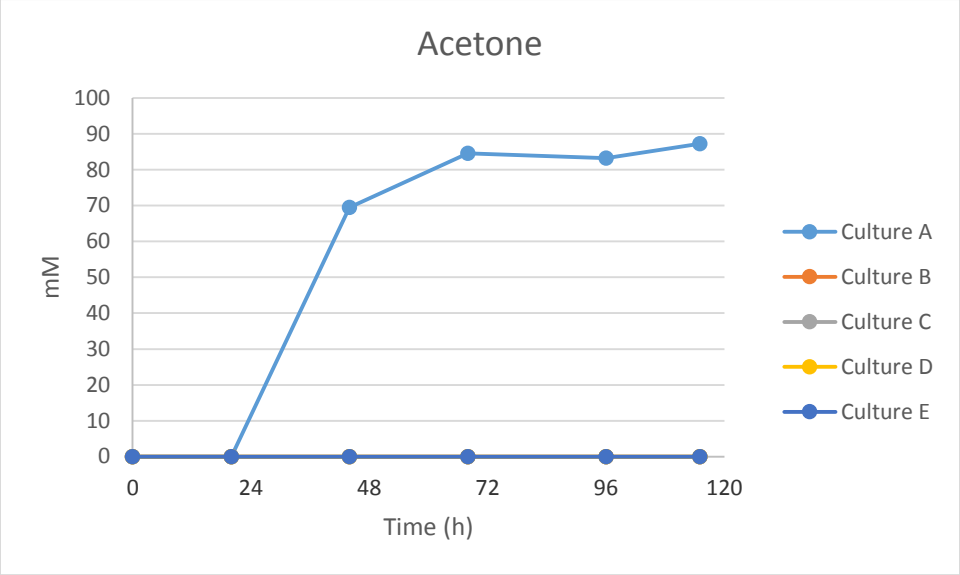

Figure C2. Acetone production in different medium condition by *C. acetobutylicum* ATCC 824. Legend is the same as Figure C1.

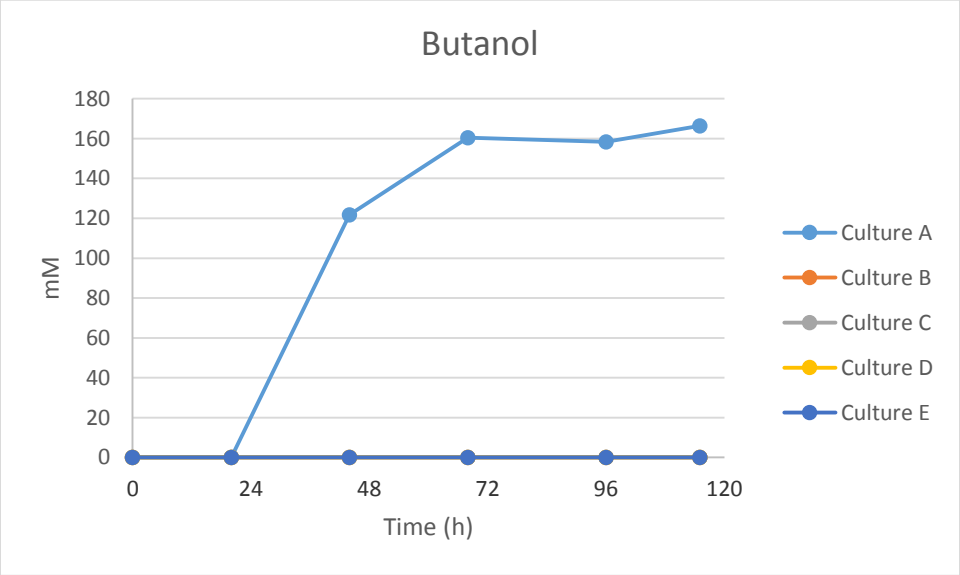

Figure C3. Butanol production in different medium condition by *C. acetobutylicum* ATCC 824. Legend is the same as Figure C1.

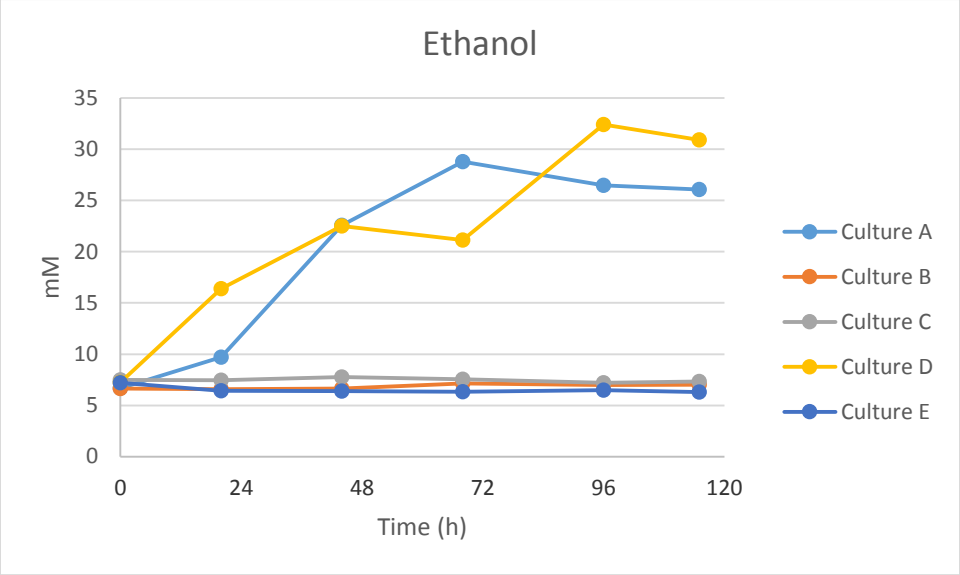

Figure C3. Ethanol production in different medium condition by *C. acetobutylicum* ATCC 824. Legend is the same as Figure C1.

Conclusion

Both hydrolysate and pretreatment liquor failed to generate solvents when just using them as unique medium. However, when added nitrogen source and other medium component except for carbon source, both of their biomass growth in different level (Figure C1). Of interesting, in pretreated liquor with nitrogen medium group, ethanol production is robust (see Figure C4).

APPENDIX D MATLAB FILES

Overview

This program included Michaelis-Menten equation, inhibition equation, activation equation, integral function description and data simulation files. The model simulated a dynamic state of Clostridium cells in ABE fermentation system, riboflavin co-production included as well.

%% File 1: Michaelis-Menten equation;

```
function K=mm(c,k,n)% K=mm(c,k,n)
K= (c.^n)./(k.^n+c.^n) ;
```

%% File 2: inhibition equation;

```
function[v]=inhibition(S,ki)
v=ki./(ki + S);
```

%% activation equation;

```
function[v]=activation(S,A,Km,Ka,alpha,beta)
v=S.*(1+beta*A/alpha/Ka)./(Km*(1+A/Ka)+S.*(1+A/Ka/alpha));
```

%% Integral function description;

```
function dxdt = equadiff(t,x)
%step 1: rate laws
V_Xyl = vmax_Xyl* mm(x(13), km_Xyl_XYL,1)* inhibition(x(20), ki_Xyl_BuOH);
V_RPE = vmax_RPE* mm(x(12), km_RPE_X5P,1) - vmaxr_RPE* mm(x(11), km_RPE_R5P,1);
V_rib = vmax_rib* activation(x(12),x(16), km_rib_X5P, ka_rib_ACE, alpha_rib_ACE,
beta_rib_ACE);
V_ribA = vmax_ribA* mm(x(8), km_ribA_GTP,1);
V_TKTa = vmax_TKTa* mm(x(11), km_TKTa_R5P,1)* mm(x(12), km_TKTa_X5P,1);
V_PFK = vmax_PFK* mm(x(5), km_PFK_F6P,1);
V_GAPDH = vmax_GAPDH* mm(x(7), km_GAPDH_GA3P,1);
V_PGK = vmax_PGK* mm(x(6), km_PGK_G13DP,1);
V_PK = vmax_PK* mm(x(9), km_PK_PEP,1);
V_LDH = vmax_LDH* mm(x(10), km_LDH_PYR,1);
V_PFOR = vmax_PFOR* mm(x(10), km_PFOR_PYR,1);
V_PTA=vmax_PTA* mm(x(3), km_PTA_ACoA,1) - vmaxr_PTA* mm(x(16),
km_PTA_ACE,1);
V_AYDH = vmax_AYDH* mm(x(3), km_AYDH_ACoA,1);
V_THL = vmax_THL* mm(x(3), km_THL_ACoA,1);
```

```
V_CoATa = vmax_CoATa* mm(x(1), km_CoATa_AACoA,1)* mm(x(16),
km_CoATa_ACE,1);
V_BHBD = vmax_BHBD* mm(x(1), km_BHBD_AACoA,1);
V_CoATb = vmax_CoATb* mm(x(1), km_CoATb_AACoA,1)* mm(x(18),
km_CoATb_BUT,1);
V_AADC = vmax_AADC* mm(x(2), km_AADC_ACA,1);
V_SADH = vmax_SADH* mm(x(17), km_SADH_ACTO,1);
V_PTB = vmax_PTB* mm(x(4), km_PTB_BCoA,1)- vmaxr_PTB* mm(x(18),
km_PTB_BUT,1);
V_BYDH = vmax_BYDH* activation(x(4),x(16), km_BYDH_BCoA, ka_BYDH_ACE,
alpha_BYDH_ACE, beta_BYDH_ACE);
V_growth = vmax_growth* mm(x(5), km_growth_F6P,1)* mm(x(8), km_growth_GTP,1)*
mm(x(10), km_growth_PYR,1)* mm(x(11), km_growth_R5P,1)* mm(x(12),
km_growth_X5P,1);%* inhibition(x(20), ki_growth_BuOH);
V_DPO1 = vmax_DPO1* mm(x(8), km_DPO1_GTP,1);

%% step 2: define the equations
dxdt(1) = + V_THL - V_CoATa - V_BHBD - V_CoATb - (V_growth * x(1)) ; % AACoA %
dxdt(2) = + V_CoATa + V_CoATb - V_AADC - (V_growth * x(2)) ; % ACA %
dxdt(3) = + V_PFOR - V_PTA - V_AYDH -(2 * V_THL) + V_CoATa - (V_growth * x(3)) ; %
ACoA %
dxdt(4) = + V_BHBD + V_CoATb - V_PTB - V_BYDH - (V_growth * x(4)) ; % BCoA %
dxdt(5) = +(2 * V_TKTa) - V_PFK - (V_growth * x(5)) - (V_growth_F6P * V_growth) ; %
F6P %
dxdt(6) = + V_GAPDH - V_PGK - (V_growth * x(6)) ; % G13DP %
dxdt(7) = + V_TKTa +(2 * V_PFK) - V_GAPDH - (V_growth * x(7)) ; % GA3P
dxdt(8) = +(0.5 * V_rib) - V_ribA - V_DPO1 - (V_growth * x(8)) - (V_growth_GTP *
V_growth) ; % GTP
dxdt(9) = + V_PGK - V_PK - (V_growth * x(9)) ; % PEP %
dxdt(10) = + V_PK - V_LDH - V_PFOR - (V_growth * x(10)) - (V_growth_PYR *
V_growth) ; % PYR
dxdt(11) = + V_RPE - V_TKTa - (V_growth * x(11)) - (V_growth_R5P * V_growth) ; % R5P
dxdt(12) = + V_Xyl - V_RPE - V_rib -(2 * V_TKTa) - (V_growth * x(12)) - (V_growth_X5P *
V_growth) ; % X5P
dxdt(13) = ( - V_Xyl ) * (x(23)); % XYL
dxdt(14) = ( +(0.6 * V_ribA) ) * (x(23)); % RIBO
dxdt(15) = ( + V_LDH ) * (x(23)); % LAC
dxdt(16) = ( + V_PTA - V_CoATa ) * (x(23)); % ACE
dxdt(17) = ( + V_AADC - V_SADH ) * (x(23)); % ACTO
dxdt(18) = ( - V_CoATb + V_PTB ) * (x(23)); % BUT
dxdt(19) = ( + V_AYDH ) * (x(23)); % EtOH
dxdt(20) = ( + V_BYDH ) * (x(23)); % BuOH
dxdt(21) = ( + V_PFOR + V_AADC ) * (x(23)); % CO2
dxdt(22) = ( + V_SADH ) * (x(23)); % PROP %
dxdt(23) = ( x(23) * V_growth )- 0.01*x(23)*(x(20)/ki_growth_BuOH); % X
dxdt(24) = + V_DPO1- (V_growth * x(24)); % DNA
dxdt = dxdt' ;
```

%% Data simulation;

```
%% Experimental data
P=csvread('dataexp.csv',2,0,[2 0 7 19]);
datatime_P=P(:,1);
Xexp_P=P(:,2);
XYLexp_P=P(:,3);
BuOHexp_P=P(:,4);
ACTOexp_P=P(:,5);
ACEexp_P=P(:,6);
EtOHexp_P=P(:,7);
BUTexp_P=P(:,8);
X5Pexp_P=P(:,10);
RIBOexp_P=P(:,9);
R5Pexp_P=P(:,11);
F6Pexp_P=P(:,12);
PYRexp_P=P(:,13);
GA3Pexp_P=P(:,14);
ADPexp_P=P(:,15);
ATPexp_P=P(:,16);
NADexp_P=P(:,17);
NADHexp_P=P(:,18);
GTPexp_P=P(:,19);
LACexp_P=P(:,20);
%Initial values
t=0:1:100;
yinitial=[
 0.00000003      %   AACoA
0.0000003   %   ACA
0.00005 %   ACoA
0.00000003  %   BCoA
%0.000003   %   E4P
%0.00003    %   F16DP
3.31E-05    %   F6P
0.00003 %   G13DP
4.60E-04    %   GA3P
9.20E-05    %   GTP
0.00003 %   PEP
7.70E-04    %   PYR
1E-03   %   R5P
%0.00003    %   S7P
4E-04   %   X5P
2.20E+02    %   XYL
8.22E-03    %   RIBO
6.12E-01    %   LAC
```

```
0    %   ACE
0.001    %   ACTO
1.59E+00    %   BUT
0.00E+00    %   EtOH
0.00E+00    %   BuOH
1    %   CO2
0.1 %PROP
1.35E-01    %   X
0.002 %DNA
];
%% Simulation
optionsode.AbsTol=1e-6;
optionsode.RelTol=1e-4;
[t,y]=ode23s(@equadiff,t,yinitial,optionsode);
AACoA_P   =    y(:,1)    ;
ACA_P =    y(:,2)    ;
ACoA_P    =    y(:,3)    ;
BCoA_P    =    y(:,4)    ;
F6P_P   =    y(:,5)    ;
G13DP_P    =    y(:,6)    ;
GA3P_P    =    y(:,7)    ;
GTP_P  =    y(:,8)    ;
PEP_P  =    y(:,9)    ;
PYR_P  =    y(:,10)   ;
R5P_P  =    y(:,11)   ;
X5P_P  =    y(:,12)   ;
XYL_P  =    y(:,13)   ;
RIBO_P=    y(:,14)   ;
LAC_P  =    y(:,15)   ;
ACE_P  =    y(:,16)   ;
ACTO_P    =    y(:,17)   ;
BUT_P  =    y(:,18)   ;
EtOH_P=    y(:,19)   ;
BuOH_P    =    y(:,20)   ;
CO2_P  =    y(:,21)   ;
PROP_P    =    y(:,22)   ;
X_P     = y(:,23)     ;
DNA_P = y(:,24);

%%END
```